The Stability of a Bicycle-Rider System

Basin of Attraction Identification and its Sensitivity to Neural Time Delay

S. Kuipers

Technische Universiteit Delft

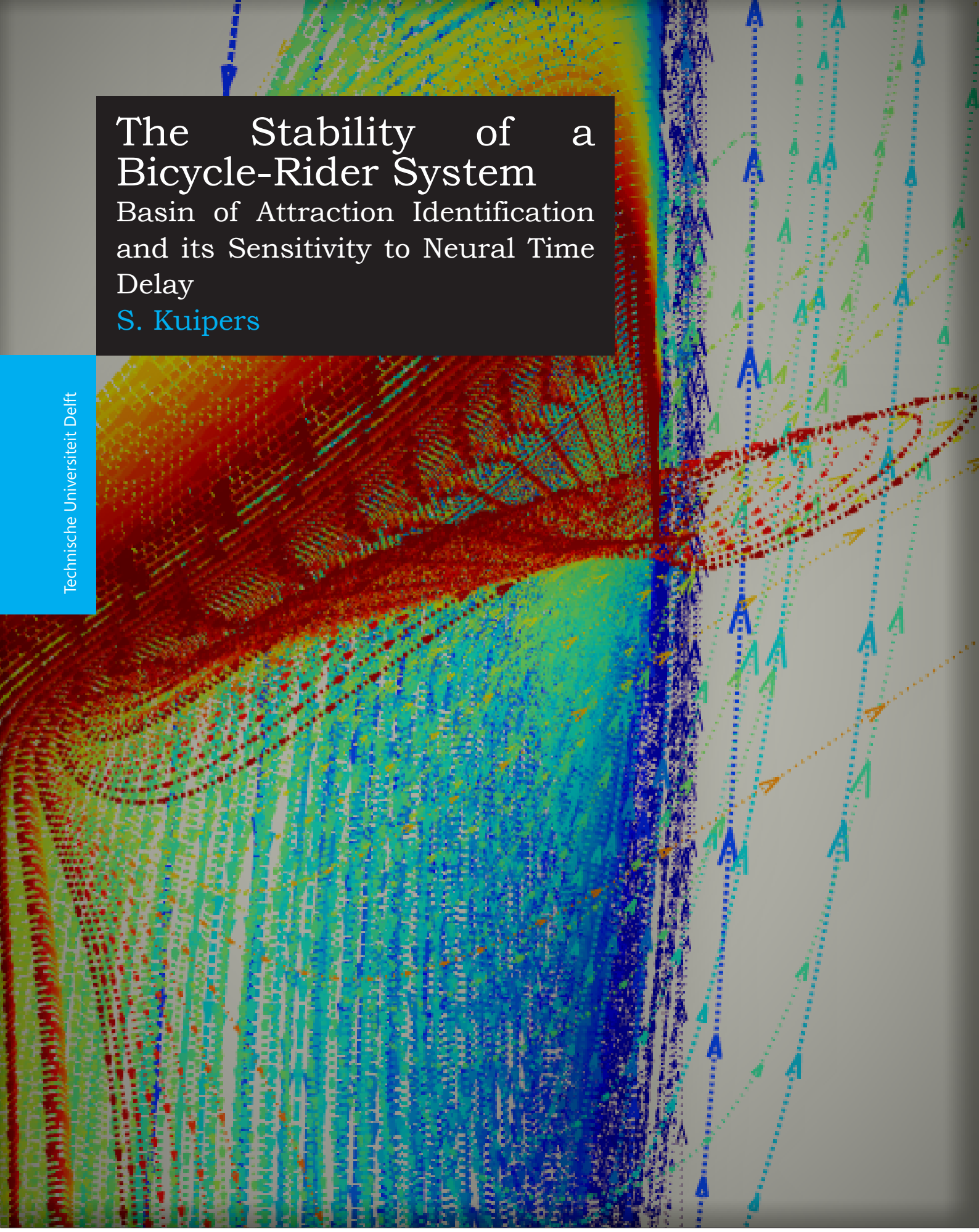

TU Delft Delft University of Technology

Challenge the future

The Stability of a Bicycle-Rider System

Basin of Attraction Identification and its Sensitivity to Neural Time Delay

by

S. Kuipers

in partial fulfillment of the requirements for the degree of

Master of Science
in Applied Physics

at the Delft University of Technology,
to be defended publicly on Friday May 29, 2020 at 10:00 AM.

Supervisor:	Prof. dr. ir. A. L. Schwab	
Thesis committee:	Ir. M. M. Reijne,	TU Delft

This thesis is confidential and cannot be made public until May 29, 2022.

TU Delft Delft University of Technology

Preface

It is late already, past 10 pm. My phone is dead and the darkness outside prevents me from looking through the window. 'Still two more hours to go', is what crosses my mind when the train stops. It is a long and boring ride, from my parents' town to my own home town; the town which has been my home for nearly a third of my life. I am sitting in an intermediate section of the train, because I prefer the mechanical noises over the eerie quietness which sporadically gets disturbed by the sounds of coughs or some wheezing.
Having to pass the time, I let my eyes glide across the mechanical constructions which make up the interior of the train's intermediate section. My eyes pause for a few seconds at every component and, whilst those seconds last, I am wondering about how the piece came to be. How many people would have cooperated to design it? How many hours did they spend on it? How many times has it been remodelled to be the way it is at this very moment? And what did the other design concepts look like? "What an incredible amount of work has gone into it. Not my kind of thing though". Yet it is fascinating; the constructions that we, as humans, can make and how much we have learned from one another over the centuries. Individually, and as a whole.
Despite these thoughts, I have never ever looked that way at my own bicycle. Regardless of owning an old moped, being able to cycle on a mono-cycle and having cycled nearly every. single. day. By now, I do realize how fascinating an object the bicycle is. One of the things on my bucket list is to copy what D.E.H Jones has done.
You pick a summer day and dip the front wheel of your bicycle in a bucket of water, bring the thing up to speed while running along, and give a push to the handlebars. Then, you study the wet traces the bicycle has left behind on the road surface. This trail gives you information, it shows you the frequency and amplitude by which the front assembly swiveled over time due to the applied perturbation. It shows you the resulting deviation of its initially, intended path of going straight ahead. It shows you the times it took for the system to eliminate the oscillations and the time it took to lose speed to friction such that it became inherently unstable and fell over.
It is not the quantitative values that matters to me, but it being the practical equivalent of what I have been doing on my laptop via simulations for nearly a year. What I have done for my thesis is tedious and boring for the lay people. What Jones did is exploring the transition of practice to theory in a playful manner, making it tangible by disclosing the connection. It is this very part what I've missed for the majority of my studies. The part that brings motivation and enhances understanding. The part that brings joy to studying.

As my main supporter, I would like to thank Maarten Kwakkenbos for listening to my entangled thoughts which did not speak to anyone's imagination. It was only fair of you to shut me up once in a while. A big thank you to Koen Wendel and Christos Christoforidis for the educational discussions and idiotic jokes. Another thank you goes to the rest of the bike (lab) gang for making the time there enjoyable. At last, and definitly not least, thank you Arend Schwab and Marco Reijne for the guidance through this process. I've enjoyed the ride.

Kuipers
Delft
May 16, 2020

Abstract

Part of the goal of Europe's Strategy Vision Zero is to eliminate all severe cycling accidents in Europe by 2030. The majority of cycling accidents are single vehicle accidents; this term indicates the absence of collisions with other road participants and implies a fall of the cyclist. Research has shown that mainly elderly cyclists are victim to those accidents. An untested hypothesis is that their slowed motor responses are one of the main reasons behind this.

This study aims to address this hypothesis by studying the influence of neural time delay on the lateral stability of bicycle-rider systems. In this study, the slowed motor responses are represented by single neural time delay values. The influence is quantified by the sizes of the identified basins of attraction of stability (BoA). The BoA contains the set of finite lateral disturbances for which stability is retained and is acquired via numerical integration. Binary threshold criteria are used to determine the stability of the solution.

The bicycle-rider system consists of two components: a bicycle model and a rider model. The bicycle is modelled using the Whipple(-Carvallo) bicycle model with the set of non-linear equations derived by Basu-Mandal [2]. The rider is modelled using an implicit experimentally validated model from literature [31]. This model consists of a PID controller with full state feedback, neuro-muscular dynamics and, in this study, is extended to include nonzero time delay.

The neural time delay value of a young cyclist has been based on literature [4]. The value is doubled to model an older cyclist. The control strategy of the young cyclist is identified using system identification techniques. The basins of the young and old cyclist are compared to study the detrimental effect of time delay on lateral stability in cycling. It declined over 80% when the time delay was doubled.

The human's ability to adapt its control to circumstances has been considered by repeating the control identification process for the rider which suffers from double the time delay. With respect to the young cyclist, a decline of over 50% was observed. Therefore, the results strongly support the hypothesis. Further research should focus on increasing complexity of the rider model to include preview and prediction. In this way, the influence of slowed motor responses can be mapped more clearly.

A secondary objective of this thesis is the preliminary development of a steer assist control model to aid the elderly cyclist balance during cycling. This development builds further on a simple control model from literature [29] which uses roll angle feedback. As a result, a nonlinear velocity dependent roll rate feedback control law was developed. This control law yields a constant basin height over the commonly used velocity range of cyclists. This height indicates the maximum allowable steer rate perturbations the bicycle-steer assist system could handle and is approximately the same height as what was identified for a young cyclist. Future research is required for improving the steer assist. This means adding maximum allowable control torque, sensorial time delays and trajectory tracking.

List of Figures

List of Tables

Contents

Acronyms

BoA Basin of Attraction *of Stability*. xi, xiii, 5, 10, 16, 18–23, 28, 29, 33, 34, 38, 40–43, 45, 47–50, 84

EoM Equations of Motion. xiii, 6–8, 10, 11, 16, 18, 19

SA Steer Assist. viii, xiii, 24, 40–43, 46, 48, 49

WCBM Whipple(-Carvallo) Benchmark Bicycle. vii, xiii, 6, 7, 9

Glossary

Basin of Attraction Set of conditions for which a system converges to the attractor. That set is then the basin of attraction of that attractor. Here, it confines the set of finite lateral disturbances for which the bicycle does not fall over. Then, the attractor is the stable, upright solution.. xiii

Capsize mode A motion characterized by a capsizing motion, similar to a coin spiralling and eventually falling on its side. The motion is unstable for velocities larger than the capsize velocity v_c.. xiii

Intuitive controller Steer assist based on [29]. The steer torque control law relies on a linear, velocity dependent roll rate and roll angle feedback.. xiii

Naive older cyclist A theoretical rider model which does not necessarily represent an elderly cyclist. It represent a cyclist which suffers from 60ms effective, neural time delay. Its control is adapted to 30ms neural time delay.. xiii

Neural time delay A time span which represents the time taken by a cyclist to register, process and respond to a external signal.. xiii

Neuro-muscular dynamics A second-order filter based on shoulder dynamics which represents the limitations of the body and, thereby, converts the neural command signal α to the exerted steering torque T_δ. xiii

Parameter set Set of feedback parameters used by the controller. The set is linearly multiplied by the states and then summed to form the neural signal α. xiii

Part i Refers to the first question answered in this thesis. xiii, 5, 14, 16, 20, 21, 23, 27, 29, 38, 51

Part ii Refers to the first question answered in this thesis. xiii, 5, 14, 16, 20, 21, 23, 27, 32, 33, 38, 51

Part iii Refers to the first question answered in this thesis. xiii, 5, 16, 23, 27, 38, 40

Smart older cyclist A theoretical rider model which does not necessarily represent an elderly cyclist. It represent a cyclist which suffers from 60ms effective, neural time delay. Its control is adapted to the neural time delay.. xiii

Steer assist Controller which exerts a steering torque on the steering axis to aid the cyclist in stabilizing a bicycle.. xiii

Weave mode A motion characterized by the pivoting motion of the front wheel around the steering axis which is unstable between the double root v_d and weave velocity v_w. xiii

Whipple(-Carvallo) Benchmark Bicycle A famous, theoretical bicycle model used for the derivation of its equations of motion.. xiii

Symbolslist

Symbol	Description	Units
$G_{\tau_d}(s)$	Neural time delay given in the Laplace domain for the constant time delay value τ_d	none
G_{nm}	Neuro-muscular dynamics, which are modelled here as a second order filter and represent the physical limitations of the human shoulders	none
α	neural signal containing the unfiltered steer torque response	Nm
δ	Steer angle, the angle of the handlebars around the steering axis. Zero angle corresponds to straight motion, positive for clockwise values	rad
T_{dist}	Disturbance torque, modelled as an initial rate of either the lean or steer angle	rad/s
$K(s,\theta(v))$	Linear feedback response of the rider, based on the estimated parameter set $\theta(v)$	Nm
$K_{\delta dd}$	Steer angle acceleration feedback gain	Nms^2/rad
$K_{\delta d}$	Steer rate feedback gain	Nms/rad
$K_{\phi dd}$	Roll acceleration feedback gain	Nms^2/rad
$K_{\phi d}$	Roll rate feedback gain	Nms/rad
$K_{\delta i}$	Integral steer feedback gain	Nm/rads
$K_{\phi i}$	Integral roll feedback gain	Nm/rads
$K_{\delta p}$	Steer angle feedback gain	Nm/rad
$K_{\phi} p$	Roll angle feedback gain	Nm/rad
ϕ	Roll angle of the bicycle-rider system around the ground-contact point of the rear wheel. Positive for clockwise values	rad
$\theta(v)$	Estimated parameter set of the rider his linear feedback control response, for forward velocity v. The set consists of the feedback parameters $(K_{\phi p}, K_{\phi i}, K_{\phi d}, K_{\phi dd}, K_{\delta p}, K_{\delta i}, K_{\delta d}, K_{\delta dd})$	multiple
T_δ	Steer torque, exerted by the rider or steer assist on the handlebars for control	Nm

Symbol	Description	Units
v_c	Capsize velocity, the upper bound velocity of the self-stable region of the bicycle	m/s
v_w	Weave velocity, the lower bound velocity of the self-stable region of the bicycle	m/s

1

Introduction

At first, some background information is given. Then, the main research objective is introduced, along with the three main steps taken to acquire that objective. After that, the building bricks which were gathered from literature, are given together with their purpose. The general outline for this Msc. thesis is given at the end.

Increasing Cycling Safety

Vision Zero has been employed by the EU as a strategy to reduce the number of road fatalities and severe injuries to 0 by 2030. Progress has been made in reducing the fatalities number of most road users, whereas the number of cyclist fatalities has stagnated over the last decade. The number of serious cyclist injuries even suffered an increase of 28% between 2010 and 2018 [1].

Cyclist fatalities mainly occur due to motor vehicle accidents, whereas the seriously injured often get hurt during single vehicle accidents. The latter term indicates that no collisions with other road users occurred. The ratio of seriously injured versus fatalities of cyclists reached nearly 15 in Europe in 2018*; 31,671 seriously injured versus 2,160 deaths [1]. Those numbers do not take into account that the number of injured cyclists is thought to be severely underestimated due to under-reporting to the police [15].

Victims of reported single vehicle bicycle accidents mainly involve males aged above 65 years old [1]. One of the main, possible causes for their falls that are often mentioned, are their slowed motor responses due to aging. This hypothesis has been proven true for falls during walking [14], but has not yet been tested for cycling and will be addressed in the first part of this Msc. thesis. General provided solutions for bicycle accident prevention concern infrastructure improvements and making protective gear mandatory. No measures targeting the older cyclist, and their impaired motor responses, are mentioned in particular. The latter part of this thesis will address this gap.

** This value is based on the numbers of 21 European countries, the remaining countries either had 'insufficient data or changes in data reporting system'*

Research Objectives

This thesis aims to increase the cycling safety of the older cyclists by studying the effects of their slowed motor responses on cycling stability and, thereafter, identifying the potential of a steer assist control law to increase their stability. A steer assist control law is one of the existing solutions for aiding the older cyclist. Other solutions fall outside the scope of this thesis.

The steer assist is a theoretical controller which purpose is to not fully control the bicycle, but to aid the cyclist by adding steer control to the control exerted by a rider. It is expected that the steer assist will increase the stability of the older cyclist and, therefore, has the potential of reducing their number of falls.

The stability of the cyclists is researched theoretically using simulations of a bicycle-rider system which is subjected to a set of finite lateral disturbances. The advantage of using simulations is the theoretical exploration of situations where ethical implications are preventing the use of physical analysis. An example is the identification of the smallest perturbations for which a cyclist falls over. Also, simulations provide a platform for testing potential solutions without building any physical construction.

The research objective can be acquired using three main steps. These three step are split up in part i to part iii and each contain their own question to be answered.

Part i: Stability of an Average Cyclist

To quantify the effects of age-related neural time delay on the stability of cyclists, the stability of an average, young cyclist needs to be identified at first. It is known that, for small disturbances, an uncontrolled bicycle is stable within a moderate forward speed range [20] and is easily controlled by a rider at unstable forward speeds [30]. However, the degree to which the bicycle can be stabilized by a rider is unknown.

This can be quantified by identifying the 'basin of attraction of stability' of the rider. This basin of attraction contains the set of finite lateral disturbances for which the rider does not fall over. Hence, the first part of this thesis will answer the following question: Which set of disturbances can a young cyclist recover from?

Part ii: Basin of Attraction of the older Cyclist

After identifying the stability of the relatively young cyclist, the basin of attraction of the older cyclist needs identification for comparison. The older cyclist is represented as the young cyclist with an additional time delay to resemble the age-related slowed motor responses. The influence of neural time delay will then reveal itself as the deterioration of the basin of attraction between the young and older cyclist. Therefore, this part will answer the question: Which set of disturbances can an older cyclist recover from?

Part iii. Steer Assist Control Law Potential

Taking a preliminary step towards the development of an assisting steering device for the prevention of falls, a steer assist control law is investigated. The controller bases its steer torque on the control law and exerts control parallel to the older cyclist. An ideal control law is defined as a controller which can handle the same degree of disturbances for every forward velocity. If the basin of attraction of the combination of the rider and assisting controller is enlarged, it would indicate the potential of the law. A positive result would support future research towards the further development of an assisting steer device, which could be used by the older cyclists such that their cycling safety is enhanced.

Conclusively, this part answers several questions. The first question is: Can the basin of attraction of an older cyclist be enlarged using a steer assist? And if so, by how much can this basin be enlarged and what are the characteristics of the steer assist?

Research Approach

The bicycle-rider system requires models of both the rider and bicycle. The well-known Whipple bicycle model (section 2.1.1) has been used throughout literature to study its dynamics [20][2][6], its non-linear equations of motion [2] can be used for simulation. Within literature, only one experimentally validated rider model (section 2.1.3) is present [31]. Neural time delays are added to this model (section 2.3), to represent the younger and older cyclists.

The bicycle and rider model will be combined (section 2.2.1) and numerically integrated (section 2.2.5) such that its basin of attraction of stability can be identified. The numerical integration is done for a set of chosen disturbances and velocities (section 2.2.2). To quantify whether the bicycle-rider system has achieved a stable solution over time, stability criteria are set (section 2.2.4). A simple controller from literature, called the intuitive controller [29], will be used as a basis for a steer assist to help stabilize

the older cyclist (section 2.1.4). Having gathered the main components, a remaining question concerns itself around the modelling of the disturbances (section 2.2.3).

If the basin of attraction decreases for increasing neural time delay, the implications of age-related slowed motor responses on the lateral stability in cycling are revealed and identified as a possible cause for falls of elderly cyclists. Then, a significant increase of this basin upon the addition of the steer assist control law would strongly support future research directed at steer assist control for the older cyclist. Future research in this direction can aid the EU in getting one step closer to the goal of strategy Vision Zero.

Thesis Outline

In chapter 2, the methodology behind the research is explained. Chapter 3 gives the results which is followed by a discussion in chapter 4. The conclusions and future recommendations are given in chapter 5.

2

Methodology

This chapter discusses the methodology used to answer the three main research question. The research questions as mentioned in the introduction were:

Part i Which set of disturbances can a young cyclist recover from?
Part ii which set of disturbances can an older cyclist recover from?
Part iii Can the basin of attraction of an older cyclist be enlarged using a steer assist?

To answer them, four models from literature have been selected. The linear and nonlinear equations of motion of the Whipple (-Carvallo) bicycle model, [20] and [2] resp., are used and combined with a rider model [31]. Using these models, and some alterations to include nonzero neural time delay, Part i and Part ii of this thesis can be answered. For Part iii, a model for the steer assist controller is required. Therefore, the model from [29] is used and build further upon

Methodology Outline

Based on the three research objectives, the methodology section can be divided into four main parts. At the foundation of the research questions lie the models selected from literature. Therefore, part 1 explains the methodology behind the four models from literature. For all three objectives, the extraction of a Basin of Attraction *of Stability* is required. Therefore, all three objectives are partially bound by the same prerequisites. These prerequisites concern e.g. stability definitions, disturbance modelling, etc. Hence, part 2 of the methodology elaborates on this. After the second methodology part, the basis has been laid for all three objectives. The next step is answering Part i and Part ii by altering the rider model such that it resembles a younger and older cyclist. Having done this, only the objective of Part iii remains unanswered. Therefore, the last part of the methodology centers itself around the evaluation and further development of the steer assist model.

To take count, the four main methodology parts for this thesis can be summarized as follows:

- Explaining the Four Models from Literature (Section 2.1)
- Laying the General Prerequisites for the Detection of a Basin of Attraction (Section 2.2)
- Altering the Rider Model to Include Neural Time Delay (Section 2.3)
- Analyzing the Steer Assist (Section 2.4)

2.1. Explaining the Four Models from Literature

This methodology part, part 1, will explain the methodology behind the four models which have been chosen from literature. As a reminder, the models this thesis is based upon are:

- *Mechanical Whipple(-Carvallo) benchmark bicycle model (Whipple, 1899)*

- Linearized equations of motion (EOM) of an uncontrolled bicycle [20]
- Nonlinear equations of motion (EOM) of an uncontrolled bicycle [2]
- Rider model [31]
- Simplified rider model used for the steer assist [29]

Given in cursive is the Whipple bicycle model, which is a bicycle model used for all other four literature models. Therefore, this model is included in this literature methodology.

Outline Methodology Part 1

Starting with the foundation of the literature models, the Whipple bicycle model will be explained first in section 2.1.1. Then, the linear and nonlinear equations are briefly discussed in section 2.1.2. After that, the rider model is elaborated upon in section 2.1.3. Aligned with the three main objectives, the steer assist is presented last in section 2.1.4.

2.1.1. Mechanical Whipple(-Carvallo) Benchmark Bicycle Model

This bicycle model is at the very foundation of this research and has been used in all four selected literature models. Its design has its limitations which shall have undeniable influence on the results produced in this thesis. Therefore, its construction will be explained briefly before diving into the EoM. First, some background information is provided. Thereafter, the basic build of the bicycle is explained, followed by the assumptions and simplifications. At last, the velocity degrees of freedom are discussed.

Background

Whipple designed a theoretical, rigid bicycle and derived its equations in 1899 [35]. A vast amount of scientists produced similar work, each using different symbols and methods used for derivation. This made cross-checking the works impossible, hence the need for a benchmark model which others could build further upon. Meijaard *et al.* did just that, building further upon Whipple's work by writing a paper on the linearized equations of a benchmark bicycle model [20]. The bicycle from this paper is called the Whipple(-Carvallo) Benchmark Bicycle (WCBM).

Rigid Bodies & Parameters

The WCBM consists of four rigid parts which each have their own center of gravity. The bicycle used here is fully defined by the 25 parameters given in black in [31], Tab. 6. The rigid parts are the

- rear wheel
- front wheel
- rear frame and rigid rider
- handlebars and front steering assembly

The rigid parts are given, in the same order as the summation above, by R, F, B and H in figure 2.1.

Assumptions and Simplifications

The bicycle model is assumed to be laterally symmetric and the wheels have circular symmetry. The inertial properties of the wheels allow general shape and mass distribution, yet the wheel-ground contact modelling is knife-edged. This indicates that there is an infinitely small line of contact between the wheels and the ground, as opposed to e.g. toroidal wheels. The lateral friction at point P and Q of figure 2.1 is infinite, indicating no side-slip is possible. The rider is rigid and fixed to the rear frame, indicating no motion between rider and frame is possible. Structural stiffness and damping, all remaining forms of friction and tyre force models are not included. Both the linear and non-linear EoM were derived using this mechanical bicycle model.

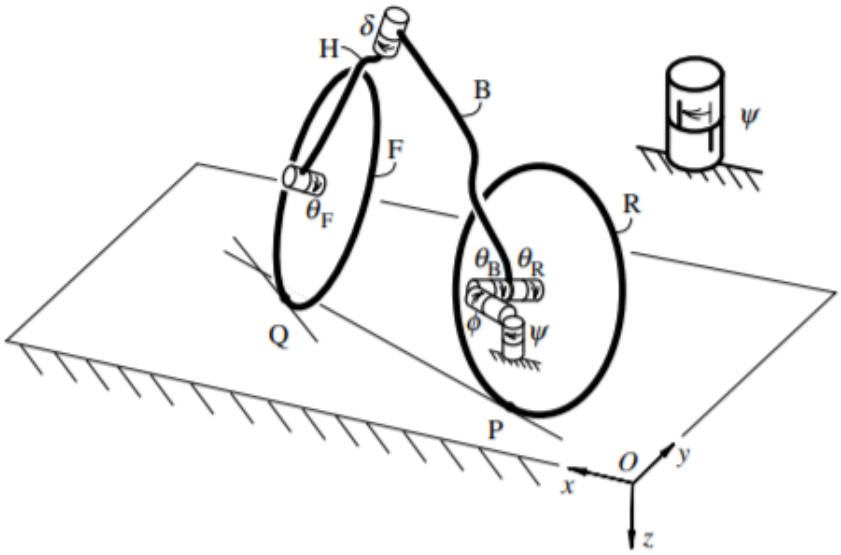

Figure 2.1: A mechanical bicycle model and its configuration parameters as defined by, and taken from, [20]. The figure shows the configuration space of their bicycle model which can be parametrized by seven dimensions. The local configuration space is defined by 5 parameters: the roll angle of the rear frame around the line of contact of the rear wheel at point P, ψ; the rear wheel rotation with respect to the rear frame B, θ_R; the front wheel rotation with respect to the front assembly H; the steer angle of the handlebars with respect to the rear frame B, δ. The global configuration is defined by three additional parameters: the yaw angle of the rear frame relative to the vertical going through point P, ϕ and the x- & y-coordinates of the rear wheel ground contact point P.

Velocity Degrees of Freedom

The configuration space of the bicycle can be defined using 7 parameters, four are eliminated due to non-holonomic constraints*. These non-holonomic constraints are rolling constraints which, in the lateral and longitudinal direction, connect the wheels with the ground. This leaves us with 3 velocity degrees of freedom, which are the

- rear frame's roll rate, $\dot{\phi}$ $[rad/s]$
- handlebar's steer rate w.r.t. the rear frame, $\dot{\delta}$ $[rad/s]$
- rear wheel's rotation rate w.r.t. the rear frame, $\dot{\beta}_R$ $[rad/s]$

The roll ϕ and steer angle δ are found in figure 2.1 using the same symbols. The rear wheel rotation β_R is represented by θ_R in the figure. This change of notation is used due to future occupation of the symbol θ.

*A holonomic constraint can be expressed as $f(q_1, q_2, ..q_n, t) = 0$, whereas a non-holonomic might be expressed as e.g. $f(q_1, q_2, ..q_n, t) \leq 0$.

2.1.2. Equations of Motion (EoM)

The linearized EoM were derived by Meijaard *et al.* [20] using the bicycle model explained above in section 2.1.1. The linearized EoM of the bicycle are used for extraction of the eigenvalues, which reveal the dynamic characteristics of the system. Its nonlinear counterpart is used for simulations which is done via numerical integration.

The linearized EoM will be explained first, then the eigenvalues are extracted and displayed in a graph to show and explain the velocity dependent characteristic behaviour of the uncontrolled bicycle. After that, the validity of the WCBM and its linearized EoM is discussed. The remainder of the section focusses on the nonlinear EoM. At the end of the first part on the EoM, a brief summary is given.

The latter part starts with the choice for the nonlinear EoM of Basu-Mandal. A very brief explanation on his work is given. At last, the main numerical integration requirement is discussed.

Linearized EoM

The first linear equation decouples the forward speed from the lateral dynamics, due to the lateral symmetry of the bicycle. This equation is,

$$\left[r_R^2 m_T + I_{Ryy} + (\frac{r_R}{r_F})^2 I_{Fyy}\right]\ddot{\beta}_R = T_{\beta_R}, \tag{2.1}$$

for which T refers to 'total', in the sense that this is the total bicycle mass. For all cases in this thesis, T_{β_R} is set to zero indicating that the rider does not exert a propulsive force to the pedals. This results in a constant forward speed $v = -r_R\dot{\beta}_R$ since the remainder of equation (2.1) consists of constant, nonzero values resulting in $\ddot{\beta}_R = 0\ rad/s^2$.

The remaining two linear EoM, the steer and lean equations, can be rearranged into two second order differential equations in the following canonical form,

$$M\ddot{q} + vC_1\dot{q} + \left[gK_0 + v^2K_2\right] = f, \tag{2.2}$$

where $q = \left[\phi, \delta\right]^T$ and $f = \left[T_\phi, T_\delta\right]^T$. The matrices M,C_1,K_0 and K_2 are constant matrices which are defined by the 25 mechanical parameters given in table E.1. The matrices C_1 and K_2 have linear and quadratic dependence on the forward velocity, respectively.

Velocity-Dependent Eigenvalues

From the linearized EoM, the characteristic polynomial equation can be established,

$$det(M\lambda^2 + vC_1\lambda + gK_0 + v^2K_2) = 0, \tag{2.3}$$

which can be used to study the stability of the system for low perturbations. As can be seen from (2.3), the eigenvalues are velocity-dependent. The eigenvalues as a function of forward velocity are displayed in the eigenvalue diagram of figure 2.2 for the uncontrolled bicycle model combined with the mechanical parameters used for [31]. Three velocities mark dynamic changing points. Those are,

- v_d, called the double-root velocity. Marks the velocity at the point of coalescence
- v_w, called the weave velocity. Marks a zero crossing and the lowest velocity of the stable region.
- v_c, called the capsize velocity. Marks another zero crossing and the highest velocity of the stable region.

For the uncontrolled bicycle those velocities are 1.01, 5.83 and 10.14 m/s, respectively.

Bicycle Mode Explanation

Every zero crossing marks a significant change in dynamics. Three main regions exist, demarcated by the velocities described previously. Between v_d and v_w, the bicycle is said to be in the *weave mode*, where its dynamics are characterized by a pivoting motion around the steering axis. Between v_w and v_c, the bicycle is self-stable; it is able to reject perturbations up to a certain degree. Above v_c, the bicycle will enter a spiralling motion like a coin having been pushed until it eventually falls on its side. This is the capsize mode. Around v_w and v_c, circular motions are encountered which are highly unstable equilibria.

To visualize the modes and the equilibria, the uncontrolled bicycle is subjected to a small perturbation at the velocities dictated by the crosses of figure 2.2. The resulting trajectories are displayed in figure 2.3.

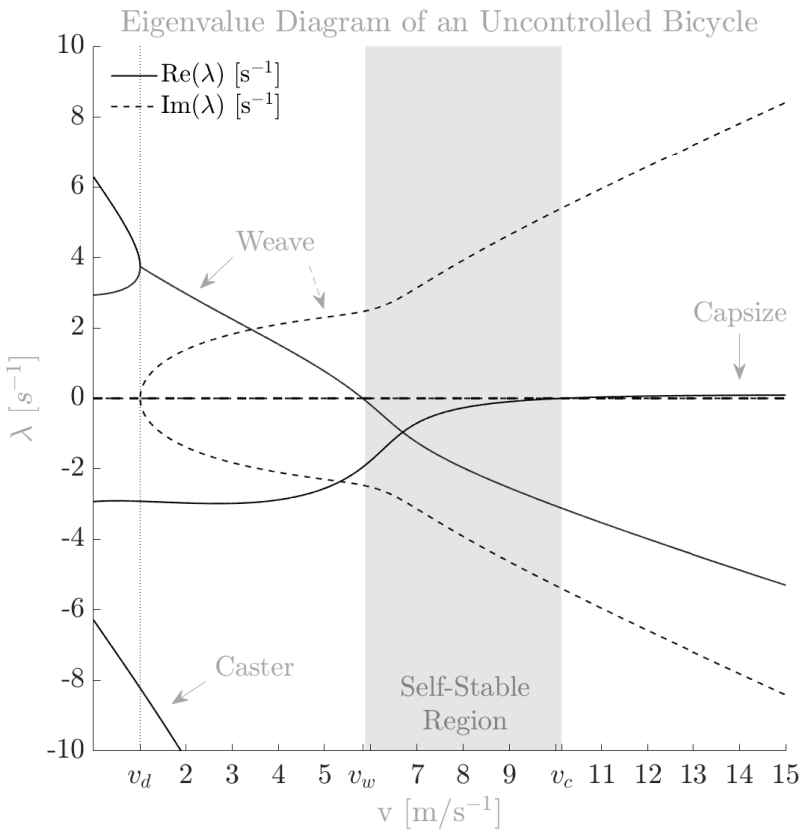

Figure 2.2: The eigenvalues of the WCBM as a function of forward velocity. The shaded region marks the velocity range for which the uncontrolled bicycle is self-stable, motions at all other velocities are unstable. The dashed lines are the imaginary eigenvalues and the solid lines are the real eigenvalues. The sole vertical line shows the velocity at the point of coalescence v_d. Before this point, the bicycle is severely unstable. After this point, the weave mode dominates the dynamics until the stable region. After the stable region, the bicycle displays capsize behaviour. The velocities corresponding to the transitions of dynamic behaviour are, for increasing velocity, called double root-, weave and capsize velocity and are denoted using v_d,v_w and v_w, respectively with corresponding mode velocities of 1.01, 5.83 and 10.14 ms^{-1}. The style of this figure has been copied from [20].

Validaty WCBM and EoM

The resulting equations of the WCBM do describe self-stability, an important dynamical bicycle characteristic which, for example, the simplest bicycle model used in [9][19][38] lacks. The equations have been verified by comparisons of the derived equations from literature which have been published prior to the benchmark paper [20]. Also, the equations were checked against two nonlinear dynamics simulations with good correspondence.

Kooijman *et al.* experimentally validated the benchmarked equations for a velocity range of approximately 3-6 m/s by comparison of the numerical and experimental eigenvalues [13]. Below 3 m/s experimental validation was difficult due to the short time window for measurements compared to the time period of the weave motion. This range of velocity covers, for the mechanical parameters used for the WCBM, the transition of the weave mode to the stable mode. For a city bicycle, the forward speeds encountered often lie within the weave to stable mode. Therefore, the Whipple model is assumed to produce valid results for this thesis.

Basu-Mandal's Nonlinear EoM

Between the set of literature on nonlinear bicycle models is the benchmarked model of Basu-Mandal [2]. Basu-Mandal has set up the nonlinear dynamics equations for an uncontrolled bicycle using two approaches; the Lagrangian and Newton-Euler approach. The bicycle model of Basu-Mandal is identical to the WCBM of Meijaard *et al.* [20] and, thus, contains the same four rigid bodies, assumptions and simplifications. For this bicycle model the equations are set up via the Lagrangian and Newton-Euler

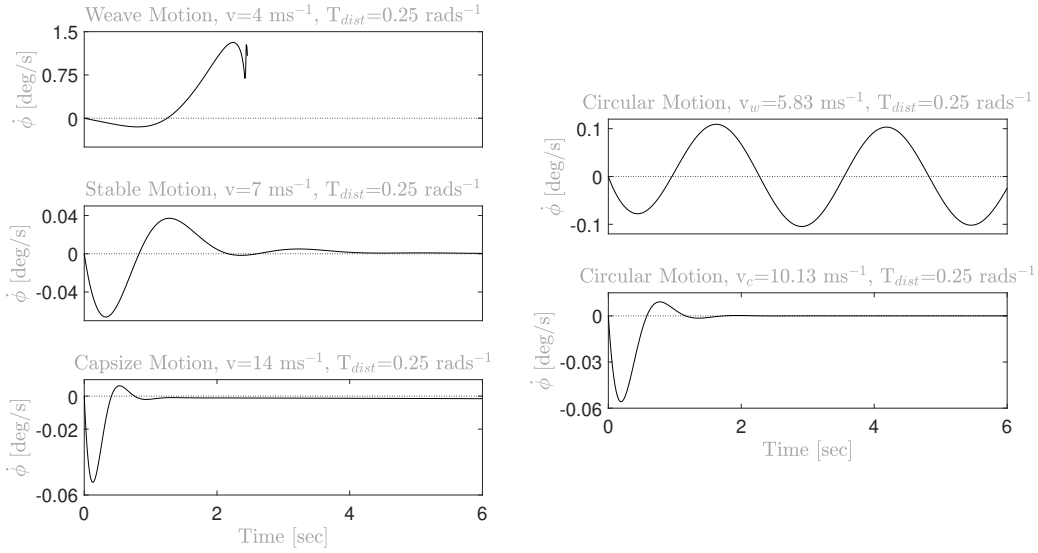

Figure 2.3: Modes of a bicycle visualized using roll rate state of the uncontrolled bicycle over time for one perturbation and three distinct initial velocities. The uncontrolled bicycle model used is the nonlinear model of Basu-Mandal [2]. The velocities for the left figures are 4, 7 and 14 ms^{-1} from top to bottom, the motions are dominated by the weave, stable and capsize mode, respectively. The right figures are simulations at the weave velocity v$_w$ (top) and the capsize velocity v$_c$ (bottom). The circular capsize motion (right-bottom graph) might seem very stable, but after 400 seconds the bicycle has ridden a full circle and has not returned to the straight-ahead motion.

approach, only the latter is used for simulation. For the full derivation of the nonlinear EoM, one is referred to the paper itself [2].

No Algebraic Solution

The model of Basu-Mandal consists of a set of equations of the governing dynamics and the constraints, which are solvable using a set of initial conditions and numerical integration. The nonlinear, analytical expression of the three velocity degrees of freedom is tens of pages long [33] which renders the method of Basu-Mandal more suitable for finding solutions of the equations of motion.

Numerical Integration Requirement

The model of Basu-Mandal is an initial value problem; to integrate the equations numerically, initial conditions are required. If the resulting states would go to zero, this would then correspond to the system going to the stable, upright position. Therefore, the BoA of stability of this system consists of the set of initial conditions for which the resulting states of the system, except the forward velocity, go to zero over time. As a result, the initial conditions of the model of Basu-Mandal influence the dimension of the BoA. E.g. the BoA can be sought for a bicycle starting of with a 45° roll angle.

The model of Basu-Mandal requires five initial conditions to solve their initial value problem. These initial conditions are,

$$q(t_0 = 0) = (\phi_0, \delta_0, \dot{\phi}_0, \dot{\delta}_0, \dot{\beta}_{r,0}), \tag{2.4}$$

The meaning of the symbols has been given in section 2.1.1. Since there are five initial conditions, the space of the BoA can be spanned by all five rendering it at least five-dimensional. A choice concerning which initial conditions to use is made in the second methodology part, section 2.2.

Validity Nonlinear EoM

Basu-Mandal *et al.* compared their results on circular motion families with previous literature, they disagreed with Psiaki [23], found one common result with Cossalter et al. [3] and Franke et al. [8] and found all but one of the same solution families as Lennartsson et al. [16]. For validation of the model, a

numerical comparison was done between the results of the two derivation methods for arbitrary inputs; numerical agreement was found up to ten digits. Basu-Mandal *et al.* also linearized the Lagrange's equations around the upright, straight ahead motion, and compared eigenvalues with the benchmark bicycle; again agreement was found. On top of that, Arend Schwab verified some of the initial conditions required for circular motion using SPACAR, according to Basu-Mandal his dissertation. Concludingly, the nonlinear EoM are assumed to be valid.

Summary

To take count, the mechanical bicycle behind the EoM has been explained in section 2.1.1, as well as the derivation and validity of the EoM themselves in this section. The typical dynamic modes of a bicycle and their relationship to the eigenvalues have been explained as well. So far, everything was concerned around the uncontrolled bicycle. The next section will be focused on its indispensable counterpart; the rider.

2.1.3. Rider Control Model

The rider control model used to represent the human cyclist is the model from [31]. The identification of the control of their rider has been performed using six steps; 1. data preparation; 2. black box identification; 3. simulation; 4. filtering; 5. gray box identification; 6. parameter reduction. For information on the first four steps, one is referred to their paper [31]. The latter two are altered and used in this thesis. Hence, step 5 and 6 will be explained in this section.

The rider is modelled as a PID controller with linear full state feedback, zero neural time delay and second order neuro-muscular dynamics. The top part of figure 2.6 explains a human way of signal processing on a general level. Translating the part covering the central nervous system to the simple theoretical model of [31] leads to the bottom block scheme of the figure. The external signals are delayed, after which they arrive at our brain. Then, we are assumed to respond linearly to the signals. This results in a neural signal α, which needs to go through a neuro-muscular filter before it can represent a torque which we are actually able to exert. Going from left to right, each block of the bottom part of figure 2.6 will briefly be explained.

It has to be noted that the order has been changed w.r.t. [31]; they implemented the time delay at the end. However, the time delay is a single, effective delay, thus it's position in the loop will yield no different result. It's position has been changed since it is a neural delay and, therefore, belongs to the part of the CNS.

Feedback States

A rider model is added to the bicycle model, their combined closed loop is given in figure 2.4. The input to the rider are the states of the bicycle; the feedback states. Using the knowledge on what our sensors are able to perceive [11], table 2.5 could be derived. It gives the sensors and the corresponding states of the bicycle which we should be able to perceive. Then based on Mcruer, whom states that a human is able to differentiate and integrate information [17], it was assumed that the cyclist perceives all of state vector y. Then, how are those signals processed in our brain?

Neural Time Delay $G_{\tau d}$

The processing in our brain takes time. In this thesis, the feedback states are first delayed and then responded to. The delay is modelled as a single, effective neural time delay and is implemented as,

$$G_{\tau_d} = e^{-\tau_d s}, \tag{2.6}$$

where τ_d is the time delay. Numerical issues were encountered for nonzero values of τ_d, therefore it was set to zero in [31]. After the processing, the signal is responded to by the controller.

Neural Controller $K(s, \theta(v))$

The neural human response to the observed, delayed signals is unknown, therefore the rider is assumed to respond linear to the feedback states. This response part covers the 'decision' and 'motor program'

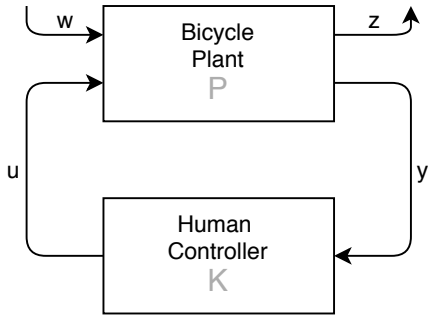

Figure 2.4: A basic block scheme of the closed loop system containing the bicycle as the plant P and the human rider as the control model K. The output of the plant y contains the state information of the plant and the output of the controller u contains the steer torque exerted by the rider. The perturbation is given by w and the output error by z.

Sensory Organ	Registered Variables
Muscle Spindles	$\delta, \dot{\delta}$
Golgi Tendon Organs	T_δ
Vestibular System	$\phi, \dot{\phi}$
Eyes	$\phi, \delta, v, x, y, \psi$

Figure 2.5: The variables which, presumably, are registered by the human sensors during cycling. On the left are the sensory organs which measure the corresponding variables given on the right.

$$y = \begin{bmatrix} \ddot{\phi} \\ \ddot{\delta} \\ \dot{\phi} \\ \dot{\delta} \\ \phi \\ \delta \\ \int \phi \\ \int \delta \end{bmatrix}, \tag{2.5}$$

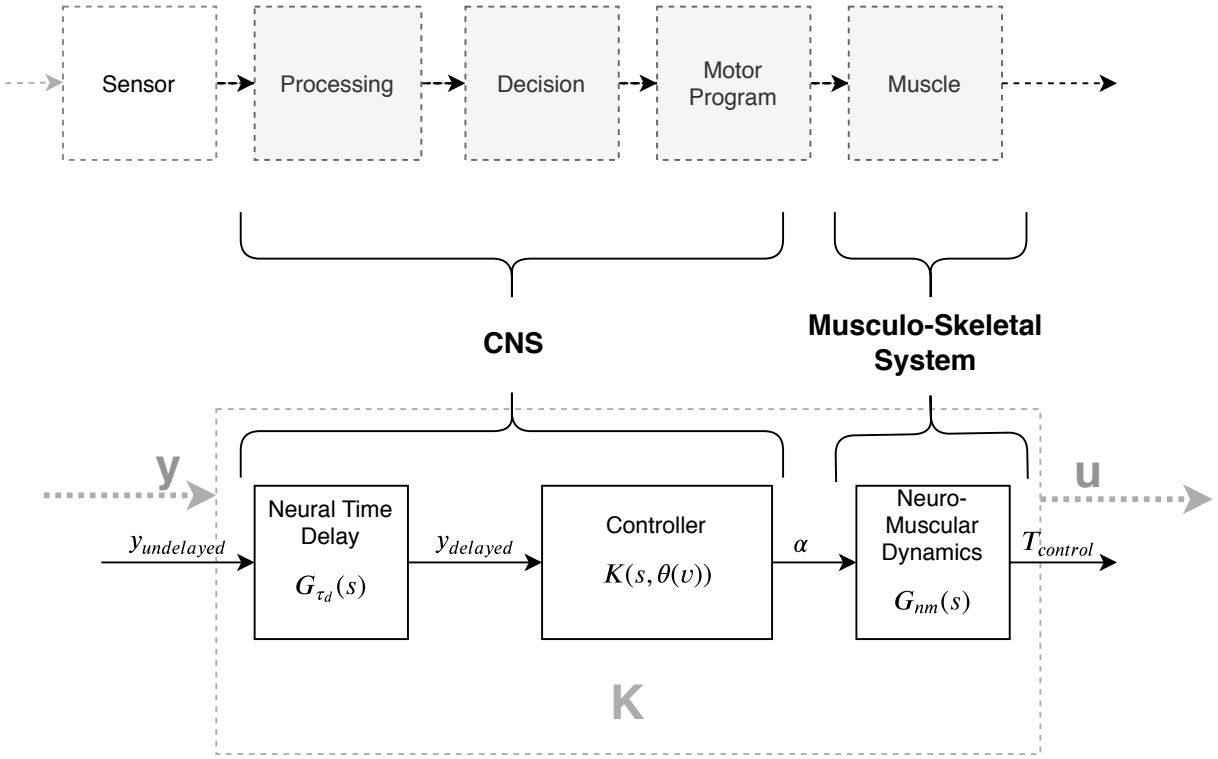

Figure 2.6: A block scheme representing the human controller. The general analog of the process is given by the top block scheme, the bottom block scheme represents the modelling used in [31]. The input to the system, $y_{undelayed}$, contains undelayed information on the states of the roll and steer angle, $y = [\phi, \delta]^T$. The delayed information on the states, $y_{delayed}$, is then delivered to the central nervous system for decision making. The central nervous system is represented by $K(s, \theta)$ and outputs a neural signal, α. The neural signal α then goes through the neuro-muscular dynamics G_{nm}, which in turns output the control torque. The output vector is $u = [T_{\phi,u}, T_{\delta,u}]^T$.

blocks of figure 2.6 and is modelled using the controller $K(s, \theta(v))$ which is based on the feedback gains $\theta(v)$. Full state feedback is assumed, which leads to the roll and steer feedback gains given in equations (2.7) and (2.8), respectively.

$$K_\phi(s, v) = \theta_{\phi p}(v) + \theta_{\phi i}(v)s^{-1} + \theta_{\phi d}(v)s + \theta_{\phi dd}(v)s^2, \tag{2.7}$$
$$K_\delta(s, v) = \theta_{\delta p}(v) + \theta_{\delta i}(v)s^{-1} + \theta_{\delta d}(v)s + \theta_{\delta dd}(v)s^2, \tag{2.8}$$

The feedback gains are θ and their subscripts ϕ and δ denote whether it is a feedback responding to a state belonging to the roll ϕ or steer δ angle, respectively. The remaining subscripts denotes whether the state is the angle's proportional p, integral i, derivative d or double derivative dd state. All control model parameters are a function of forward velocity v, hence the notation $\theta(v)$. The feedback gains of (2.7) and (2.8) are summed up and together they result in a neural signal α. This signal contains responses which a human body cannot exert, therefore it has to be filtered first.

Neuro-Muscular Dynamics G_{nm}

Neuro-muscular dynamics are included to represent the limitations of the human body and are denoted using G_{nm}. The neuro-muscular dynamics are assumed to be time-invariant, they are represented by a second-order filter which filters out the high frequency-components and induces a lag in the response.

This neuro-muscular model is based on the model introduced by Mcruer [18]. The equation for the second order filter is given in (2.9). The input to the neuro-muscular dynamics is the neural signal α which contains the unfiltered control torque response and the filter converts it to the filtered steer torque output. The values for the cross-over frequency ω_c and damping coefficient ζ are $2.17 \cdot 2\pi$ rad/s and $\sqrt{1/2}$, respectively, which are values taken from a study on shoulder dynamics [26].

$$G_{nm}(s) = \frac{\omega_c^2}{s^2 + 2\zeta\omega_c s + \omega_c^2} \quad \Leftrightarrow \quad \begin{bmatrix} \dot{T}_\delta \\ \ddot{T}_\delta \end{bmatrix} = \begin{bmatrix} 0 & 1 \\ -\omega_c^2 & -2\zeta\omega_c \end{bmatrix} \begin{bmatrix} T_\delta \\ \dot{T}_\delta \end{bmatrix} + \begin{bmatrix} 0 \\ \omega_c \end{bmatrix} \alpha, \quad T_{nm} = \begin{bmatrix} 1 & 0 \end{bmatrix} \begin{bmatrix} T_\delta \\ \dot{T}_\delta \end{bmatrix}, \tag{2.9}$$

The process from left to right of figure 2.6 has been explained. The next step is the identification of the unknown parameters.

Human Response Identification through Parameter Estimation

To take count, a gray box rider model has been explained so far. This gray box rider model is combined with the bicycle model to form the closed loop gray box model of figure 2.4. The unknowns of the model are the parameters $\theta(v)$ which dictate the linear state response of the controller. The identification process of these unknowns is explained here, because this process is repeated for the riders used in this thesis.

The unknown control parameters θ can be estimated via optimization. The gray box system is supplied the experimentally measured disturbance w. Then, the optimal set of parameters is sought for which the gray box describes the true steer angle y the most accurately. A more technical explanation is given below.

The unknown feedback parameters are estimated using optimization algorithms. These algorithms minimize an objective function $V(\hat{\theta})$ which is dependent on the error $\epsilon(t, \hat{\theta})$ between the gray box response $\hat{y}(t\|\hat{\theta})$ and measured output signal y. In mathematical terms, this objective function can be defined as,

$$V_N(\hat{\theta}) = \frac{1}{N}\sum_{t=1}^{N} \frac{1}{2}\epsilon(t, \hat{\theta})^2 = \frac{1}{N}\sum_{t=1}^{N} \frac{1}{2}(y(t) - \hat{y}(t|\hat{\theta}))^2, \tag{2.10}$$

where $y(t)$ is the experimentally measured data of the steer angle δ, $\hat{y}(t|\hat{\theta})$ the steer angle response of the gray box model based an estimated parameter set $\hat{\theta}$ and ϵ is the error between the experimental and simulated data. The optimal estimated parameter set can then be defined as,

$$\theta^* = \arg\min_{\theta} V_N(\theta), \tag{2.11}$$

The algorithms used for optimization are a genetic algorithm and a LSQNONLIN solver. To measure how well the model with the optimal estimated parameters describes the true bicycle-rider systems response, the variance-accounted-for (VAF) is used,

$$VAF = 1 - \frac{\sum_{k=1}^{N}(y(t) - \hat{y}(t, \theta^*))^2}{\sum_{k=1}^{N} y(t)^2}, \tag{2.12}$$

where $y(t)$ contains the experimental data and $\hat{y}(t)$ is the estimated output of the model in response to experimental input data $u(t)$. For information on the experimental procedure used to acquire the data for this parameter estimation process, one is referred to the sources [31] & [24].

Feedback Parameter Reduction

With the information given so far, a rider model with known, linear, full state feedback parameters can be derived. However, is the assumption of full state feedback true? Or, if that assumption holds true, are all states of y given in (2.5) used for controlling the bicycle?

To extract the crucial feedback states, a reduction technique is used in [31]. This reduction process is repeated in this thesis for the delayed riders. To perform the reduction, the variance of the parameters near the found optimal parameter set is required. This variance is found on the diagonal of the parameter covariance matrix, which is defined as,

$$\theta_i' = \theta_i / \theta_i^*, \tag{2.13}$$

$$J^T J = \frac{\partial^2 V_N}{\partial \theta'^2}, \tag{2.14}$$

$$cov_{\theta'}^2 = \frac{1}{N} e^T e (J^T J)^{-1}, \tag{2.15}$$

where i is the number of parameters. The parameters are normalized by their optimal parameter θ_i^* (2.13), such that all parameters will have value 1 at the optimum. The diagonal of this matrix contains the variances of the parameter. The height of the variance of a parameter during the optimization search indicates its degree of redundancy for the solution.

The parameter with the highest variance is eliminated and the process is repeated. After every reduction, the VAF is checked. If it drops below 50%, the process is terminated. This reduction will be used for the young and older cyclist to determine which set of critical parameters are required for control and whether this depends on the time delay.

Summary

So far, the bicycle models have been explained as well as the rider model. The identification of the unknown control parameters of the rider using experimental data has been explained, after which a method for identifying the crucial feedback parameters of a cyclist has been given. All models discussed so far are sufficient for answering Part i and Part ii of this thesis. The one question remaining, is whether a steer assist can aid the older rider during cycling. Therefore, the next section will be concerned with explaining the steer assist model.

2.1.4. Steer Assist Controller

The intuitive controller from [29] is a selected candidate from literature to function as a steer assist to enhance the basin of attraction of older cyclists. The model will be added to the human rider model which has just been described in section 2.1.3. In the paper, the steer assist model is called an 'intuitive controller', hence both that name and 'steer assist' refer to the same model.

Mathematical Model

The intuitive controller has the mathematical model given in equation (2.16). The first term uses the roll rate $\dot{\phi}$ to stabilize the weave mode and the second the roll angle ϕ to stabilize the capsize mode. Due to the bicycle's velocity-dependent stability, the steer assist has to be velocity-dependent as well. At v_{max}, the system has the most negative, highest eigenvalue and is likely thought to be most stable.

$$T_{\psi_f} = \begin{cases} -K_v(v_{max} - v)\dot{\phi}, & \text{for } v < v_{max} \\ -K_c(v - v_{max})\phi, & \text{for } v \geq v_{max} \end{cases} \tag{2.16}$$

Eigenvalues

The eigenvalues of the WCBM, with the mechanical parameters from [20] combined with the steer assist as used in [29], are given in the left graph of figure 2.7. As can be seen, $Re(\lambda_{weave})$ is stable over a larger range than compared with the uncontrolled bicycle (see figure 2.2) and $Re(\lambda_{capsize})$ has been stabilized over the whole forward speed range. For velocities below v_d, double frequencies can be expected in the resulting motion. Also, the frequencies seem to be increasing over velocity after v_{max}. Looking at the gains, the roll rate feedback gain stays below -40 Nmsrad^{-1}, which can be assumed to be the maximum allowable feedback gain a motor gain handle. This is of course dependent on the roll rate $\dot{\phi}$ as well, however, the roll rate cannot be bounded by control.

Any further explanation on how the intuitive controller will be used for enhancing the stability of the older cyclist is discussed in section 2.4.

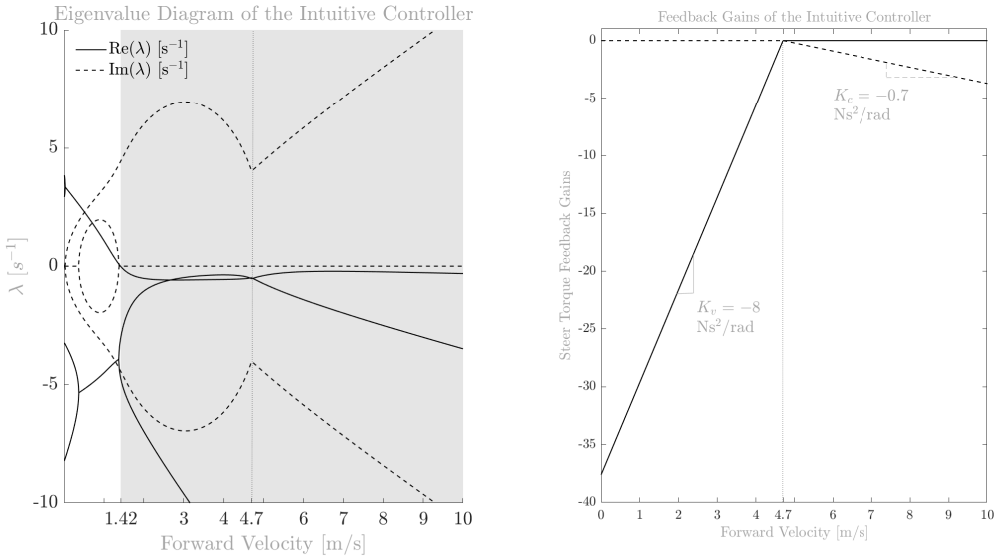

Figure 2.7: Eigenvalues of the combined intuitive controller from [29] and WCBM from [20] (left) and the gains of the controller (right), both over forward velocity. The dotted line contains the imaginary eigenvalues Im(λ) and the black, solid the real eigenvalues Re(λ). The shaded region gives the self-stable region of the bicycle system. On the right figure are the steer torque feedback gains of the intuitive controller given with corresponding slope of the lines in the text boxes. The solid line gives the roll rate feedback gain and the dashed line the roll angle feedback gain.

2.1.5. Summary Part 1 Methodology

Part 1 of the methodology was dedicated to the explanation of the selected models from literature which will form the basis of this thesis. In section 2.1.1, the bicycle model used for the derivation of the EoM has been explained, after which the EoM themselves were explained in section 2.1.2. The gray box rider model and the estimation of its control parameters has been explained in section 2.1.3. These three models are sufficient for Part i and Part ii of this thesis, which was the identification of the BoA of the young and older cyclist. Part iii, the exploration of the enhancement of the BoA of the older cyclist requires the steer assist. The steer assist, or 'intuitive controller', has been explained in section 2.1.4. The total system is visualized in figure 2.8. All the literature models which are used in this thesis have been explained. The next step is answering the question "How can a basin of attraction be identified using the models from literature?". The next section, section 2.2, will elaborate on this.

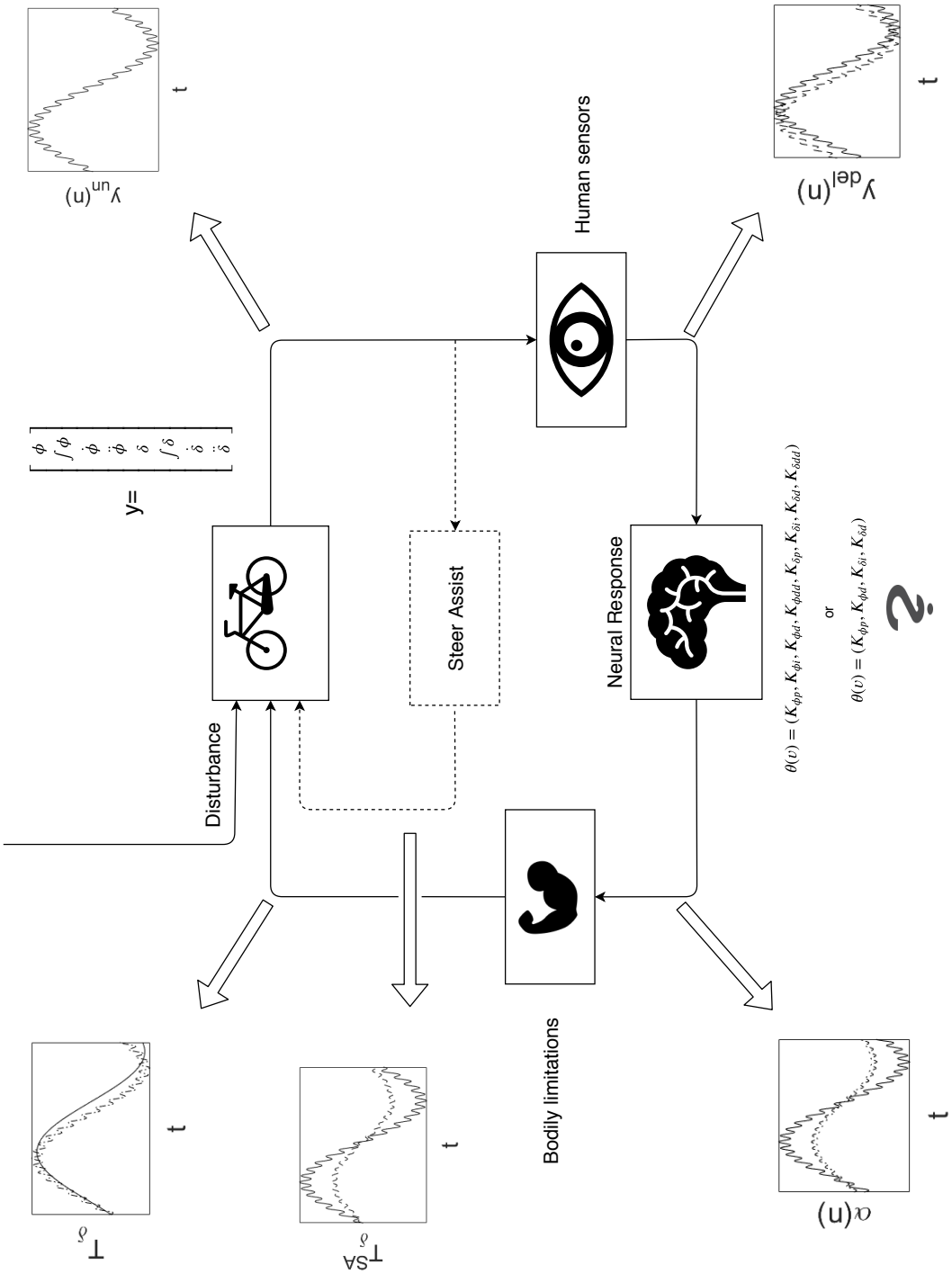

Figure 2.8: Total system of the bicycle-rider system used for the identification of the basin of attraction of neurally delayed riders. Using experimental data, the feedback parameters given above the question mark are identified. The full state feedback is reduced to find the crucial feedback parameters. The neural delay is adapted to represent young and older cyclists. After identifying their basins of attraction, the steer assist is added to the system to explore its potential.

2.2. Laying the General Prerequisites for the Detection of a Basin of Attraction

All three research questions require the detection of the BoA. As stated previously, the BoA is the set of initial disturbances and velocities for which the bicycle-rider system retains stability over time. In the previous section, section 2.1, the models selected from literature have been explained. To connect the parts between the models and the detection of the basin, the following questions need answering:

- How are the rider and bicycle model connected? (Section 2.2.1)
- What initial configurations will be considered? (Section 2.2.2)
- How will the disturbances be modelled? (Section 2.2.3)
- How can solutions of the system be classified as 'stable' and 'unstable'? (Section 2.2.5)
- Which solver will be used for the numerical integration of the equations? (Section 2.2.5)

This section, part 2 of the methodology, is dedicated to answering those questions. Combined, they form the general prerequisites for the detection of a BoA.

2.2.1. Connecting the Models

The connecting between the rider and the model is by the implementation of a steer torque in the nonlinear EoM. The derivation of the equation and the exact implementation of the steer torque is explained in Appendix A.

2.2.2. Initial Configurations

As stated in 2.1.2, five initial conditions need to be supplied to the system such that it can be solved using numerical integration. To recapitulate, these conditions were,

$$q(t_0 = 0) = (\phi_0, \delta_0, \dot{\phi}_0, \dot{\delta}_0, \dot{\beta}_{r,0})$$

which are the roll angle ϕ_0, steer angle δ_0, roll rate $\dot{\phi}_0$, steer rate $\dot{\delta}_0$ and rear wheel rotation rate $\dot{\beta}_{r,0}$. Since the dimension of the BoA is spanned by the initial conditions, its dimension reaches up to five. Discussed in 2.1.2 is that this thesis confines itself to the BoA of stability of *longitudinally steady motion*; the forward velocity is approximately constant. This results in $q(t_0 = 0) = (0, 0, \dot{\phi}_0, \dot{\delta}_0, \dot{\beta}_{r,0})$ and reduces the dimension by two. The rear wheel rotation rate $\dot{\beta}_{r,0}$ determines the first dimension of the BoA since it defines the forward speed. The remaining velocity degrees of freedom are used for the disturbance modelling and, thereby, fill up the remaining two dimensions of the BoA.

City bikes hardly go any faster than 10 ms^{-1}, therefore this will be taken as the maximum velocity. Then, the initial forward velocities will range between 0 and 10 ms^{-1}. Since no clear palpability exists for the initial disturbances, its range will be determined by the maximum perturbation the bicycle-rider system is able to handle. The two remaining, undetermined initial conditions are the lean and steer rate. Those will be used to model the disturbances. How this is done is explained below in section 2.2.3.

2.2.3. Disturbance Modelling

To identify the BoA of a bicycle-rider system, the system needs to have a certain speed and needs to be subjected to a perturbation. However, modelling a disturbance is not as straight-forward. Some background information is given first, thereafter a solution for disturbance modelling is given.

Problem and Solution

Studies on crash analysis reveal the various external causes of single-vehicle accidents, such as bumps in the road, collisions with poles and wind gusts [25]. Studying the effects of external disturbances on

bicycle balance based on experiments, would pose ethical challenges for the larger disturbances.

Theoretically studying the individual disturbance effects on the stability of a bicycle-rider system is unrealistic due to the varying size and nature of the disturbances. However, it is possible to, approximately, map the disturbances onto the velocity degrees of freedom of a theoretical bicycle. This can be done using impact equations [27].

The state of the system is modelled at time t^+ after impact, such that the system is still in the same configuration but did endure a change in velocities. As a result, the disturbance can be modelled using either, or both, the roll $\dot{\phi}$ and lean rate $\dot{\delta}$. Then, the basin of attraction of stability for steady motion can be defined by the initial forward velocity v, roll rate $\dot{\phi}$ and/or steer rate $\dot{\delta}$.

BoA Dimension Reduction

Identifying a three-dimensional BoA three times, one for each thesis part, will be quite time-consuming. Therefore, only one of the initial rates is used for the disturbance modelling.

The steer δ and roll angle ϕ, of a bicycle are coupled by the equations of motion [20]. Therefore, a disturbance of one angle will induce a change in the other and vice versa. The primary control method employed by a cyclist is via steering [32]. Therefore, direct interaction between disturbances and control can only be observed if the disturbances are applied onto the steer angle. For this reason, the disturbances will be modelled as initial steer rates.

The BoA will consist of the sets of initial steer rates $\dot{\delta_0}$ and forward velocities for which the bicycle-rider system retains stability over time. The disadvantage of this modelling method is the loss of palpability to the magnitude of the perturbations; what does an angular steering perturbation of 3 rad/s feel like?

So far the dimension and nature of the basin of attraction has been determined, which indicates that the initial conditions for the system have been chosen. Then, if the system is simulated for a set of initial conditions, how does one determine if the solution belongs to the sought BoA? This is determined using stabiliy criteria which are explained next in section 2.2.4.

2.2.4. Stability Criteria

As stated in section 2.1, the nonlinear, analytical EoM of a bicycle are complex. For this reason, numerical integration is used instead of solving the equations algebraically. It is not feasible to observe the solution of every initial condition set by eye until the bicycle falls over. Therefore, stopping criteria need to be defined which stop the numerical integration automatically as soon as the bicycle has lost stability. The criteria are defined as thresholds on the steer angle δ, the roll angle ϕ and the simulation time t.

Roll Angle Threshold

If the roll angle exceeds 90 degrees, the simulation is terminated and the solution is flagged as unstable. For a 90 degree roll angle, the rider would lie on its side on the ground and has have fallen over. This is, of course, an extreme example and it is very likely that this threshold can be set much lower. However, setting it to the maximum physical angle allows the observation of extreme cases for which stability was retained as well as the change in the maximum occurring roll angles between the riders.

Steer Angle Threshold

For a 90 degrees steer angle, if the cyclist has not fallen over yet, the intended direction would be completely lost. This is deemed as dangerous, since this might result in a collision with other road users or with a sidewalk. Therefore, a 90 degrees steer angle is also classified as 'unstable'.

Simulation Time Limit

The maximum simulation time t_{sim} is chosen based on the view that it should not influence the classification of stability. One might argue that e.g. 4 seconds might be enough time to intervene if the motion is unstable, but there is no substantiation for selecting an exact limitation on the time.

However, long simulation times yield long computation times. Therefore, 15 seconds was tried first but this took too long. Preliminary simulations yielded a sharp transition for the t_{ttf} at the border of the BoA, where t_{ttf} <1 second. Therefore, t_{sim} was set to 3 seconds. This seemed too short for the older cyclist, therefore the t_{sim} was doubled to 6 seconds.

Marginally Unstable Motions

Due to the set criteria, some marginally unstable motions are flagged as 'stable'. These are motions which go on for more than t_{sim} seconds without the system breaching the angular threshold criteria. Often these motions are oscillatory motions when dealing with controlled bicycles, characterized by the pivoting motion of the front assembly around the steering axis. A majority of those motions for the uncontrolled bicycle are capsizing motions, characterized by the slowly increasing lean angle and the spiralling, global trajectory that results from it.

The latter mentioned motion is deemed harmless, due to the short and slow trajectory through state space over time. The first motion is an unwanted motion. However, from the t_{ttf} the initial conditions corresponding to those motions can often be identified by eye, since the transgression of a stable set of initial conditions to an unstable one will not yield a sharp transition for marginally unstable motions. If a large BoA outline with this slow transition of t_{ttf} is observed, a choice can be made to redo the simulation with an adjusted t_{sim} such that those motions are flagged correctly.

Damping Coefficient Extraction

The stability classification is rather binary, you either fall or you don't. Whereas, stability in terms of eigenvalues contains a lot more information. To be able to extract more information, it has been tried to fit a harmonic function to the roll rate solutions such that the damping coefficient could be determined. No accurate results could be found, more information is given in appendix C.

2.2.5. Numerical Integration method

To select a method for the numerical integration of the system, a convergence study has been performed. The full convergence study can be viewed in appendix D. As a result, the ODE15s solver of MATLAB has been selected with an absolute and relative tolerance of 10^{-8}.

2.3. Altering the Rider Model to Include Neural Time Delay

So far, it is possible to integrate a bicycle-rider system and identify a basin of attraction for a rider with zero time delay. However, to answer Part i and Part ii of this thesis, two rider models with nonzero time delays are required. One which represents the young cyclist and one which represents the older cyclist.

This section, the third part of the methodology, answers the following questions:

- How are the numerical issues of [31] circumvented? (section 2.3.1)
- How will the young and older cyclist be modelled? (section 2.3.2)
- Which rider identification steps need to be repeated? (section 2.3.3)

The last question might not seem as an intuitive question. To study the effect of time delay on stability, why not just add it to control strategy as identified in [31]? This is further explained in appendix section J.6.

2.3.1. Solving the Numerical Issues

As it is now, the rider model has 0 ms neural time delay. In [31] they experienced numerical issues for the nonzero neural time delay due to their classical control approach. A transfer function was used to convert disturbance input to bicycle output, which had the following form,

$$y(\theta) = G(\theta)w, \tag{2.17}$$

$$G(\theta) = \left[P_{yw} + P_{yu}(I - K(\theta)P_{yu})^{-1}K(\theta)P_{yw}\right], \tag{2.18}$$

The drawback of converting the model to this form lies within the term $(I - K(\theta)P_{yu})^{-1}$. As a reminder, the controller is modelled as,

$$K(s) = G_{nm}G_{\tau_d}\left[K_\phi K_\delta\right], \tag{2.19}$$

where $G_{\tau d} = e^{-\tau_d d}$ which will have an inverted form in $G(\theta)$ resulting in a term which describes anti-causal behaviour.

This problem is circumvented using build-in MATLAB command which creates a coded simulink environment which is able to keep memory and, thereby, is able to properly implement the time delay without any numerical issues.

Implementation Validation

The implementation could be validated w.r.t (2.19) using the frequency response of both implementations. An arbritrary dataset and a time delay of 30 ms were selected and then the frequency response was extracted using the nyquist command in MATLAB. The real parts of the frequency response of both modelling approaches were compared using the MSE. The MSE was of order -27, whereas the smallest value of the real parts was of order -3 for a sampling frequency of 0.005. Thereby, the alternative implementation is assumed to be valid.

2.3.2. How will the young and older cyclist be modelled?

For Part i and Part ii of this thesis, the BoA of a young and older cyclist will be identified. Then, how are those young and older cyclist modelled? This is done using different time delay values. However, that does not answer all the modelling questions. E.g. is the older cyclist modelled by adding an additional time delay to the young cyclist or does the control between the two differ? First off, time delay values need to be selected.

Effective Neural Time Delay Values

A human cannot immediately respond to external stimuli, a neuro-muscular time delay is present if muscular action is required. This delay is dependent on a lot of factors such as proximity, limb mass, age etc. D.H. Weir studied the delay for motorcycle handling and found a 0.1 s delay for steering torque and 0.3 s for upper body lean [34]. Doyle found a delay between the manipulated variable and response to be in the range of 60 and 150 ms [7][22]. De Vlugt *et al.* found a mean neural time delay of 30 msec [4] and Schouten *et al.* [26] of 28.4 ms for the shoulder dynamics upon performing an experiment to identify intrinsic and reflexive properties of the shoulder. The average age of the group of Vlugt *et al.* was 26.8 years and for Schouten *et al.* 25.8 years. Neural time delays refer to the delay of the afferent signal and do not include lag due to neuro-muscular dynamics, hence the lower values compared to Weir and Doyle.

The mean neural time delay of 30 ms foud by De Vlugt *et al.* [4] has been adopted to represent the young cyclists which are of an average age of 26.8 years. To find the influence of time delay on the basin of attraction of a bicycle-rider system, this value is doubled. Therefore, the rider with 60 msec time delay is called the 'older cyclist'.

Control Strategy of the Old Cyclist

The time delay values have been selected for evaluation. To study the pure effect of time delay, the control strategy of the young cyclist will be maintained and an additional 30 ms will be added. The BoA of this cyclist will be identified again. A decline in BoA would indicate the detrimental effect of time delay on stability. However, what if the cyclist can adapt its control strategy? To be able to let the old cyclist adapt its control strategy, the experimental data of the young cyclist is used. Suffering from 60 ms neural time delay, the old cyclist is allowed to compensate its strategy such that the same response to the experimental data is given as was done by the young cyclist. Therefore, the rider has to be identified again. Then, its basin of attraction is identified and compared to the young cyclist.

2.3.3. Rider Identification Process

The estimated feedback parameters of [31] compensate for the lack of a nonzero neural time delay. Therefore, implementing nonzero time delay and retaining the feedback parameters would, in a sense, lead to double integration of time delay in the model. Also, the experimental validity would be lost since the model's perturbation response would no longer describe the experimental data. And above all, it is not known whether the same reduced parameters set would be found as in [31]. For the reasons above, the rider identification process needs to be repeated..

For the purpose of comparison, the evaluation of the stability of the cyclist with zero time delay has been done in appendix J.

Parameter Reduction and Estimation

The rider identification process is repeated. Six out of fifteen data sets are selected for which the parameter reduction process is performed such that the most reduced parameter set can be selected for which the experimental data is still described accurately (VAF>90%). This process is not done for all fifteen data sets due to its time consuming nature. An example of an arbitrary result of this process is illustrated by (2.20). From the full parameter set, a smaller set is selected to be used on the fifteen data sets.

$$\begin{aligned} \theta &= [K_{\phi p}, K_{\phi i}, K_{\phi d}, K_{\phi dd}, K_{\delta p}, K_{\delta i}, K_{\delta d}, K]^T, \\ \theta_{reduced} &= [K_{\phi i}, K_{\phi d}, K_{\phi dd}, K_{\delta i}, K_{\delta d}]^T, \end{aligned} \tag{2.20}$$

After that, the reduced parameter set will be estimated for all fifteen data sets. Per experimental velocity group, three data sets are available. Thus, after the estimation process, the rider's control has been identified for five velocities. These estimated parameter values can then be used to define the rider's control as a continuous function over forward velocity..

Feedback Continualization

The feedback gains are estimated only for the experimental velocities, which are 2.1, 3.2, 4.3, 6.1, and 7.3 ms^{-1}. For the detection of the BoA of the cyclist, simulation is preferred for a higher velocity resolution. Therefore, the feedback gain will be made continuous. Since three sets of parameters are estimated per velocity, a choice has to be made on how to make the parameters velocity dependent.

Since the bicycle's dynamics change with velocity, it is likely that the rider's control changes over velocity as well and especially during a change of modes of the uncontrolled bicycle. However, since knowledge lacks concerning the rider's exact control strategy, assumptions have to be made.

It is likely that a rider won't abruptly change strategy for increasing or decreasing forward velocity. In his dissertation, Moore predicted based on theory and concluded based on experiments, that the control gains could reasonably be represented by a function with linear dependence on velocity for velocities above 2 ms^{-1}[21]. Therefore, a linear regression of the parameter sets $f_{\theta_{LR}}(v)$ will be used to see if this prediction holds. To prevent a big misfit with the truth, two linear interpolated functions will

be used as well. One which goes through the parameter sets which had the highest VAF per velocity $f_{\theta_{LI,HV}}(v)$ and another that goes through the mean parameter sets per velocity $f_{\theta_{LI,mean}}(v)$.

If $f_{\theta_{LI,mean}}(v)$ and $f_{\theta_{LI,HV}}(v)$ yield similar results, then the fifteen data sets all yield similar solutions per velocity group and it will indicate that the BoA is not as sensitive to small variations in the control parameters. The quality of the fit will be measured using the coefficient of determination R^2, which is defined as follows,

$$R^2 = 1 - \frac{\sum_i (K_i - \overline{K})^2}{\sum_i (f_i - \overline{K})^2}, \tag{2.21}$$

where the discrete data is represented by K_i, the function fitted through the data by f_i and the mean of the discrete data by $\overline{K}$. The coefficient measures the proportion of variance of the discrete, estimated feedback parameter predicted by the functions fitted through them. A value of 1 indicates a good fit and 0 indicates a baseline fit which predicts $\overline{K}$. Negative values indicate a bad fit.

The root mean square error (RMSE) between the three basins will indicate the similarity between the derived BoA's based on the three functions. The RMSE is calculated as follows:

$$RMSE = \sqrt{\sum_{i=1}^{n} (y_i - z_i)^2}, \tag{2.22}$$

where y_i contains the value of $T_{\delta,max}(v)$ at integration point i of the BoA based on one controller and z_i of another controllers. The maximum allowable perturbation $T_{\delta,max}(v)$ is the equivalent of the BoA height. A RMSE of 0 indicates that the BoA's of two controllers match exactly.

2.3.4. Rider Modifications Summary

To recapitulate:

- The modelling of the neural time delay is altered such that the problem, with the numerical issues for nonzero time delay, is circumvented.
- A rider with 30 ms neural time delay will be evaluated as the young cyclist and the older cyclist is modelled with 60 ms neural time delay.
- Two old cyclist rider models will be used. One whom retained the young cyclist's control strategy (naive, old cyclist) and one whom can adapt its control to its time delay (smart, old cyclist).
- To retain experimental validation and to prevent an indirect double implementation of the time delay, the parameter reduction process identical to the one in [31] is repeated for both the young and older cyclist for six data sets.
- Based on the selected, reduced parameter sets, the parameter are estimated for all fifteen data sets.
- The gains are made continuous over forward velocity for the identification of a higher resolution BoA

These are the main steps taken such that the models can be used to answer Part i and part Part ii of this thesis. Section 2.4 elaborates on analyzing the steer assist to answer Part iii of this thesis.

2.4. Analyzing the Steer Assist

To analyze the potential of enhancing the BoA of the older cyclist using a steer assist (SA), the objective of Part iii, the model of [29] is used. This section contains part 4, the last part, of the methodology which concerns itself with the analysis and development of a steer assist based on the controller from [29].

2.4.1. Validity of the Answer

The research question on whether the elderly cyclist's stability can be enhanced using a steer assist can only be answered up to a certain degree, because no interaction between the rider and SA is taken into account.

The potential of the SA, based on the control law of the intuitive controller from [29], is investigated by adding the control from the steer assist to the control exerted by the older cyclist. Thereby, it is implicitly assumed that the old cyclist retains its general control strategy while being aided by the steer assist. Then, if the basin of attraction of the combined controller is enlarged with respect to the basin of attraction of the older cyclist, it would indicate the potential of the steer assist.

It would mean for the cyclist that no control adaption is required, hence it should be fairly easy to cycle straight, under the influence of perturbations, with the steer assist. The results will be very preliminary, since no trajectory tracking is considered nor interaction between cyclist and steer assist. However, a positive result would support future research. However, prior to this preliminary assessment, the ideal control law has to be developed first.

2.4.2. General Approach

The stabilization performance of the SA, based on the intuitive controller from [29], is analyzed without a human rider. The control law will be adapted until an ideal control law has been developed. Before starting this approach, one main question needs answering: What is considered optimal control for the SA? To bound this question, design criteria are set.

2.4.3. Design Criteria

This section presents the design criteria for the steer assist control law.

Maximum Motor Control

As stated in section 2.1.4, the maximum roll rate feedback of the intuitive controller in [29] is 40 Nmsrad^{-1}. Therefore, this is assumed to be the upper bound of what a physical actuator would be able to handle.

Constant Basin Height

To make sure that the rider can easily adapt to a SA, the rider should be aware of the stabilization capabilities of the SA. This will be the easiest when the SA behaves constant over velocity. Therefore, a SA which has a constant basin height is sought. This means that the SA would be able to reject the same degree of perturbations for every forward velocity.

Low Speed Control

It is known, that for decreasing velocity the uncontrolled bicycle gets significant worse in dampening out oscillations (see positive real eigenvalues in figure 2.2) and, therefore, gets increasingly harder to control. Loss of control at low speeds is one of the factors identified at the cause of falls, which might also be the cause behind the high numbers of falls of the elderly during mounting and dismounting their bicycle [25]. Therefore, bicycle stabilization for low speeds is important as well. Hence, the weave velocity v_w will be evaluated for every control law design.

Weave Stabilization

The roll angle feedback K_v is selected to tilt the capsize eigenvalue into the left-half complex plane such that the capsize mode is stabilized. The capsize instability is easily stabilized by a human and for the bicycle used here, the capsize velocity lies above the maximum velocity of 10 ms^{-1} considered. Hence, the capsize mode does not need stabilizing, therefore, only the feedback on the roll rate is retained. Thus, our only focus lies on,

$$K_\phi(s,v) = \begin{cases} K_v(v_{max} - v)s, & \text{for } v < v_{max} \\ 0, & \text{for } v \geq v_{max} \end{cases} \tag{2.23}$$

for which v_{max} and K_v needs to be optimized such that the stability of the bicycle-rider system is raised, yet without exerting too much control.

3

Results

This chapter discusses the results obtained following the methodology of chapter 2. In this chapter, the three main parts of this thesis are answered, therefore the outline is as follows:

- Part i Which set of disturbances can a young cyclist recover from? (Section 3.1)
- Part ii which set of disturbances can an older cyclist recover from?(Section 3.2)
- Part iii Can the basin of attraction of an older cyclist be enlarged using a steer assist? (Section 3.4)

Before starting on the answer to Part i, it might be useful to get acquainted with some common notations and abbreviations used in this chapter.

Notations & Abbreviations

The cyclist is represented by a controller $K(s, \theta)$, which responds linearly to the delayed states using the parameter set $\hat{\theta}$, for which the diacritic is dropped in the remainder of this thesis. The full parameter set θ contains the following feedback gains

$$\theta = [K_{\phi p}, K_{\phi i}, K_{\phi d}, K_{\phi dd}, K_{\delta p}, K_{\delta i}, K_{\delta d}, K_{\delta dd}]^T, \tag{3.1}$$

for which the subscript denotes the lean ϕ or steer δ angle and its derivative or integral state the feedback parameter belongs to. The feedback gains are the summation of the feedback parameters multiplied by their corresponding state as given in section 2.1.3, eqs. (2.7) and (2.8). The states are delayed by the neural time delay τ_d and the linear response is filtered by the neuro-muscular dynamics G_{nm}. The accuracy by which the gray box model describes the data is the VAF; Variance-Accounted-For. The data sets have their unique id numbers and three unique data sets were acquired per velocity group. A velocity group refers to a set of velocities lying close to one another.

3.1. Part i. Which set of disturbances can a young cyclist recover from?

This section answers the first research question of this thesis belonging to Part i. A more technical synonym of this question is:

> What is the basin of attraction of a bicycle-rider system which suffers from a 30 ms single, effective neural time delay?

As a reminder, answering this question is necessary to evaluate the influence of neural time delay on the stability of cyclists.

Part i. Outline

The substantiation behind the chosen value of 30 ms was given in section 2.3.2. To answer this question, several subquestions need answering. These questions also form the structure of this section:

- How can the control of the young cyclist be modelled? (Section 3.1.1)
  - Which feedback gains are crucial for the young cyclist and what are their values?
  - What are the velocity-dependent feedback parameter functions based on those values?
  - What do those functions and values tell us about the control of the young cyclist?
- What are the basins of attraction of the controller with those functions? (Section 3.1.2)
  - How do the basins between the three functions compare?

The first three questions are necessary for the identification of the control strategy employed by the young cyclist. The process is rather tedious and is clouded by numbers in tables which do not particularly speak to the imagination. Therefore, only a brief summary of the most crucial results concerning the young rider's control strategy will be given below and one is referred to appendix F for a more elaborate explanation on the results of this process.

3.1.1. Part i. Young Cyclist Control Strategy

In this section, the crucial feedback gains for the young cyclist are sought. Those feedback gains are found using the parameter reduction process explained in section 2.1.3. To recapitulate, the full state feedback parameter set consisted of,

$$\theta(s) = [K_{\phi p}, K_{\phi pi}, K_{\phi d}, K_{\phi dd}, K_{\delta p}, K_{\delta i}, K_{\delta d}, K_{\delta dd}]^T. \tag{3.2}$$

For the young cyclist, this set could be reduced to,

$$\theta(s) = [K_{\phi p}, K_{\phi d}, K_{\delta i}, K_{\delta d}, K_{\delta dd}]^T, \tag{3.3}$$

while retaining a VAF>90%. For these five gains, only for data set 256, the VAF dropped to 88.66% which is still deemed sufficient. Data sets 248 and 249 could be described with 3 and 2 gains, respectively, for VAF>90%. The remaining three data sets suffered a drop in VAF of nearly 10% and more when reducing any further than the set given by (F.1). Therefore, this set of five is chosen to describe the control of the young cyclist. More information on the reduction and estimation process is given in appendix F.

The five feedback parameters are estimated for all fifteen data sets. At this point, the control of the young cyclist has been identified for five discrete velocities based on fifteen data sets. The next step is making the dependence of the control continuous over forward velocity.

Continuous Control over Velocity

To identify the BoA of the young cyclist, a control strategy is required which also covers the velocities in between. As explained in section 2.3, the discrete, estimated feedback parameters $\theta(v)$ are made continuous over velocity by a linear regression $f_{\theta_{LR}}(v)$ and two methods for linear interpolation, $f_{\theta_{LI}}(V)$. The result of the process is given by figure 3.1. The equations of the linear regression and the coefficients of determination of the functions with respect to the discrete, estimated parameters are given in appendix F. The coefficients confirm the intuitive, the linear regression provides the worst fit ($\overline{R^2}$=0.38) and the linear interpolation of the mean values the best ($\overline{R^2}$=0.70).

Control Interpretation

The feedback states the rider responds to are the same as identified in [31], except for an additional steer acceleration state $K_{\delta dd}$. The acceleration state makes sense, since acceleration does functions as a lead and is able to compensate for the time delay. The remaining states are of similar sign and order as identified in [31] and, thereby, also abide the principle of steer-into-the-fall.

3.1.2. Part i. Basin of Attraction Identification

To answer the question of Part i, the rider model is combined with the nonlinear bicycle model and the initial value problem is solved for a set of finite lateral disturbances as defined in section 2.2.3. This process is repeated for the controller with τ_d=30 ms for each feedback parameter function $f_\theta(v)$. The result of the simulations are given in figure 3.2. The feedback parameters are interpolated and extrapolated beyond 2.1 and 7.4 ms^{-1}, hence beyond 2 and 7.5 ms^{-1} the BoA is discarded.

Basin of Attraction Analysis of the Young Cyclist

As can be seen in figure 3.2, all three functions yield roughly the same BoA for the young cyclist. To quantify the resulting BoA's of controllers $K(s, f_{\theta_{LR}}(v))$, $K(s, f_{\theta_{LI,HV}}(v))$ and $K(s, f_{\theta_{LI,mean}}(v))$ and to be able to, quantitatively, compare them with the BoA's of the older cyclist, the surface areas and the average heights of the BoA's are used. To quantify the similarity between the BoA's of the controllers based on the feedback functions $f_\theta(v)$, the root mean square error (RMSE) is used. The results are given in table 3.1.

The metrics support the visual observation concerning the similarity of the BoA's of all three controllers; the surface areas and average heights of the basins of the controllers deviate at most 1.63% and 1.52% from the mean values 50.62 radms^{-2} and 9.21 rads^{-1}, respectively. However, the overall trend of the BoA outline is most similar between $K(s, f_{\theta_{LI,mean}}(v))$ and $K(s, f_{\theta_{LI,HV}}(v))$ (RMSE=0.60) and less similar between controllers $K(s, f_{\theta_{LI}}(v))$ and $K(s, f_{\theta_{LR}}(v))$ (RMSE>1). This was also partially reflected in the R^2 of the parameter functions, for which $K(s, f_{\theta_{LR}}(v))$ had an average R^2 of 0.38, compared to 0.59 and 0.77 for the linear interpolations.

	Young cyclist		
RMSE	$K(s, f_{\theta_{LR}}(v))$	$K(s, f_{\theta_{LI,mean}}(v))$	$K(s, f_{\theta_{LI,HV}}(v))$
$K(s, f_{\theta_{LR}}(v))$	-	1.10	1.15
$K(s, f_{\theta_{LI,mean}}(v))$	1.10	-	0.60
$K(s, f_{\theta_{LI,HV}}(v))$	1.15	0.60	-

Surface Area [radms^{-2}]	**Average Height** [rads^{-1}]
51.39	9.32
50.68	9.24
49.80	9.07

Table 3.1: Root-mean square error (RMSE) between the basin of attraction height of the three bicycle-rider systems (left table) and the surface area and average basin height per bicycle-rider system (right table). The bicycle-rider system consists of the nonlinear equations of motion of Basu-Mandal [2] and a rider model $K(a, f_\theta(v))$ with neuro-muscular dynamics G_{nm} and single, effective neural time delay τ_d of 30 ms. The function $f_\theta(v)$ is based on the estimated parameter sets $\theta(v)$ where LR refers to linear regression, $LI, mean$ to a linear interpolation between the mean parameter sets and LI, HV to a linear interpolation between the parameter sets with the highest variance accounted for.

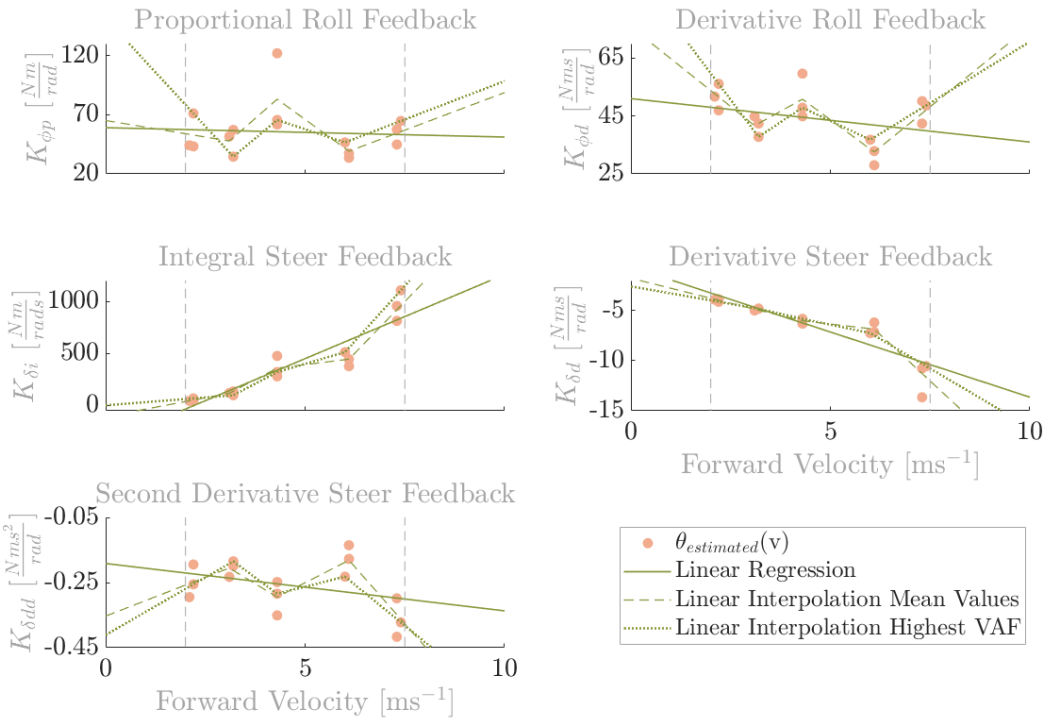

Figure 3.1: The discrete, estimated five state parameters $\theta(v) = (K_{\phi p}, K_{\phi d}, K_{\delta i}, K_{\delta d}, K_{\delta dd})$ and their continualizations, resulting from gray box identification of controller $K(s, \theta)$ with neuro-muscular dynamics G_{nm} and neural time delay τ_d=30 ms. The discrete estimated parameters are the filled circles. The solid line is a linear regression, the dashed line a linear interpolation between the mean values of the estimated parameters per velocity group and the dotted line a linear interpolation between the parameter sets with the highest VAF per velocity. A velocity group consists of three parameter sets for close velocities. The top-left figure contains the data concerning the proportional roll parameter, $K_{\phi p}$. The top-right figure contains the data concerning the derivative roll parameter, $K_{\phi p}$, the mid-left figure concerning the integral steer parameter, $K_{\phi p}$, the mid-right figure concerning the derivative steer and the bottom figured displays the second derivative steer parameter fits. All corresponding coefficients of determination are given in table F.1. In this study, only values in between the velocities of the two vertical lines are considered.

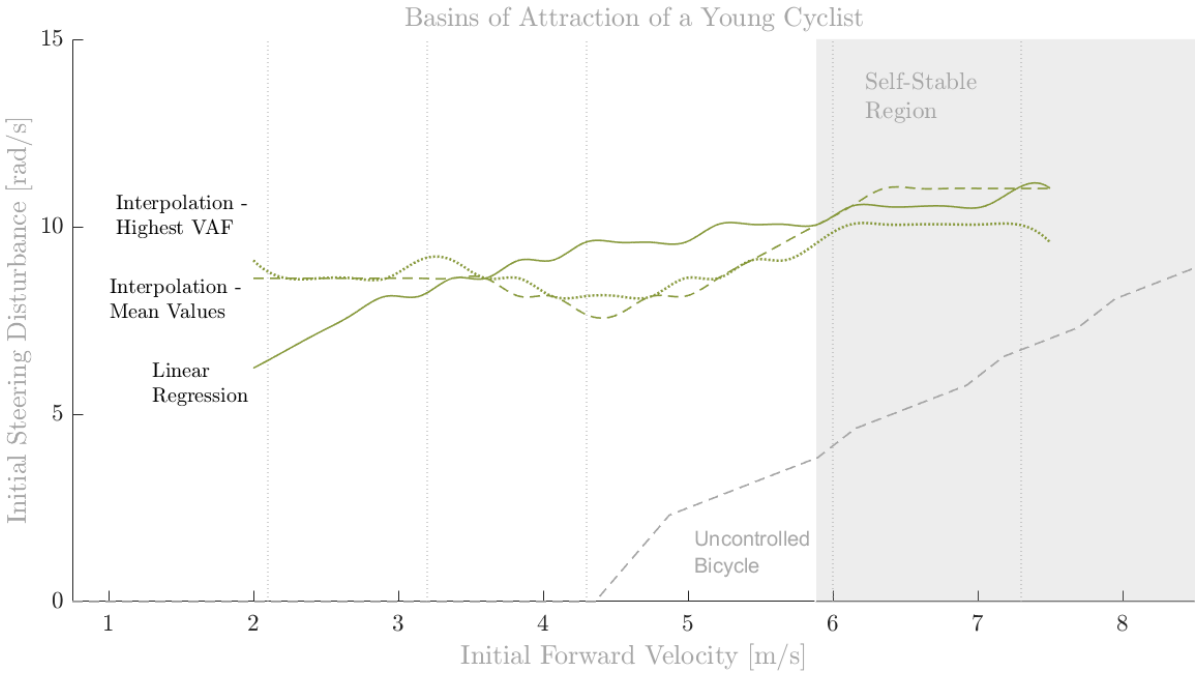

Figure 3.2: Basin of attraction outlines of bicycle-rider system consisting of the WCBM combined with a rider, based on the gray box model consisting of controller K($s, f_\theta(v)$), second-order neuro-muscular dynamics G_{nm} and an effective neural time delay, τd, of 30 ms. The function $f_\theta(v)$ is based on discrete estimated parameter sets $\theta(v)$. Parameter sets $\theta(v)$ are based on neural time delay τ_d and velocity v. The shaded region is the self-stable region of the uncontrolled bicycle and ranges from 5.88 to 10.13 ms^{-1}. The dashed, vertical lines are the velocities at which the experimental data was acquired and the parameter sets were estimated. These velocities are approximately 2.1, 3.2, 4.3, 6.0 and 7.3 ms^{-1}. The solid line represents the control model for which the parameter sets, θ, were made continuous over velocity using a linear regression. The parameters of the controller corresponding to the dashed line, were linearly interpolated mean parameters. For the dotted line, the parameters were linearly interpolated between the parameter containing the highest VAF.

3.2. Part ii. Which set of disturbances can an older cyclist recover from?

This section answers the first research question of this thesis belonging to Part ii. A more technical synonym of this question is:

> What is the basin of attraction of a bicycle-rider system which suffers from a 60 ms single, effective neural time delay?

In the previous section, section 3.1, the basin of attraction of a young cyclist has been identified. Then, what would be the influence of time delay on this basin if an additional 30 ms is added? Section 3.2.2 reveals the results. However, who says that an older cyclist is not able to adapt its control response to its slowed motor responses?

In this section, the control of an old cyclist who does adapt its control strategy will be identified. This will be done based on the experimental data of the young cyclist and an additional 30ms time delay will be added to the gray-box model before the control is identified again. The cyclist who does adapt its control will be referred to a the 'smart', old cyclist. The old cyclist who does not adapt its control will be referred to as the 'naive', old cyclist.

Do note that neither of the old rider models represent an actual elderly cyclist. It represents a cyclist with increasing time delay, such that the influence of neural time delay on cycling stability can be observed.

Part ii. Outline

The substantiation behind the chosen value of 60 ms was given in 2.3.2. To answer this question, several subquestions need answering. These questions also form the structure of this section:

- How can the control of the smart, old cyclist be modelled? (Section 3.2.1)
  - Which feedback gains are crucial for the smart, old cyclist and what are their values?
  - What are the velocity-dependent feedback parameter functions based on those values?
  - What do those functions and values tell us about the control of the smart, older cyclist?
- What are the basins of attraction of the controller with those functions? (Section 3.2.2)
  - What is the direct influence of time delay on lateral stability in cycling?
  - How do the basins between the three velocity-dependent control functions of the smart, old cyclist compare?
  - What is the indirect influence of time delay on lateral stability in cycling?

3.2.1. Part ii. Crucial Feedback Gains

In this section, the crucial feedback gains for the smart, old cyclist are sought. Those feedback gains are found using the parameter reduction process explained in section 2.1.3. To recapitulate once more, the full state feedback parameter set consisted of,

$$\theta(s) = [K_{\phi p}, K_{\phi pi}, K_{\phi d}, K_{\phi dd}, K_{\delta p}, K_{\delta i}, K_{\delta d}, K_{\delta dd}]^T. \tag{3.4}$$

For the older cyclist, this set could be reduced to,

$$\theta(s) = [K_{\phi p}, K_{\phi d}, K_{\phi dd}, K_{\delta p}, K_{\delta i}, K_{\delta d}, K_{\delta dd}]^T, \tag{3.5}$$

while retaining a VAF>90%. In general, the data sets could be described using more reduced parameter sets compared to the reduced set of (3.5). However, not the same reduced sets were found for all six data sets. Appendix H did study the BoA's of the smart, older rider when a six-state feedback

set was handpicked, to see if it would yield significantly different results compared to using seven-state feedback for describing the cyclist's control.

The result was a significant difference between both $K(s, f_{\theta_{HV}})$ (RMSE=0.95) which resulted in a BoA decline of approximately 21%, but only a minor difference between both $K(s, f_{\theta_{mean}})$ (RMSE=0.42) which resulted in a BoA decline of only 1.45%. This led to more questions concerning the correlation between the BoA, number and nature of feedback states and the metric VAF. Appendix I contains a study on the sensitivity of the BoA to the feedback state dimension and on the measure VAF, which also influences the correlation. For the young cyclist, quite a spread was found between difference parameter sets of the same data set which all yielded VAF>90%. For the older cyclist, this spread was smaller.

The selection of the seven feedback gains given in (3.5) has been made, instead of all eight, since $K_{\phi i}$ does not have a logical, physical interpretation and it was the only feedback parameter which was not crucial for all of the data sets. Therefore, this feedback state could be eliminated. Also, six state feedback was not chosen regardless of the high VAFs since the substantiation for eliminating $K_{\phi p}$ lacks.

For this reduced set, the seven feedback parameters are estimated for all fifteen data sets. After the estimation, the control of the smart, older cyclist has been identified for five discrete velocities. The next step is to make control parameters continuous over forward velocity.

Continuous Control over Velocity

As explained in section 2.3, and as has been done for the young cyclist, the discrete, estimated feedback parameters $\theta(v)$ are made continuous over velocity by a linear regression $f_{\theta_{LR}}(v)$ and two methods for linear interpolation, $f_{\theta_{LI}}(v)$. The result is given by figure 3.3. The equations of the linear regression and the coefficients of determination of the functions are given in appendix G.

Control Interpretation

The control interpretation of the estimated seven state feedback parameters is given in appendix G.

3.2.2. Part ii. Basin of Attraction Identification

The velocity-dependent functions of figure 3.3 are added to the nonlinear bicycle model of Basu-Mandal, along with the remainder of the rider structure, and the system as a whole is numerically integrated. The result, given in figure 3.4 and quantified by the measures given in table 3.2, answers the question of Part ii of this thesis.

Effect of Increasing Delay

Also plotted in figure 3.4 is the basin of attraction of the naive, old cyclist. This would be the result if the cyclist has no awareness of the neural time delay. The BoA shrank by approximately 81% when comparing the average area's of the three controllers for the young and old cyclist. Another interesting observation is that all RMSE's approximately doubled for the increasing time delay (see table 3.2); the stability becomes more sensitive to the control exerted by the rider.

The detrimental effect of neural time delay is clearly visible, since nearly no stable region remains outside the BoA of the uncontrolled bicycle. This seems to indicate that the inherent stability of the bicycle can aid in preventing falls. Just below v_w of the uncontrolled bicycle, the bicycle has a slowly growing motion for which the bicycle falls after 6 seconds. Therefore, this behaviour is classified as stable even though the eigenvalues dictate marginal instability. It seems that this behaviour might aid the older cyclist in stabilizing the bicycle.

Comment on Simulation Time Influence

However, falling after 6 seconds also holds for the old cyclist here. For the young cyclist, a sharp transition of the time-to-fall t_{ttf} was observed outside the border of the BoA. All unstable solutions yielded a t_{ttf}<1 second for an increase of $\Delta T_{\delta,disturbance}$<1 rads^{-1}. Whereas for the old cyclist, its slowed re-

sponses resulted in slowly growing oscillating motions for velocities below 5 ms^{-1}, approximately.

A lower simulation time limit t_{sim} would have rendered these solutions stable and the BoA of the old cyclist would be larger. A longer t_{sim} would result in a decrease of the BoA. It is debatable as to whether oscillating for 6 seconds would result in a fall for elderly cyclists. One might argue that the time is more than sufficient to intervene. Someone else might argue that intervening could lead to a maladroit movement and a fall. Or it can be argue that for such a motion the cyclist may have collided with a sidewalk or another road participant.

Regardless of the outcome, it is not a safe nor stable motion and should therefore be classified as 'unstable'. For higher velocities, the BoA would only marginally change if the time limit for stability would be halved. The BoA would disappear for velocities below approximately 5 ms^{-1}. Therefore, the BoA's of the naive, older cyclist are likely to be slightly smaller than taken into account here.

Unstable Linear Regression Controller

The stability regions of $K(s, f_{\theta_{LI,mean}}(v))$ and $K(s, f_{\theta_{LI,VAF}}(v))$ are very similar for all velocities (RMSE=0.45 $rads^{-1}$). For $K(s, f_{\theta_{LR}}(v))$, the stability region is non-existent for all nonzero perturbations around 4.3 m/s initial forward velocity. This results in large RMSE's of 2.32 and 2.51 $rads^{-1}$ with respect to the BoA's of the other controllers; those values are over 5 times larger compared to the RMSE between $K(s, f_{\theta_{LI,mean}}(v))$ and $K(s, f_{\theta_{LI,VAF}}(v))$.

The R^2 of $f_{\theta_{LR}}(v)$ was low for $K_{\phi dd}$ (R^2=0.019) and $K_{\delta i}$ (R^2=0.097), but the mean trend of the parameters was still predicted well (R^2>0). To analyse the sensitivity of the perturbation response to the variance of the feedback parameters, a sensitivity analysis has been performed in appendix K. This sensitivity analysis studies the perturbation responses for fixed percentage changes of individual feedback parameters.

The result revealed a high sensitivity of the system with respect to the roll acceleration feedback $K_{\phi dd}$, a relatively high sensitivity with respect to the proportional steer feedback $K_{\delta p}$ and a significantly lower sensitivity to the other feedback parameters. At 4.3 ms^{-1}, the linear regression is 17.18% off for $K_{\phi dd}$ and 4.39% off for $K_{\delta p}$, with respect to the mean value. Both deviations are towards the destabilizing side. Therefore, the main reason for the unstable response is the roll acceleration feedback value which is worsened by the deviation of the proportional steer feedback.

Overall, $K(s, f_{\theta_{LR}}(v))$ is excluded from further evaluation due to its stability issues at 4.3 ms^{-1}.

Results Remaining Controllers

Ignoring the basin of $K(s, f_{\theta_{LR}}(v))$, the older cyclist whom adapts its control strategy is able to handle average perturbations of 4.05 $rads^{-1}$ and has a basin size of 22 $radms^{-2}$, both approximately. A very slight overall increase in basin height can be observed for increasing velocity.

Similar as was observed of the older cyclist in section 3.1, the inherent stability of the uncontrolled bicycle seems to aid the controllers in stabilizing the bicycle. For velocities above v_w of the uncontrolled bicycle, all controllers seems to follow the BoA outline of the uncontrolled bicycle. This might be because the uncontrolled bicycle's response is not delayed and thereby aids the cyclist in rejection the perturbations, before the cyclist is able to exert any control. Whether this is true, can only be said if more experimental data is available between the experimental velocities 6.0 and 7.3 ms^{-1}, since it might also just be coincidence due to the identified and interpolated control at and in between those velocities.

	Smart, old cyclist			**Surface Area**	**Average Basin**
RMSE	$K(s, f_{\theta_{LR}}(v))$	$K(s, f_{\theta_{LI,mean}}(v))$	$K(s, f_{\theta_{LI,HV}}(v))$	**[radms^{-2}]**	**Height [rads^{-1}]**
$K(s, f_{\theta_{LR}}(v))$	-	2.32	2.50	13.23	2.51
$K(s, f_{\theta_{LI,mean}}(v))$	2.32	-	0.45	21.41	3.91
$K(s, f_{\theta_{LI,HV}}(v))$	2.50	0.45	-	23.05	4.22

	Naive, old cyclist				
RMSE	$K(s, f_{\theta_{LR}}(v))$	$K(s, f_{\theta_{LI,mean}}(v))$	$K(s, f_{\theta_{LI,HV}}(v))$		
$K(s, f_{\theta_{LR}}(v))$	-	2.62	1.99	8.95	1.70
$K(s, f_{\theta_{LI,mean}}(v))$	2.62	-	1.56	7.38	1.30
$K(s, f_{\theta_{LI,HV}}(v))$	1.99	1.56	-	12.89	2.33

Table 3.2: Root-mean square error (RMSE) between the basin of attraction height of the three bicycle-rider systems (left table) and the surface area and average basin height per bicycle-rider system (right table). The bicycle-rider system consists of the nonlinear equations of motion of Basu-Mandal [2] and a rider model $K(s, f_\theta(v))$ with neuro-muscular dynamics G_{nm} and single, effective neural time delay τ_d of 60ms. The function $f_\theta(v)$ is based on the estimated parameter sets $\theta(v)$ where LR refers to linear regression, $LI, mean$ to a linear interpolation between the mean parameter sets and LI, HV to a linear interpolation between the parameter sets with the highest variance accounted for.

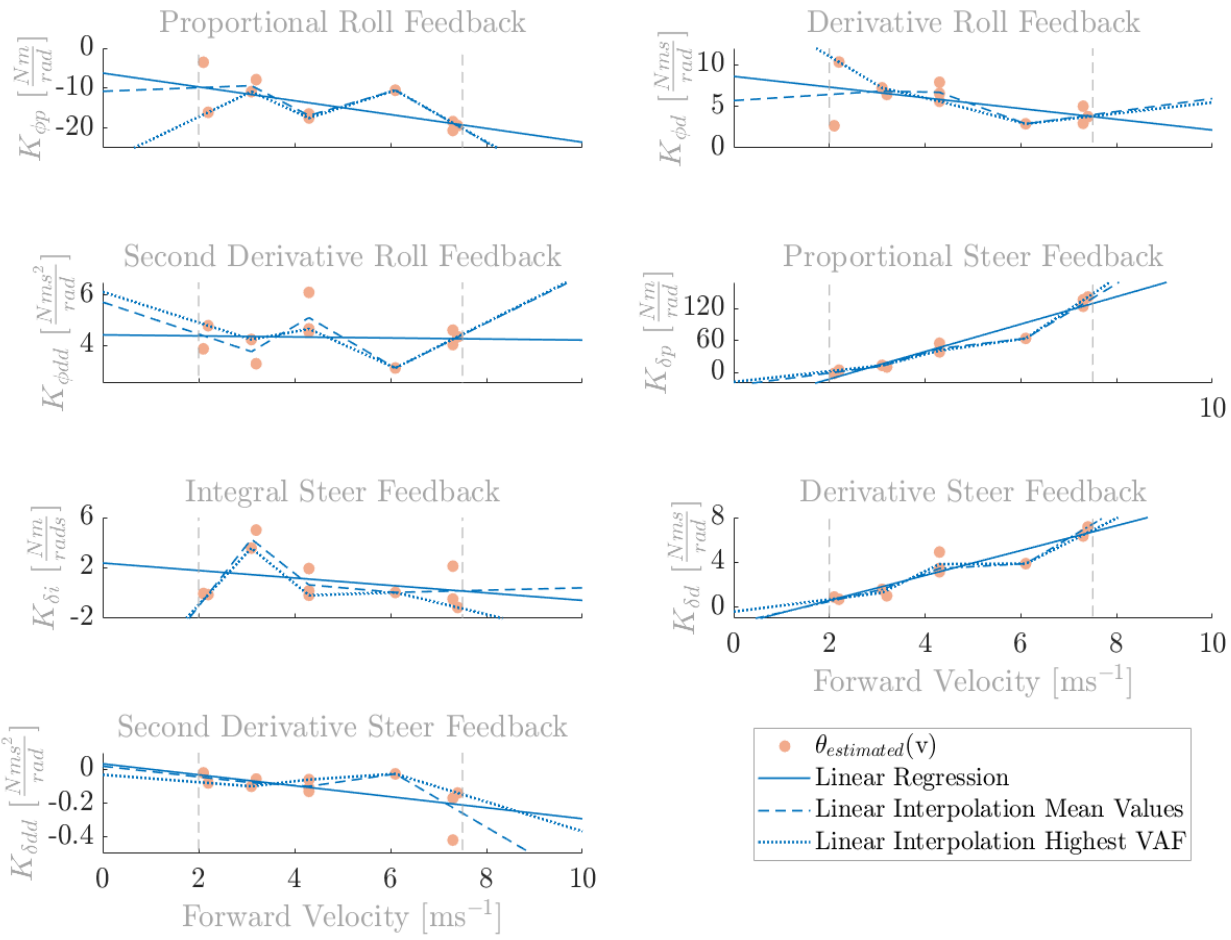

Figure 3.3: The discrete, estimated seven state parameters $\theta(v) = (K_{\phi p}, K_{\phi d}, K_{\phi dd}, K_{\delta p}, K_{\delta i}, K_{\delta d}, K_{\delta dd})$ and their continualization resulting from gray box identification of of controller $K(s, \theta)$ with neuro-muscular dynamics G_{nm} and neural time delay τ_d=60 ms. The discrete estimated parameters are the filled circles. The solid line is a linear regression, the dashed line a linear interpolation between the mean values of the estimated parameters per velocity group and the dotted line a linear interpolation between the parameter sets with the highest VAF per velocity. A velocity group consists of three parameter sets for close velocities. The top-left figure contains the data concerning the proportional roll parameter, $K_{\phi p}$. The top-right figure contains the data concerning the derivative roll parameter, $K_{\phi p}$, the mid-left figure concerning the integral steer parameter, $K_{\phi p}$, the mid-right figure concerning the derivative steer and the bottom figured displays the second derivative steer parameter fits. All corresponding coefficients of determination are given in table G.2. Only values at velocities between the two vertical lines are considered in this study.

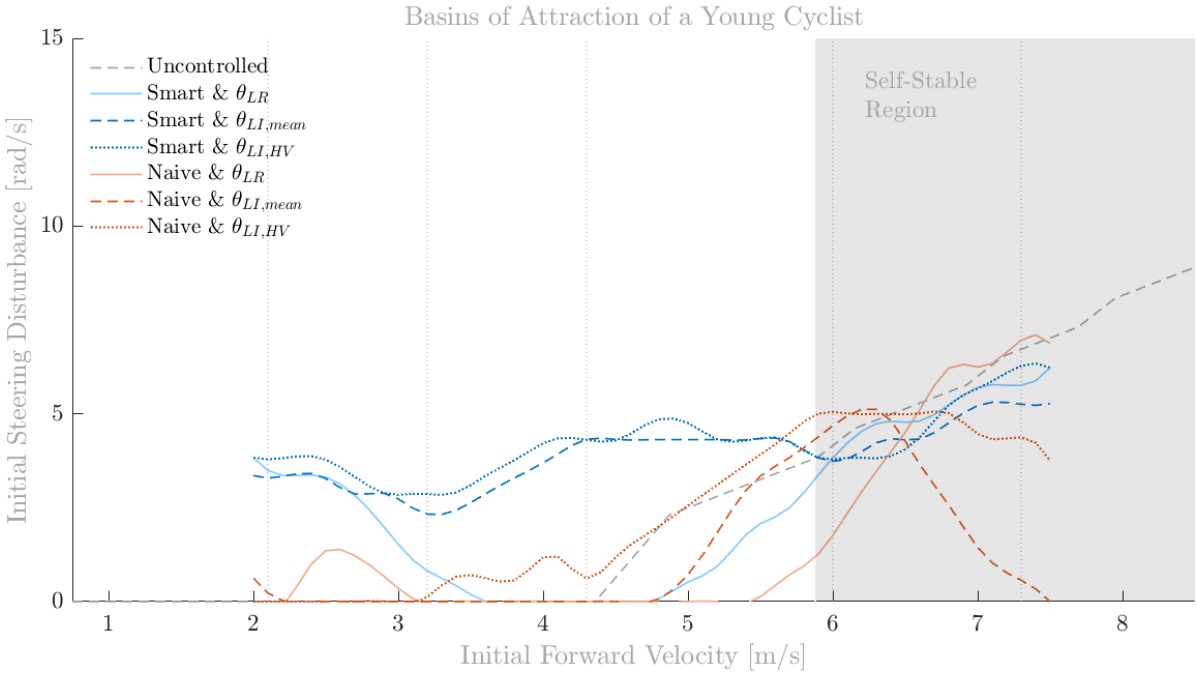

Figure 3.4: Basin of attraction outlines of bicycle-rider system consisting of the WCBM combined with a rider, based on the gray box model consisting of controller K(s, θ), second-order neuro-muscular dynamics G_{nm} and an effective neural time delay, τd, of 60 ms. The shaded region is the self-stable region of the uncontrolled bicycle and ranges from 5.88 to 10.13 ms^{-1}. The dashed, vertical lines are the velocities at which the experimental data was acquired and the parameter sets were estimated. These velocities are approximately 2.1, 3.2, 4.3, 6.0 and 7.3 ms^{-1}. The blue lines demarcate the stability region of the smart, old cyclist and the red lines of the naive, old cyclist. The smart, old cyclist did adapt its control strategy to its neural time delay and the naive cyclist did not. The solid lines represents the control models for which the parameter sets, θ, were made continuous over velocity using a linear regression. For the dashed lines they were linearly interpolated between the mean parameters. For the dotted lines, the parameters were linearly interpolated between the parameter containing the highest VAF.

3.3. Results of Part 1 & 2 of the Research Objective

So far, the answer to Part i and Part ii of this thesis have been answered in sections 3.1 and 3.2, respectively. The BoA's of the young and older cyclist have been identified. The answer to these two questions were required to test the hypothesis provided in the introduction of this thesis. The hypothesis addressed is as follows,

Hypothesis: One of the main causes for falls occurring amongst older cyclist is their age-related slowed motor responses.

This hypothesis is addressed by comparing the basins of attraction of the young and older cyclist. If the BoA would shrink for increasing time delay, this would then give a strong indication towards the truth of the hypothesis. However, due to the theoretical nature of this study, the hypothesis can merely be addressed and not tested.

Nonlinear Velocity-dependency

Figure 3.4 of section 3.2 showed that the linear regression did not yield a continuous basin of attraction. For both cyclists, the controller based on the linear regression also showed deviated significantly from the other controllers. For the young cyclist, the linear regression had a RMSE>1 with respect to the controllers based on the linear interpolations. Those controllers had a RMSE of only 0.60 compared to one another. For the older cyclist, the values lie even further apart. The RMSE values between the linear regression and the other two are above 2.25. Between the controllers based on linear interpolation, the RMSE was only 0.45.

It might be that the cyclist changes control approximately linear over velocity. However, for this rider model, it is likely that the parameters also compensate for more complex human control characteristics, such as prediction. This might result in a nonlinear velocity dependence of the feedback gains and, hence, in an inaccurate representation of human control of the linear regression feedback functions. Therefore, the controller based on the linear regression is excluded from further evaluation.

BoA Surface Comparison

The BoA's all seems to show a small increase in basin height over velocity. This might be due to the increasing, inherent stability of the bicycle over forward velocity. A comparison of the average basin height and basins surface is given in table H.3. The BoA of the rider shrank by approximately 55% for both controllers for increasing time delay. The results give a strong indication towards the hypothesis. For Part iii, section 3.4, the hypothesis will therefore be assumed true.

	Basin of Attraction [radms^{-2}]				
	Young Cyclist	Naive Cyclist	Change	Smart Cyclist	Change
$K(s, f_{\theta_{LI,mean}}(v))$	50.68	7.38	85.44	21.41	57.75%
$K(s, f_{\theta_{LI,HV}}(v))$	49.80	12.89	74.12	23.05	53.71%

Table 3.3: Changes in surface area and average height of the basins of attraction of a bicycle-rider system with 30 and 60 ms neural time delay. The bicycle-rider system consists of the nonlinear equations of motion of Basu-Mandal [2], internal controller $K(s, f_\theta(v))$, neuro-muscular dynamics G_{nm} and neural time delay τ_d. The feedback parameter function is based on linear interpolation between either the mean estimated parameters, $f_{\theta_{LI,mean}}$ or between the estimated parameters with the highest variance accounted for $f_{\theta_{LI,HV}}$.

Neural Time Delay and Motion Characteristics

The time to fall t_{ttf} increased significantly for increasing time delay. The young cyclist has a t_{ttf}<1 s. The naive, old cyclist has a t_{ttf}<5 s, a high number caused due to the rider's inability to quickly dampening out the oscillations. The smart, old cyclist adapted its control and that resulted in a t_{ttf} of maximum 3.5 seconds. Interesting is that, if the simulation time t_{sim} would have been set at 3 seconds instead of the 6 which have been used, then the BoA's of the old cyclist would have been fairly similar.

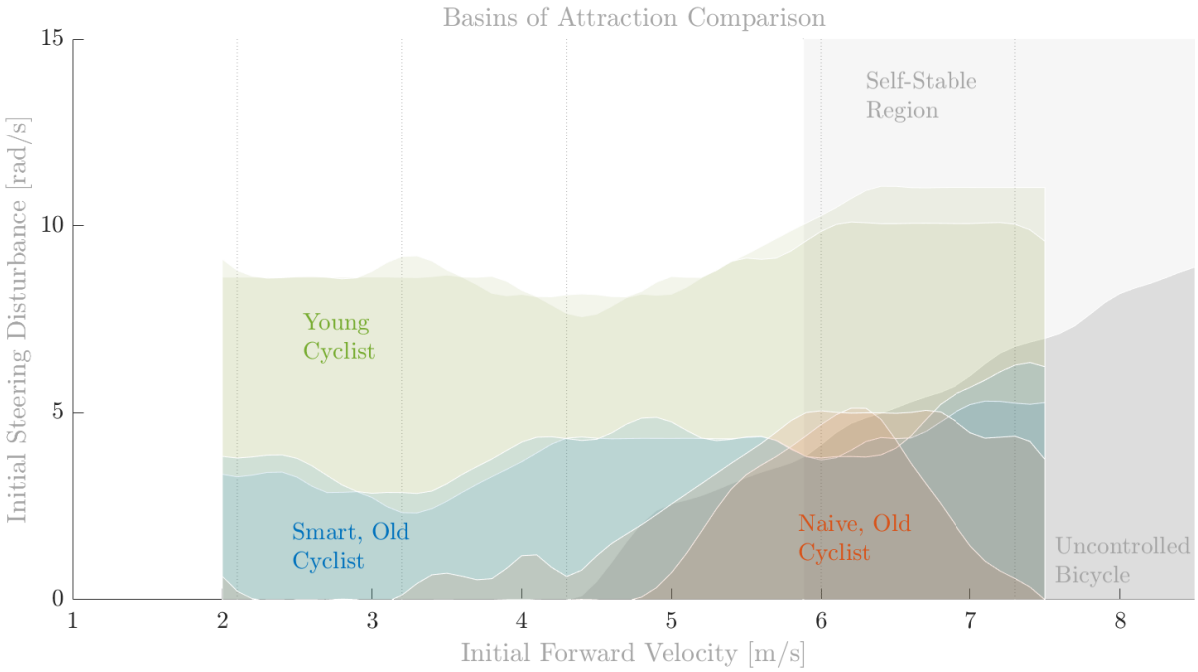

Figure 3.5: Basins of attraction of stability of a bicycle-rider system consisting of the nonlinear WCBM[2] equations combined with a rider[31]. The rider is based on a gray box model consisting of controller K(s, θ), second-order neuro-muscular dynamics G_{nm} and a neural time delay, τd, of 30 and 60 milliseconds. The young cyclist (green patches) suffers from 30 ms neural time delay. The smart, old cyclist (blue patches) suffers from 60 ms neural time delay. The naive, old cyclist (red patches) suffers from 60 ms effective neural time delay, but has its control tuned to 30 ms neural time delay. The square, gray shaded region is the self-stable region of the linear uncontrolled bicycle and ranges from 5.88 to 10.13 ms^{-1}. The dashed, vertical lines are the velocities at which the experimental data was acquired and the parameter sets were estimated. These velocities are approximately 2.1, 3.2, 4.3, 6.0 and 7.3 ms^{-1}. The outlines are based on linear interpolations of discrete, estimated feedback parameters.

Comments on Feedback Parameter Redundancy

The overparametrization of the system is quite troublesome. The feedback parameter reduction and estimation process had also been repeated for the rider with τ_d=0ms, and the reduction of [31] could not be found unless a bound was placed on $K_{\phi p}$ (see appendix J). One question which arises is the degree to which the rider model is still (experimentally) validated. If, with a more and a less reduced parameter set, the gray box model can still just as accurately describe the experimental data, do they both also describe the same basin of attraction? If not, then how valid is this model?

As was done for the young cyclist, the maximum allowable perturbations for all parameter sets of the reduction with VAF>90% have been plotted have been plotted in I. Overall, the results still indicate that increasing time delay yields a decrease for the maximum allowable perturbations. However, various parameter sets which describe one data set with VAF>90% show quite a spread in maximum allowable perturbations. Therefore, the results are rendered less reliable.

3.4. Part iii. Can the BoA of an older cyclist be enlarged using a SA?

The first part of this thesis has been addressed previously, and the hypothesis concerning the effect of slowed motor responses on cycling stability seems true. Then, knowing that the BoA declines for increases neural time delay, is it possible to increase the BoA upon adding a steer assist (SA) to the bicycle-rider system? This question is related to the second research objective and is the third research question of this thesis which is answered in this section.

Design Approach

Before answering the research question of Part iii, an ideal SA control law needs to be developed. This is done by adding the SA as the sole rider to the bicycle, evaluation its eigenvalues and BoA, and adapting it's law until the design criteria are met. The design criteria were set in section 2.4. To sum them up, they were,

- constant basin height
- good low speed control
- total motor control under 40 Nmsrad^{-1}
- no double frequencies

As a basis to start with, the controller from [29] is used. The capsize stabilization control law is not used. First, the roll rate control law as used in the paper, but adapted to the mechanical parameters of the bicycle here (see appendix E), will be evaluated. For the development of the controller, the eigenvalues are used. The state space implementation of the SA integrated with the bicycle can be found in appendix B.

Outline

Three main steps are taken to develop a control law which abides by the design criteria. The first control law, CL1, is analog to the intuitive controller from [29]. Based on the results, linear control laws are explored. Then, the need for nonlinear control laws became evident. The outline is as follows,

- CL1. Analog Control Law (Section 3.4.1)
- CL2. Linear Control Laws (Section 3.4.2)
- CL3. Nonlinear Control Laws (Section 3.4.3)

3.4.1. CL1. Analog Control Law

The ideal control law of the SA is unknown, therefore the approach will be partially heuristic. The first logical step is to find a control law somewhat analog to what has been used in the paper [29]; except for the exclusion of the roll angle feedback K_ϕ. The maximum control velocity, v_{max}, is set at 6.7 ms^{-1}. Then, letting $K_{\phi d}(0)$=-40 Nms/rad as the upper bound gain at zero forward velocity, the control law results in,

$$K_{\phi d}(v) = \begin{cases} K_v(6.7 - v) = 40, & \text{for } v < 6.7 \\ 0, & \text{for } v \geq 6.7 \end{cases} \tag{3.6}$$

which yields the feedback parameter $K_v = -5.97$ Ns^2/rad. Therefore the first control law to be applied will be,

$$K_{\phi d}(v) = -5.97(6.7 - v)s \text{ for } v < 6.7, \tag{3.7}$$

for which the stability will be evaluated based on its eigenvalues prior to the numerical integration.

CL1. Stability Analysis

The next step is to analyze the stability of this control law using the eigenvalue diagram. The feedback gain $K_{\phi d}(v)$ is given in the right graph of figure 3.6 and the corresponding eigenvalue diagram is given in the left graph. The modes are given in the figure. Please note the two black arrows of the weave mode; at 6.7 ms^{-1}, Re(λ_{weave}) and Re($\lambda_{capsize}$) nearly touch but do not cross.

At v_d of 1.01 ms^{-1}, the two positive real eigenvalues of the uncontrolled bicycle merges into one real eigenvalue, which becomes negative at 5.83 ms^{-1}. The SA moves those values to nearly zero and 1.36 ms^{-1}, respectively. In between those velocities, v_d and v_W, two frequencies are found of which one is very well damped and stable. The other is unstable and contains frequencies twice as high as those of the uncontrolled bicycle. This motion slowly becomes asymptotically stable for increasing velocity below v_w. This transition should show an oscillating motion which becomes cyclic at v_w and stable thereafter.

To visualize this, the roll rate perturbation responses, for initial forward velocity range 0.5-2 ms^{-1} and initial steer perturbation of 0.1 $rads^{-1}$, are plotted in time domain and phase space in figure 3.8, left and right respectively. The right-bottom graph gives the close-up phase space of the origin of the figure above.

What can be seen from those simulation plots is that the motions of about 1 ms^{-1} clearly contain two frequencies, which is in accordance with the eigenvalue diagram of figure 3.6; it shows two complex pairs between 0.5231 ms^{-1} and 1.153 ms^{-1}. Whereas a clean, stable cyclic motion is clearly visible for the yellow trajectory given in the zoomed in phase space figure (right-bottom). This trajectory is travelled at 1.40 ms^{-1}, just above the weave velocity in the stable region.

From figure 3.6, it can be observed that the bicycle and SA combined are stable from the v_w at 1.36 ms^{-1}, until the remainder of the forward speed range. The uncontrolled bicycle had a v_w of 5.88 ms^{-1} and was also stable over the remainder of the forward speed range, hence, the SA enlarges the stable velocity range significantly by decreasing v_w by 76.87%. Re(λ_{weave}) is marginally stable over the forward speed range, whereas Re($\lambda_{capsize}$) is significantly more stable over this range.

Capsize behaviour is not caught by the stability criteria of the numerical integration, see section 2.2, and is therefore marked as a stable solution. The weave mode is significantly stabilized by the SA law. Therefore, a large stability region can be expected. To see whether the expectation based on the linear equations holds true, the nonlinear system is numerically integrated.

CL1. Basin of Attraction

The result of the integration process is given in figure 3.7. The BoA will be analyzed from left to right.

The stability region indeed increases significantly between 1 and 2 ms^{-1}. Increasing the velocity further, the height of the BoA increases significantly and stagnates shortly after. Thus, for linear decreasing control a constant basin height is reached between approximately 2 and 4.5 ms^{-1}, after which the height starts to decline until no control is exerted anymore at 6.7 ms^{-1} and the remainder of the basin is just that of the uncontrolled bicycle.

Overall, the SA significantly enlarges the BoA compared to the uncontrolled bicycle, which is promising. However, the double frequencies at low velocities and the dip in the BoA cause the control law to fail the design criteria.

Then, what control is needed to maintain a constant basin height? The basin height does not have a clear relationship with the eigenvalue diagram. The largest, negative eigenvalue was found at 6.7 ms^{-1} yet this corresponded to the lowest basin height. To deduce correlations between the control law and BoA, a set of control laws will be analyzed in the next section by varying the linear feedback parameter and observing the changes of the region for which the basin height was constant.

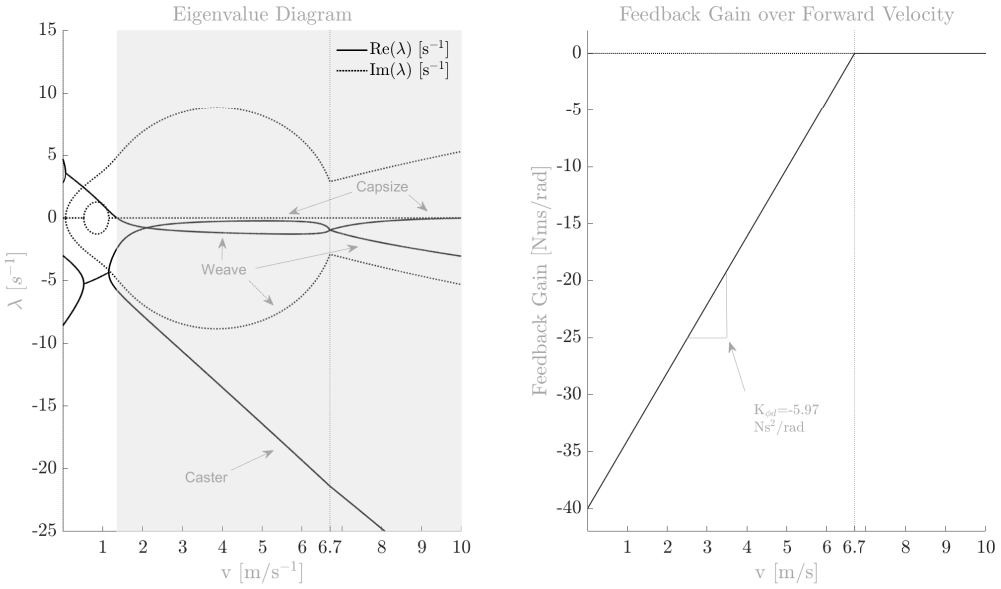

Figure 3.6: The eigenvalue diagram and feedback gain plot over forward velocity the Whipple(-Carvallo) benchmark bicycle controlled by an intuitive controller analog to [29]. The controller uses roll rate feedback of the form $T_\delta(v,s) = K_v(v_{max} - v)\dot{\phi}$, where in this case K_v=-5.97 Nms/rad and v_{max}=6.7 ms^{-1}. The resulting weave velocity is v_w=1.36 ms^{-1}. Note the arrows, the lines do not cross but merely touch at the vertical dashed line.

3.4.2. CL2. Linear Control Laws

To eliminate the dip at 6.7 ms^{-1}, v_{max} is set to 10 ms^{-1}, which is the maximum velocity considered in this thesis and the maximum velocity assumed a person on a city bike would go. If v_{max} is set at 10 ms^{-1}, then the decade, K_v, should be at max 4 Ns^2/rad over forward velocity. For larger values, the design criterion concerning the maximum feedback would be breached.

To get a feeling of the connection between K_v and the stability regions, the basins of attraction for four values of K_v will be calculated whilst keeping v_{max} at 10 ms^{-1}. The chosen feedback decade values are -1, -2, -3 and -4 Ns^{2}rad^{-1}. The corresponding controllers will be denoted using $K(s, f_{K_v=-1}(v))$, $K(s, f_{K_v=-2}(v))$ etc. The eigenvalues will be analyzed prior to the numerical integration, just as with the previous control law.

CL2. Eigenvalue Analysis

The eigenvalues and gains of the controllers $K(s, f_{K_v}(v))$ are given in the left and right graph of figure 3.9, respectively. A decrease of K_v seems to be proportional with an increase in the weave velocity v_w and a decrease in oscillation frequency of the resulting motion $Im(\lambda_{weave})$. In other words, less roll rate feedback results in slower oscillatory motions but the oscillations are also less dampened. Also, high control at low velocities seems to induce double frequencies in the motion due to the coalescence of Re($\lambda_{capsize}$) and Re(λ_{caster}).

CL2. Basins of Attraction

In figure 3.10, the basins of attraction outlines of the controller $K(s, f_{K_v}(v))$ are compared for the four values of K_v. From these basins of attraction, the influence of the damping exerted by the SA can be observed.

For less control, K_v=-1 Ns^{2}rad^{-1}, the BoA is similar as for the uncontrolled bicycle, except for a shift to lower velocities. An increase in control increases the basin height and tends to mold the outline towards a more logarithmic shape. The lowest v_w is acquired for $K(s, f_{K_v=-4}(v))$ and is 1.42 ms^{-1}, which is only slightly lower than what has been achieved using the analog control law.

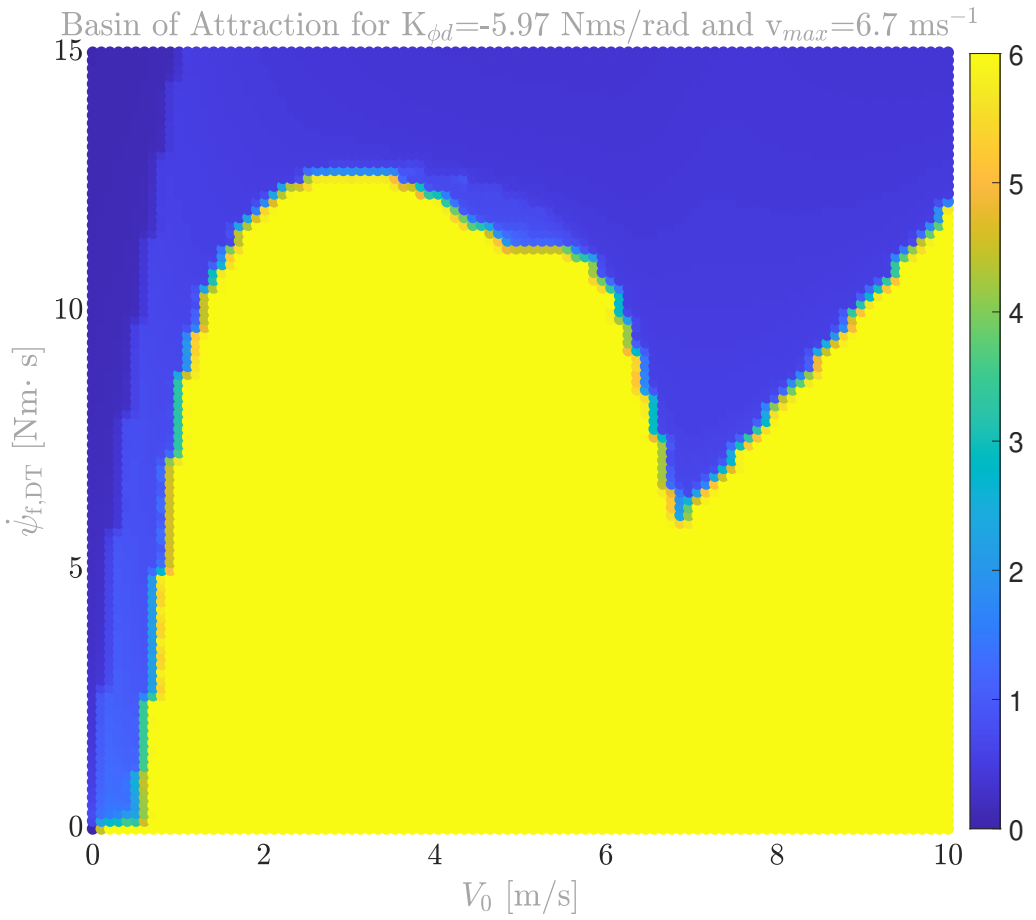

Figure 3.7: Stability Region of a controller based on [29], combined with the Whipple(-Carvallo) benchmark bicycle which is subjected to finite lateral disturbances and numerically integrated for a maximum of 6 seconds. The roll rate feedback parameter K_v is -5.97 Nms/rad and becomes zero at the velocity v_{max} of 6.7 ms^{-1}. The weave velocity v_w of the system is 1.36 ms^{-1}. The basin of attraction of stability is given by the yellow surface and all unstable solutions are represented by the other-coloured dots. The colour of the dots indicate the time is takes to fall, with warmer colours representing longer times.

CL2. Conclusion

Conclusively, more roll rate feedback control easily leads to higher basin height, but shows limited performance in decreasing v_w. A higher K_v is required between approximately 2 and 4 ms^{-1} to create a constant basin height, whereas lower K_v, than the values used here, is required for the higher velocity range. Therefore, nonlinear dependence on velocity is needed.

The 30 ms delayed rider from section 3.1 has a basin height range between 8 and 10 rads^{-1}. Then, would it be possible to create a constant basin height of around 8 rads^{-1} using an adapted SA control law? The ideal control law would then need the feedback values corresponding to the black crosses in figure 3.10.

3.4.3. CL3. Nonlinear Control Laws

The control law will be adapted such that the feedback gain has nonlinear dependence on forward velocity and such that $K_{\phi d}$ crosses the proximity of the values corresponding to the black crosses of figure 3.10. The feedback gains of the crosses are,

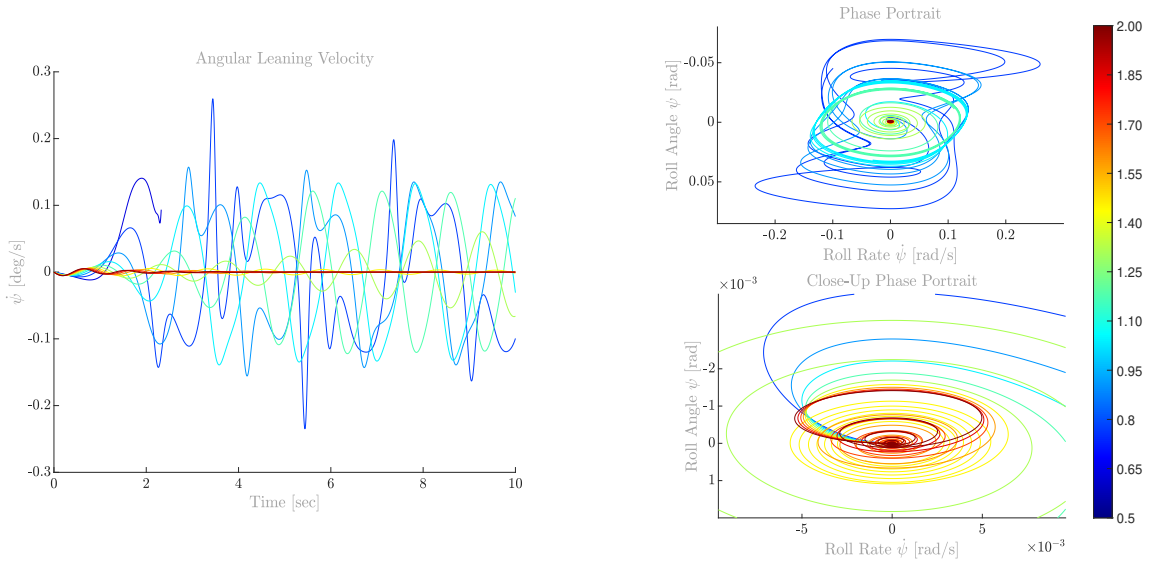

Figure 3.8: Roll rate perturbation response, $\dot{\phi}(t)$, over a range of velocities between 0.5 and 2 ms^{-1}. The perturbation is an initial steer rate of 0.1 $rads^{-1}$. In the left figure the response is given in the time domain, in the right figure in phase-space. The bottom-right is close-up of the origin of the figure above. The labels of the color bar indicate the forward speed.

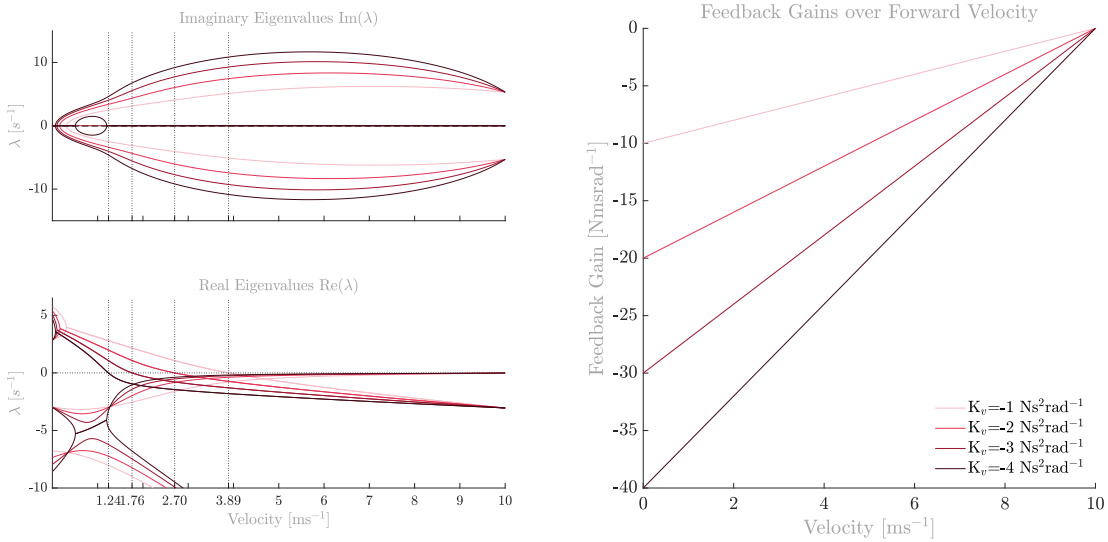

Figure 3.9: Eigenvalue diagram and feedback gains of the Whipple(-Carvallo) benchmark bicycle controlled by a steer assist. The steer assist is based on [28] and the three used roll rate feedback gains are given in the right graph. The imaginary eigenvalues $Im(\lambda)$ (left-top graph) dictate the frequencies of the motion and the real eigenvalues $Re(\lambda)$ (left-bottom graph) dictate the damping coefficient of those frequencies. The vertical lines mark the zero-crossings of the $Re(\lambda)$, which are also called the weave velocities v_w. For any forward velocity above the weave velocity, the motion is asymptotically stable.

$$K_{\phi d}(1.4) = -3 \cdot (10 - 1.4) = -25.8 \text{ Nms/rad} \tag{3.8}$$
$$K_{\phi d}(2.8) = -2 \cdot (10 - 2.8) = -14.4 \text{ Nm/rad} \tag{3.9}$$
$$K_{\phi d}(4.4) = -1 \cdot (10 - 4.4) = -5.6 \text{ Nm/rad}, \tag{3.10}$$

Those values are plotted in figure 3.11 using black crosses and they lie on the dashed lines, which represent the gains explored previously.

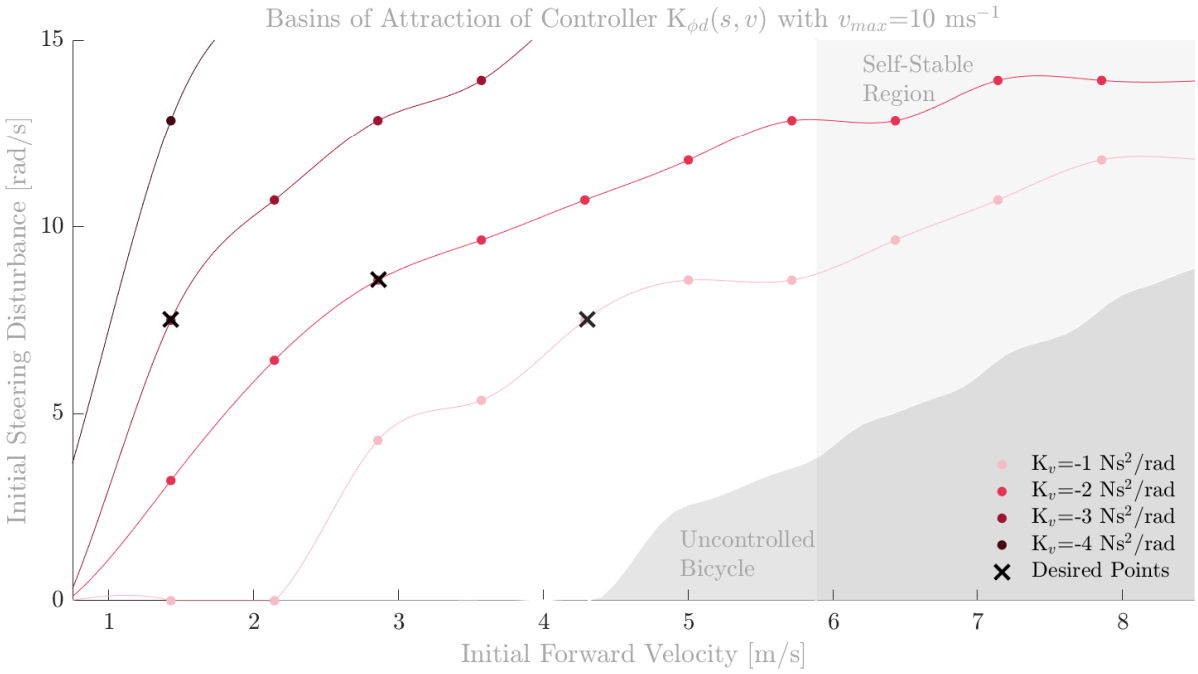

Figure 3.10: Stability region outlines of a bicycle-rider system consisting of the WCBM combined with a rider, based the intuitive controller from [29], denoted by $K(s, f_{K_v}(v))$ with various values of K_v. The square shaded region is the self-stable region of the uncontrolled bicycle according to the eigenvalues and ranges from 5.88 to 10.13 ms^{-1}. The dark gray patch is the BoA of the uncontrolled bicycle.

CL3. Function 1

Fitting a second order function through the desired points using the basic curve fitting tool of MATLAB, returns us the first function given in (3.11), denoted by $K(s, f_{\phi d}(v))$. This function is drawn in blue in the figure. After the third cross at 4.4 ms^{-1}, $f_{\phi d}(v)$ is higher than $f_{K_v=-1}(v)$, but decreases again after 7 ms^{-1} and then becomes lower again at 8.2 ms^{-1}.

From what has been learned so far, this will yield a smaller basin height compared to $K(s, f_{K_v=-1}(v))$ in between 4.4 and 8.2 ms^{-1}. The basin height of $K(s, f_{K_v=-1}(v))$ is approximately 12 rads^{-1} at 8.2 ms^{-1}, hence $f_{\phi d}$ will likely not yield a constant basin height. The beginning of the curve of $f_{\phi d}$, however, does fulfill the requirements. An exponential function might come closer to the desired control law.

CL3. Function 2

An heuristic attempt of using an exponential function resulted in the second function given by (3.12), denoted by $K(s, g_{\phi d}(v))$. This function has the desirable high control characteristics for low velocities, but exerts more control in the higher velocity region. However, the amount of control at high velocities seems too high to acquire a constant basin. No good trade-off could be found for retaining the control in the low speed region whilst reducing the control in the higher regions.

CL3. Function 3

Therefore, the velocity dependence within the exponential has been made second order, resulting in the third function given by (3.13) and denoted by $K(s, g_{\phi d}(v))$. The feedback values of this function lies in between both new functions for the main part, at the cost of some control for very low velocities below 1.5 ms^{-1}. The only concern for this function is the positive roll rate feedback values above approximately 7.5 ms^{-1}, however, that velocity lies well within the uncontrolled self-stable region. Then, if unwanted dynamic behaviour appears at this point, a v_{max} can be set at the sign change of the feedback since the bicycle is already stable on its own at this point.

$$f_{\phi d}(v) = -0.88v^2 + 12v - 41, \tag{3.11}$$
$$g_{\phi d}(v) = (v - 40)e^{-0.35v}, \tag{3.12}$$
$$h_{\phi d}(v) = (4v - 30)e^{-0.03v^2} \tag{3.13}$$

Three new control laws have been selected and will be analyzed using their eigenvalues.

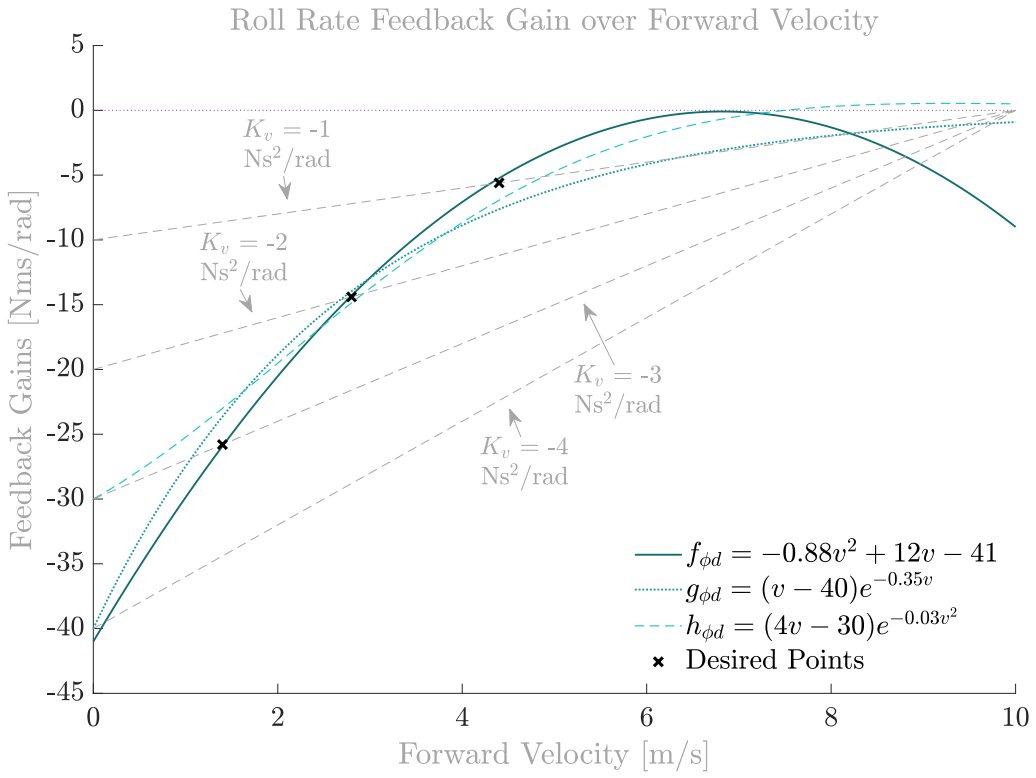

Figure 3.11: Potential roll rate feedback control laws for a SA bicycle controller, inspired by the intuitive controller from [29]. The intuitive controller is of the form $T_\delta = K_v(v_{max} - v)\dot{\phi}$. The dashed lines show the roll rate gain using v_{max}=10 ms^{-1} for three values of K_v. The coloured lines give potential, nonlinear control laws for which the feedback gain functions are given in the legend. The black crosses correspond to desired roll rate feedback gains at the corresponding forward velocities.

CL3. Stability Analysis

The eigenvalues of the functions given in (3.11) to (3.13) are displayed in figure 3.12.

All weave velocities lie in between 2.45 and 2.73 ms^{-1}, which is fairly large. One needs not to forget that, even though it is not a common cycling velocity, it is a velocity reached before getting on and off the bicycle. Especially for the elderly, it would be preferable to be stable, or at least marginally unstable, at speeds between 1.5 and 2 ms^{-1}. For the remainder of the forward velocity range, all three control laws yield stability.

Control law $f_{\phi d}$ again shows a dip in the real and imaginary values around 7 ms^{-1}, which, from what has been learned, will likely also correspond to a dip in the BoA. Also, this control law leads to double frequencies at very low speeds. The dip is eliminated using control law $g_{\phi d}$ and the double frequency for low velocities nearly as well. The last controller has no double frequencies nor, for higher speeds, a clear visible dip in the real eigenvalues.

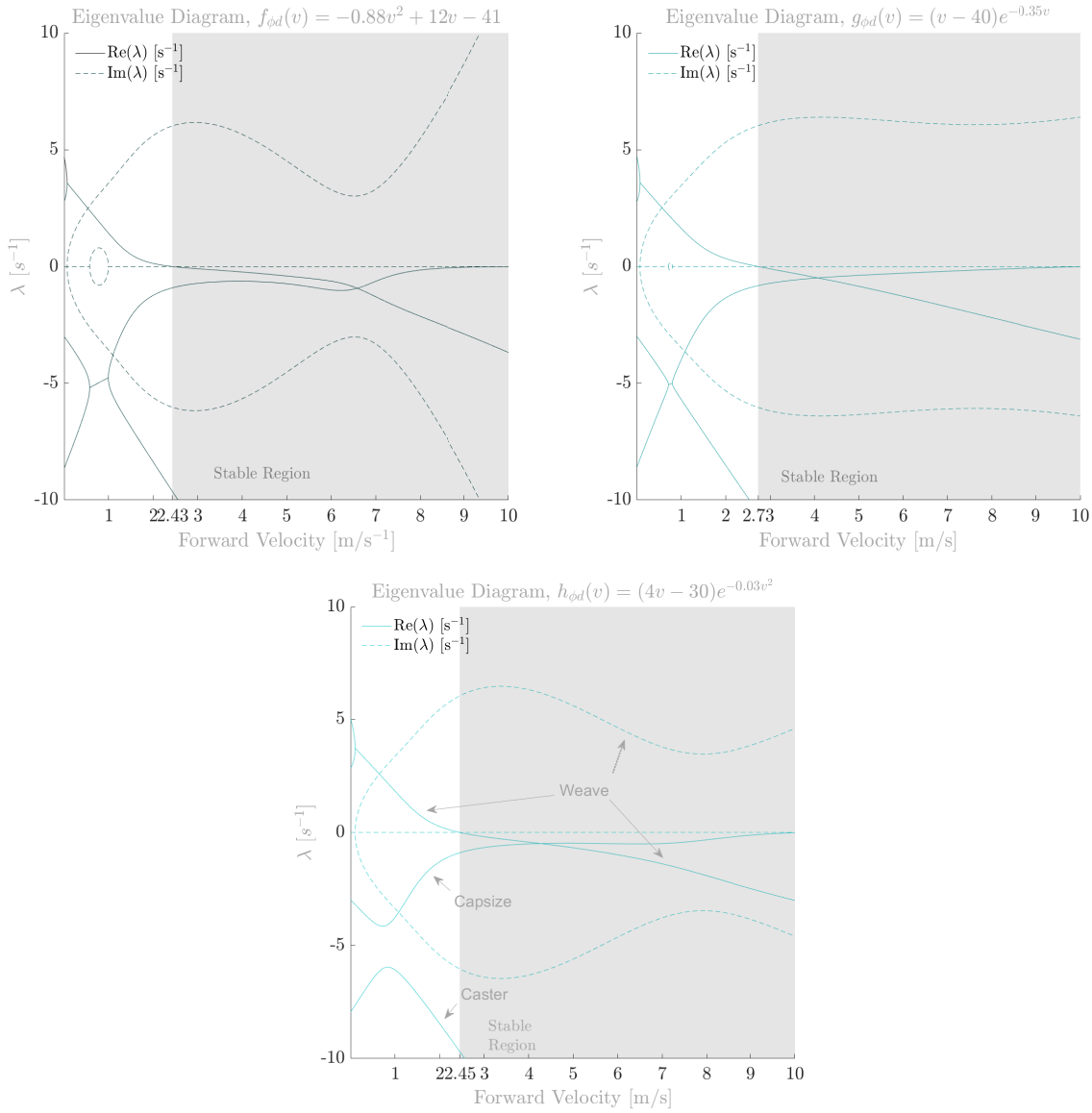

Figure 3.12: Eigenvalue diagrams of the WCBM controlled using a roll rate feedback control law. The top-left graph shows the eigenvalues λ for second order roll rate feedback, the top-right graph for exponential roll rate feedback and the bottom graph for exponential roll rate feedback with second order dependency on the forward velocity. The shaded regions cover the velocities for which the combined system is stable.

Basins of Attraction

The outlines of the basins of attraction of the three controllers are given in figure 3.13. As expected, $K(s, f_{\phi d}(v)$ indeed has a loss of basin height for the higher velocity range. Also, $K(s, f_{\phi d}(v)$ has a lower basin height at 7.22 ms^{-1} than $K(s, h_{\phi d}(v)$ which seems odd since according to figure 3.11 their feedback gains cross.

Simulation at that velocity reveals that the initial steer perturbation results in a slight decline of forward velocity, see figure 3.14. This then results in different feedback gains. After 0.6 seconds, the bicycle reaches a forward velocity higher than 8.4 ms^{-1} for both controllers. This velocity is is significantly larger than their initial velocity. At this point, the feedback parameters of both controllers are of different magnitude and sign. Therefore, their BoA height differs.

For controller $K(s, g_{\phi d}(v))$, its basin significantly increases over forward speed and the basin height

is not constant. For controller $K(s, f_{\phi d}(v))$, a dip in basin height still occurs after which the height steeply increases. Only $K(s, h_{\phi d}(v))$ has a constant basin height of 7.5 rads^{-1} for velocities above 2 ms^{-1}. Therefore, this controller will be used for the evaluation of the BoA of a bicycle-rider system aided by a SA.

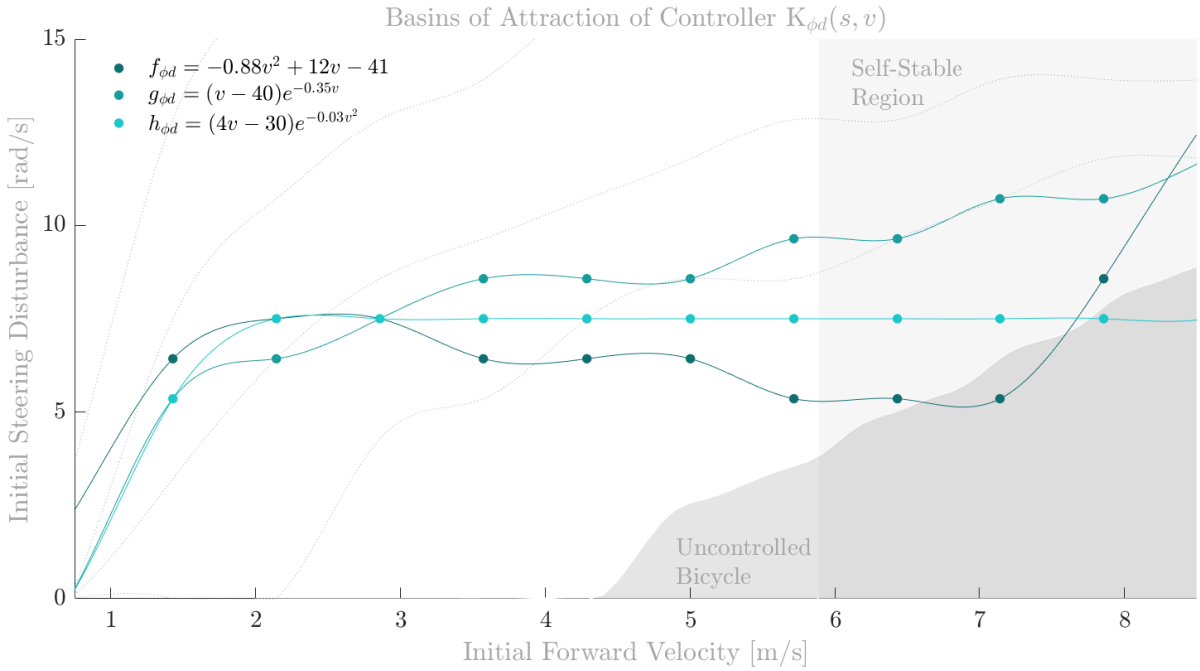

Figure 3.13: Stability region outlines of a bicycle-rider system consisting of the WCBM controlled using various roll rate feedback control laws. The square, gray shaded region is the self-stable region of the uncontrolled bicycle according to the eigenvalues and ranges from 5.88 to 10.13 ms^{-1}. The dark gray shaded region demarcates the BoA of the uncontrolled bicycle.

Combined BoA

Then, the remaining step is to combine the 60 ms delayed rider with the developed SA for which the basin height remains constant over forward velocity. The human rider, for which the feedback parameters were linearly interpolated, is eliminated for further evaluation due to the basin collapse around 4.3 ms^{-1}. Then, adding the SA to the human rider results in the BoA given in 3.15.

As can be seen is that, for both the rider and SA individually, the basin height remained fairly constant over forward velocity. However, adding both controllers together results in a high basin height for low velocities which declines over increasing speed until it reaches the self-stable region of the uncontrolled bicycle. The basin of the smart, old cyclist grew by 207%, when being aided by the SA.

Discussion SA

The SA provides a possible solution to enlarge the BoA of elderly cyclist under the assumption that the cyclist maintains the same control as without the SA. To reveal the real potential of the SA, a new experiment to identify the riders' control when being aided by the SA is required. Then, the BoA needs to be re-identified to see whether it indeed grew with respect to the BoA of an elderly cyclist. And, as stated before, the older cyclist here does not represent and elderly cyclist since the chosen time delay was not based on literature. Therefore, the control identification also needs to be performed for the elderly cyclists without being aided by the steer assist. This would then also require knowledge of an accurate effective, neural time delay value of the elderly participants which might yet require another experiment similar to [4].

The results are promising in the sense that the results revealed that it is not necessary for a cyclist to change its control strategy when being aided by the SA. Therefore, it is likely that it merely requires the

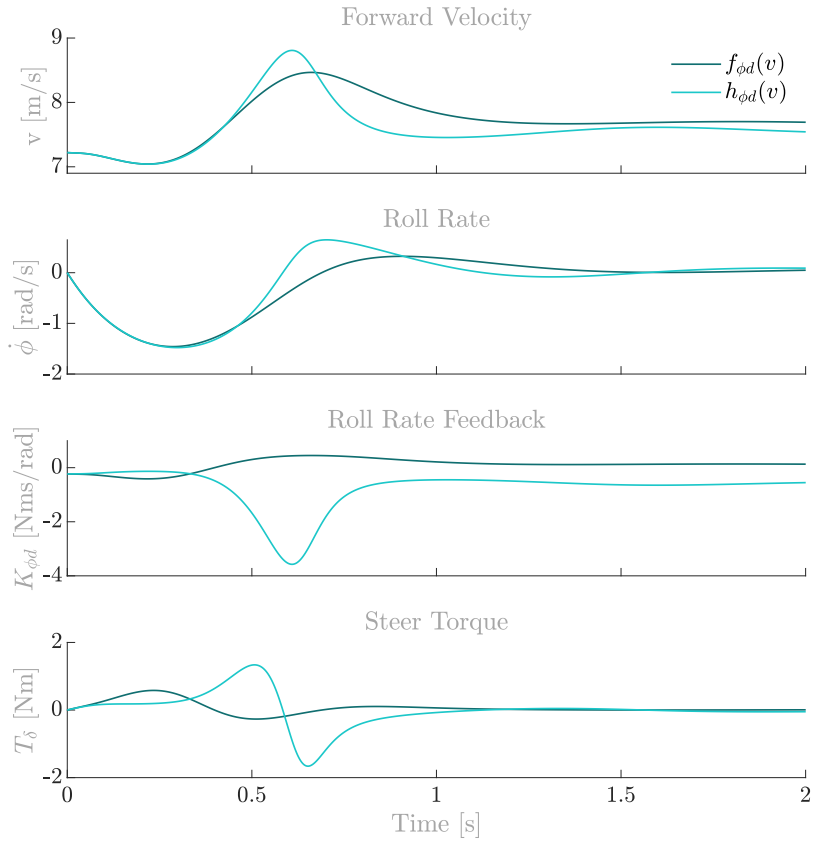

Figure 3.14: Nonlinear simulation of steer assist controllers $K(f_{\phi d}(v), \dot{\phi})$ and $K(h_{\phi d}(v), \dot{\phi})$ combined with the Whipple benchmark bicycle, simulated for an initial disturbance of 6 rads^{-1} and initial velocity 7.221 ms^{-1}. Roll rate feedback of the controllers are $f_{\phi d}(v) = -0.88v^2 + 12v - 41$ (dark blue) and $h_{\phi d}(v) = (4v - 30)e^{-0.03v^2}$ (light blue).

cyclist to get familiar with the feeling rather than having to learn how to cycle with assisting steer control.

However, the results are very preliminary. Not just because the interaction between steer assist and elderly cyclist has not been taken into account and because the older cyclist does not accurately represent an elderly cyclist. But also because no sensorial time delays have been taken into account; the design does not allow trajectory tracking; and it does not have a maximum bound on the exerted torque control since the SA control is still roll rate dependent. Prior to further research cycling with the SA, the SA should be modelled more accurately but incorporating the points above.

Summary Steer Assist

To provide a reliable SA, the control law has been adapted such that without any control exerted by the human rider, the aided bicycle is able to handle constant maximum allowable perturbations for velocities between 2 and 8.5 ms^{-1}. This identified BoA is derived without taking into account sensorial time delays and maximum allowable control torque and is therefore a preliminary result.

Combined with the old cyclist, the BoA of the old cyclist doubled. This proves the potential of the steer assist. However, the relationship between the individual basins of attraction of two controllers and their combined basin is still unclear.

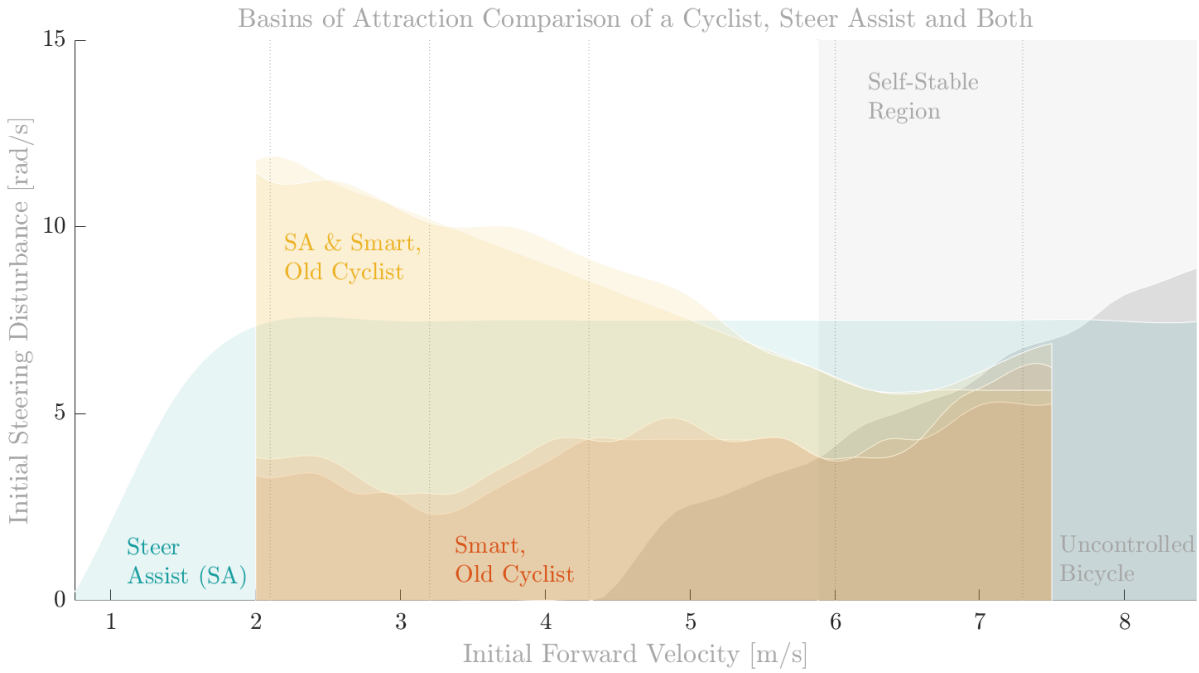

Figure 3.15: Stability region outlines of a bicycle-rider system consisting of a human rider based on [31] and the Whipple(-Carvallo) benchmark bicycle, controlled using various roll rate feedback control laws. The blue shaded region is the self-stable region of the uncontrolled bicycle according to the eigenvalues and ranges from 5.88 to 10.13 ms^{-1}. The dashed, black line demarcates the BoA of the uncontrolled bicycle.

4

Discussion & Future Recommendations

This chapters provides the overall discussion and the resulting future recommendations. The discussion focuses mainly on the process adopted for this thesis and the corresponding results. For comments on the rider model and the experimental process behind the data, one is referred to their source [24]&[31].

Discussion Outline

First, the hypothesis will be addressed using the major finding of this thesis. Every theoretical study is limited by the modelling aspects and a discrepancy between the model and the truth will always exist. However, addressing those limitations and proposing future recommendations might shrink the gap between theory and truth. This is done after discussion the main results concerning the human rider. The next part to discuss concerns itself with the steer assist development results. This part is also finalized by some limitation and future recommendation discussions. At the end, the future recommendations are summarized by bullet points. Thus, a summary of the outline and the questions addressed here are as follows:

- What can be said about the hypothesis based on the main results? (Section 4.1)
- What are the main results of the steer assist development? (Section 4.2)
- What are the future recommendations emerging from this study? (Section 4.3)

4.1. Hypothesis

The hypothesis was introduced in the main introduction of this thesis. As a reminder, the hypothesis can be stated as follows,

> One of the main, possible causes for the falls of elderly cyclists are their slowed motor responses.

The results found in Part i and Part ii of this thesis, sections 3.1 and 3.2, strongly indicate towards this hypothesis. The BoA of two old cyclists have been identified. One whom was unaware of the neural time delay and, therefore, retained the same control strategy as was exerted by the young cyclist. And one old cyclist whom could adapt its control strategy to the perturbation responses of the experimental data of a young cyclist. Both rider models were compared with a young cyclist, to observe the influence of neural time delay on the lateral stability in cycling (see figure 3.5).

For the first old cyclist, stability was completely lost for velocities below 5 ms^{-1} and its basin of attraction shrank significantly by approximately 81% (see figure 3.2). For the latter mentioned old cyclist, the surface area and height of the basin of attraction both declined by approximately 55% (see table H.3, section 3.3). This shows the detrimental effect an increased slowed motor response has on the

degree of perturbations a cyclist can handle, even if one tries to adapt its control. Therefore, it is very likely that the elderly cyclist is more prone to falling over for disturbances which the young cyclist can handle. Combined with the physical fragility of the elderly, this would then lead to an increasing share amongst the seriously injured cyclist, as is observed by the numbers [1].

4.2. Steer Assist Development

Assuming that the hypothesis is true, the second objective of this thesis could be addressed. The second objective was the development of a steer assist to aid the stability of the older cyclist based on certain design criteria. This process was followed by a preliminary assessment of its potential to aid an elderly cyclist in stabilizing a bicycle.

Below the double root velocity v_d of the uncontrolled bicycle, the maximum allowable perturbations decline rapidly for even the highest feedback parameter (see figure 3.10). Too much control for low velocities results in double frequencies and only marginally decreases the weave velocity v_w (see figure 3.9). Overall, negative, but linearly increasing roll rate feedback results in an increase of BoA height over forward velocity (see figure 3.10). The overall BoA outline trend shifts from linear to sublinear with increasing surface for stronger control. A constant BoA height required negative, higher order roll rate feedback.

The development of the steer assist has been done according to several design criteria. The most important criteria was the degree of perturbation rejection over forward velocity; it was required to be constant. This could only be managed by an exponential control law with second order dependency on velocity (see figure 3.13). Part of the design emphasis focused on the control for low velocities. Stabilization for the extreme low velocities required significantly more control than at low velocities. Whether extremely increasing control for decreasing velocity in the low velocity region is a desired characteristic, is questionable.

The assessment is called 'preliminary', since no interaction between cyclist and steer assist has been taken into account. If the elderly cyclist indeed uses a control strategy similar to the older cyclist, then the cyclist can retain its control strategy and benefit from increased stability due to the steer assist. Combined, increasing stability for low velocities is found. Above the weave velocity v_w of the uncontrolled bicycle, the stability seems to exhibit a slight increase.

4.3. Future Recommendations

This section first discusses several aspects of this thesis which led to future recommendations. At the end of this section, the future recommendations are summarized.

Inherent Bicycle Stability

The inherent stability of the bicycle seems to aid the stability of both old rider models. The BoA height of both old rider models start to increase for the same velocities as where a nonzero BoA height for the uncontrolled bicycle was found (see figure 3.5). To further investigate this, more experimental data is required for velocities in between 6.0 and 7.3 ms^{-1}. If a clear correlation can be found, this would support future research towards creating a bicycle with lower v_w for the elderly such that the lateral stability in cycling can be mechanically enhanced.

Neural Time Delay of the Elderly Cyclist

This research studied the effect of slowed motor responses on the basin of attraction of stability of cyclists by adding two values of a single, effective time delay to the rider's observed states. The neural time delay value of the young cyclist was based on literature [26][4]. That value was doubled to represent an older cyclist. This cyclist does not represent the elderly cyclist, but is merely used to study the effect of increased time delay. To find an effective time delay value that can represent the delay an elderly cyclist suffers from, a study similar to [26] and [4] should be conducted with participants aged 65 and above.

Sensitivity of the BoA

The young rider model, with the time delay based on literature, has been identified using experimental data and is therefore implicitly validated. However, this identification yielded multiple solutions for the riders with 0 and 60 ms time delay (appendix J and section 3.2, resp.) which both described the data with VAF>90%. Then the question arose, as to whether different sets of parameters which are equally capable of describing the experimental data, would also yield the same degree to which perturbations could be handled. This issue was addressed in appendix H by representing the older cyclist with six, instead of seven, feedback states.

The results of that appendix revealed that for a single data set, more or less reduced parameter sets which still had a VAF>90%, could yield different basin heights. This was backed-up by looking into the matter more closely, as was done in appendix I. However, it seems that the average parameter sets per velocity group still yielded similar BoA's, regardless of the dimension (RMSE=0.42). Therefore, sufficient data is required per velocity.

Validity Validation Metric VAF

How come that two parameter sets describing the same data set with both VAF>90% can yield different BoA heights? (see appendix I) VAF is the normalized difference between the experimental and simulated roll rate signals, but for falling over only the few oscillations right after being perturbed are of significance and not the whole signal. This led to some parameter sets with high VAF which did not properly describe the beginning of the signal and, as a result, could handle a different magnitude of perturbations compared to another set. Therefore, VAF is only a good measure when the simulation input data of the identified theoretical system is similar to the experimental input data. That being said, the rider model qualified by VAF is only accurate when subjected to similar sized perturbations as was done with the experiment.

Crucial Feedback States

Also, it is recommended to seek out the crucial feedback parameter using experiments similar to what has been done by [5]. This path will provide more certainty as to which feedback states are actually responded to by a human cyclist. Even if only a few feedback states can be eliminated, it will be more likely that the optimization will yield an unique solution than when using full state feedback.

Linear Velocity Dependent Control Strategy

To find the relationship between velocity and feedback parameters, it is of importance to find the crucial feedback parameters and to increase the complexity of the rider model. For the rider model used here, the control could not properly be represented based on a linear regression. The feedback gains compensate for the lacking components of the gray-box model, such as preview and prediction. This might render the velocity dependency of the feedback gains nonlinear, while it might be that the control can be represented by linear regression.

Including a More Complete Passive Rider

The model used here did include the inertial properties of the cyclist by adding it to the rigid rider attached to the rear frame. However, the rider is not modelled to have its hands at the handlebars. Therefore, no extra inertia and damping is added to the front assembly. For a rider with zero time delay, the gains would compensate for the lack of this modelling aspect. For a delayed rider, however, the perturbation response of the front assembly will be as if the rider would cycle with the hands off for as long as the time delay holds.

It cannot be said whether this would increase or decrease the BoA difference between the young an old cyclist. The magnitude of the steer response would be less, but the added damping would oppose the principle of steer into the fall which would then decline stability. Also, both models do describe the experimental data well, which indicates that the feedback gains already compensate for the lack of the modelling aspect. Future recommendations are to include a passive rider by kinematically connecting

the rider with the handlebars as what was done in [30].

Other Limitations

Even if the results were to be reliable, other limitations still have their influence on the reliability of the results. Part of those limitations are concerned with the experiment behind the data for which one is referred to its sources [31][24]. Examples of those limitations are the environment of the experiment as well as the physical limitations imposed on the rider's motion. Also, the dynamics of an uncontrolled bicycle on a treadmill with the weight of a rider on top, have not been validated yet.

Further Development of the Steer Assist

The overall results of the steer assist seem promising and it would be interesting to implement the recommended control strategy. However, for this design process, the torque exerted by the steer assist was not limited by a maximum value. Only the roll rate feedback value was. Also, no delay was implemented for the registration and process time of the steer assist. Above all, no trajectory tracking is considered. Those factors are recommended to be included for any further design on the steer assist. Then, an experiment can be conducted to identify the interaction between cyclist and steer assist and to see if the combined system has indeed become more stable.

Summary Future Recommendations

The future recommendation are summarized below using bullet points.

- The mechanical development of a bicycle for the elderly which is mechanically more stable and which has a lower v_w using basin of attraction identification and studying the effect on the lateral stability of elderly in cycling
- Identifying the neural time delay of the elderly for movement of the upper extremities, similar as what has been done by [26] & [4]
- For validation of a control model which is later subjected to larger perturbations, the VAF should only be applied on the data right after perturbation or a metric should be used which puts emphasis on that part of the data by e.g. the usage of weights
- Taking into account that VAF, combined with long perturbation response signals, is not an accurate metric for validation rider models which later are used for larger perturbations.
- Eliminate feedback paths using experimental research, e.g. as has been done by [5], such that redundant feedback channels can be eliminated during the stage of gray-box modelling
- Increasing rider model complexity to include preview and prediction as well as a more correct passive rider model
- Further developing the steer assist control law by taking into account sensorial delays, trajectory tracking and maximum allowable control torque.

5

Conclusion

The first two questions were answered to address the hypothesis concerning the relationship between slowed motor responses of the elderly and the number of elderly cycling victims. The method to address the hypothesis was to identify the relationship between neural time delay and lateral stability in cycling. Mapping this relationship has been done using the identification of the basin of attraction of stability which consists of the set of finite, lateral disturbances for which the bicycle-rider system did not fall over. The basins of attraction of a young rider model has been compared with the basins of two older rider models. One older rider model was naive, and retained the same control strategy as the young rider did while suffering from double the time delay. The other older rider model was smart and did adapt its control response. Regardless, the basin of attraction shrank significantly for both. Therefore, the results strongly indicate towards the hypothesis. Thus, it can be assumed that the slowed motor responses of the elderly are one of the main causes behind their falls.

Furthermore, a preliminary development of a steer assist control law has been performed. The goal of this development is future implementation of a further developed control law such that the number of elderly cycling victims can be reduced by enhancing their lateral stability in cycling. As a result, a nonlinear velocity-dependent roll rate feedback control law has been developed which yielded a constant basin height. The basin height was similar to the basin height of a young rider.

Appendices

A

Nonlinear EOM of Basu-Mandal: Steer Torque Implementation

The rider model is connected with the nonlinear bicycle model of Basu-Mandal [2] by the steer torque implementation. This appendix briefly explains the model of Basu-Mandal and the implementation of this steer torque implementation.

A.1. Configuration

As for the standard configuration, a lean angle to the left or a counter clockwise steer angle is defined as positive. The bicycle itself is the same as used in [20], however, different symbols are used (see figure A.1. Another important difference is the starting configuration, for which the bicycle is assumed to lie on its side on the ground. Therefore, a lean angle of $\phi - pi/2$ corresponds to the straight-up bicycle. Throughout this thesis, the following notations will be used:

- ϕ refers to the roll angle
- δ refers to the steer angle

Other denotations will be explained long the way. If one is interested in the supplementary material, do note that the symbols are different. In the MATLAB script, the symbols of Basu-Mandal hold and their meanings can be found in the corresponding paper [2].

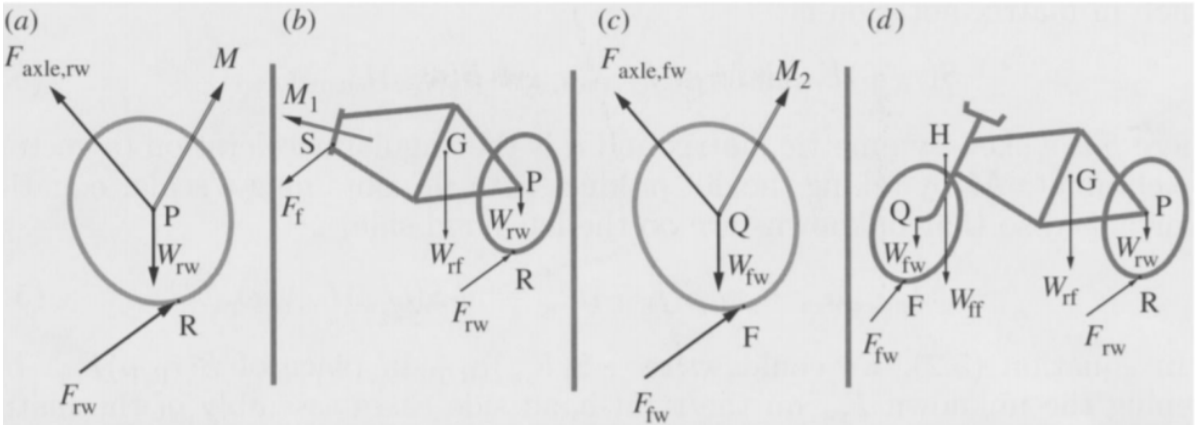

Figure A.1: The free body diagrams of, from left to right, the rear wheel, the rear wheel and frame, the front wheel, and at last the entire bicycle. Points G & H are centres of mass of the rear and front frames, respectively. This figure has been taken from [2].

A.2. Newton-Euler Equations

The Newton-Euler equations of the WCBM consist of 33 independent simultaneous linear algebraic equations and 33 unknowns, hence it has an unique solution. Of these 33 equations, 9 scalar equations come from the momentum balance, 6 emerge from the constraint equations and another 18 scalar equations emerge from further kinematic relations. The 33 unknowns are,

$$(a_p, a_g, a_H, a_Q, \alpha_{rw}, \alpha_{rf}, \alpha_{ff}, \alpha_{fw}, F_{rw}, F_{fw}, \ddot{\beta}_r, \ddot{\psi}_f, \ddot{\beta}_f) \tag{A.1}$$

of which all are vector unknowns. The first four unknowns are the acceleration vectors of the centres of mass of the corresponding four rigid bodies, denoted by their subscript, and given in figure A.1, the next four vectors are the angular accelerations of the rear wheel, rear frame, front frame and front wheel, respectively, and the following two vectors contain the components of the front and rear ground contact forces. Remaining are three vector components of which the first represents the angular acceleration of the rear wheel, the second the angular steering acceleration and the last the angular acceleration of the front wheel.

The set above can be solved for the 33 unknowns, however, the solution of those equations does not contain the desired accelerations of the Euler angles $\ddot{\theta}$, $\ddot{\psi}$ and $\ddot{\phi}$. To obtain those, the equation of the angular acceleration of the rear frame can be used since its velocity is defined as,

$$\omega = \begin{bmatrix} e_3 & R_1 e_1 & R_2 R_1 e_3 \end{bmatrix} \begin{Bmatrix} \dot{\theta} \\ \dot{\psi} \\ \dot{\phi} \end{Bmatrix}, \tag{A.2}$$

where R_1 and R_2 are defined as,

$$R_1 = R(e_3, \theta) \tag{A.3}$$

$$R_2 = R(R_1 e_1, \psi), \tag{A.4}$$

and R represents the rotation matrix. Hence, it can be derived that,

$$\alpha_{rf} = e_3\ddot{\theta} + R_1 e_1 \ddot{\psi} + R_2 R_1 e_3 \ddot{\phi} + S(R_1 e_1 \dot{\psi} + e_3 \dot{\theta}) R_2 R_1 e_3 \dot{\phi} + S(e_3 \dot{\theta} R_1 e_1 \dot{\phi}), \tag{A.5}$$

where S stands for skew-symmetric matrix. Equation (A.5) can then be solved for $\ddot{\theta}$, $\ddot{\psi}$ and $\ddot{\phi}$, since α_{rf} is part of the unique solution of the 33 Newton-Euler vector equations and the Euler angles are scalar unknowns. Hence, equations (A.5) consists of three scalar equations and three scalar unknowns, which thus yields an unique solution. If one is interested in writing down the full form of this derivation, paper [10] might aid in finding the derivative of rotation matrices. For the full derivation of the equations, one is referred to the paper of Basu-Mandal itself [2].

A.3. Validation

The resulting equations using the Newton-Euler and Lagrange derivation methods cannot be compared by the eye. Therefore, Basu-Mandal *et al.* chose several arbitrary coordinates and their first derivatives, then derived their acceleration using the equations from both methods. Correspondence was found to machine precision and the results are shown in table 1 of their paper [2]. Also, the results from the Lagrangian approach have been linearized and cross-checked with the WCBM of Meijaard *et al.* and agreement up to 13 digits was found. Other models containing the nonlinear equations of motion of an uncontrolled bicycle have not yet been properly cross-checked, do not lean for simulation use or are not publicity available (e.g. [36][33]). The Newton-Euler MATLAB script of Basu-Mandal not only leans for rapid simulation, it is also easily modified and understood, such that a controller can be added. Hence, the model of Basu-Mandal will be adapted and used throughout this thesis for simulation.

A.4. Steering Torque Input

To control the bicycle, the rider needs to exert a torque on the handlebars and this torque needs to be implemented in the equations. Applying a torque directly into the equations is done as follows. The angular momentum balance equations of the rear frame and rear wheel of the bicycle around an arbitrary point S on the front fork axis based on figure A.1 (b) is,

$$\begin{aligned} &r_{R/S} \times F_{rw} - F_{g,rw} r_{P/S} \times e3 - F_{g,rf} r_{G/S} \times e3 + M_1 = \\ &I_{cm,rf}\alpha_{rf} + \omega_{rf} \times I_{cm,rf}\omega_{rf} + m_{rf} r_{G/S} \times a_G + I_{cm,rw}\alpha_{rw} + \omega_{rw} \times I_{cm,rw}\omega_{rw} + m_{rw} r_{P/S} \times a_P, \end{aligned} \tag{A.6}$$

where F_g is gravitational force, F_{rw} the ground contact force at point R, $r_{x/y}$ shortest distance between point x and y, e3 the body-fixed z-axis, α angular acceleration, I_{cm} moment of inertia about the center of mass, m mass, a acceleration and ω angular velocity. The subscripts rw and rf refer to 'rear wheel' and 'rear frame', respectively. M_1 is an unknown bearing moment with no component along the bearing axis nor in the direction of a unit vector along the steering axis, $\hat{n}_f$. Hence, M_1 can be eliminated by taking the dot product with this unit vector. Adding a steering torque T to the applied forces and eliminating M_1 results in,

$$\begin{aligned} &\hat{n}_f(r_{R/S} \times F_{rw} - F_{g,rw} r_{P/S} \times e3 - F_{g,rf} r_{G/S} \times e3) + T = \\ &\hat{n}_f(I_{cm,rf}\alpha_{rf} + \omega_{rf} \times I_{cm,rf}\omega_{rf} + m_{rf} r_{G/S} \times a_G + I_{cm,rw}\alpha_{rw} + \omega_{rw} \times I_{cm,rw}\omega_{rw} + m_{rw} r_{P/S} \times a_P), \end{aligned} \tag{A.7}$$

By taking the dot product of $\hat{n}_f$, vector equation (A.6), which consists of three scalar equations, is reduced to one scalar equation which concerns itself around the steering axis, which is scalar equation (A.7). Hence, the steering torque could be added straight into the scalar equations. Reorganizing equation (A.7) such that the unknown terms are on the left-hand side and the known terms on the right hand side leaves us with,

$$\begin{aligned} &\hat{n}_f(-I_{cm,rw}\alpha_{rw} - I_{cm,rf}\alpha_{rf} + r_{R/S} \times F_{rw} - m_{rw} r_{P/S} \times a_P - m_{rf} r_{G/S} \times a_G) = \\ &\hat{n}_f(F_{g,rw} r_{P/S} \times e3 + F_{g,rf} r_{G/S} \times e3 + \omega_{rf} \times I_{cm,rf}\omega_{rf} + \omega_{rw} \times I_{cm,rw}\omega_{rw}) - T, \end{aligned} \tag{A.8}$$

where T is clockwise for positive values.

B

State Space Implementation

This appendix shows the derivation of the state space of the bicycle-rider system based on the general equations of motion in the canonical form. For the derivation of the linear equations of motions themselves, one is referred to [20].

B.1. Linear Equations of Motion

As stated in chapter 2.1, the linear equations of motion of the uncontrolled bicycle can be expressed as,

$$M\ddot{q} + vC_1\dot{q} + \{gK_0 + v^2K_2\} = f, \tag{B.1}$$

where $q = \{\phi, \delta,\}^T$ and $f = \{T_\phi, T_\delta,\}^T$. Converting this to its state space form yields,

$$\begin{Bmatrix} \ddot{\phi} \\ \ddot{\delta} \\ \dot{\phi} \\ \dot{\delta} \end{Bmatrix} = \left[\begin{array}{cc|cc} -M^{-1}vC_1 & & -M^{-1}(gK_0 + v^2K_2) & \\ \hline 1 & 0 & 0 & 0 \\ 0 & 1 & 0 & 0 \end{array}\right] \begin{Bmatrix} \dot{\phi} \\ \dot{\delta} \\ \phi \\ \delta \end{Bmatrix} + \left[\begin{array}{cc} M^{-1} & \\ \hline 0 & 0 \\ 0 & 0 \end{array}\right] \begin{Bmatrix} T_\phi \\ T_\delta \end{Bmatrix}, \tag{B.2}$$

which can also be written in the following simplified form,

$$\dot{a} = Aq + Bu, \tag{B.3}$$

Add Integral State

To add the control of the rider, we need to increase the state vector by one to include the steering integral. Also, upper body lean torque is omitted in this thesis, which results in $T_\phi = 0$. Applying the latter and increasing the state vector results in,

$$\begin{Bmatrix} \ddot{\phi} \\ \ddot{\delta} \\ \dot{\phi} \\ \dot{\delta} \\ \delta \end{Bmatrix} = \left[\begin{array}{cc|cc|c} -M^{-1}vC_1 & & -M^{-1}(gK_0 + v^2K_2) & & 0 \\ \hline 1 & 0 & 0 & 0 & 0 \\ 0 & 1 & 0 & 0 & 0 \\ \hline 0 & 0 & 0 & 1 & 0 \end{array}\right] \begin{Bmatrix} \dot{\phi} \\ \dot{\delta} \\ \phi \\ \delta \\ \int \delta \end{Bmatrix} + \left[\begin{array}{cc} M^{-1} & \\ \hline 0 & 0 \\ 0 & 0 \\ \hline 0 & 0 \end{array}\right] \begin{Bmatrix} 0 \\ T_\delta \end{Bmatrix}, \tag{B.4}$$

Add Neuro-muscular Dynamics

The transfer function between neural signal and steering torque output is the second order function given and discussed in section **??**, rewriting this transfer function to state space results in,

$$\begin{Bmatrix} \ddot{T}_\delta \\ \dot{T}_\delta \end{Bmatrix} = \begin{bmatrix} -2\zeta\omega_c & -\omega_c^2 \\ 1 & 0 \end{bmatrix} \begin{Bmatrix} \dot{T}_\delta \\ T_\delta \end{Bmatrix} + \begin{bmatrix} \omega_c^2 \\ 0 \end{bmatrix} \alpha_{neural}, \tag{B.5}$$

Combining the state spaces of the extended, uncontrolled bicycle, eq. (B.4), and the neuromuscular dynamics, eq. (B.5) results in,

$$\begin{Bmatrix} \ddot{\phi} \\ \ddot{\delta} \\ \dot{\phi} \\ \dot{\delta} \\ \delta \\ \ddot{T}_\delta \\ \dot{T}_\delta \end{Bmatrix} = \left[\begin{array}{cc|cc|c|cc} -M^{-1}vC_1 & & -M^{-1}(gK_0 + v^2K_2) & & 0 & 0 & 0 \\ \hline 1 & 0 & 0 & 0 & 0 & 0 & 0 \\ 0 & 1 & 0 & 0 & 0 & 0 & 0 \\ \hline 0 & 0 & 0 & 1 & 0 & 0 & 0 \\ \hline 0 & 0 & 0 & 0 & 0 & -2\zeta\omega_c & -\omega_c^2 \\ 0 & 0 & 0 & 0 & 0 & 1 & 0 \end{array}\right] \begin{Bmatrix} \dot{\phi} \\ \dot{\delta} \\ \phi \\ \delta \\ \int \delta \\ \dot{T}_\delta \\ T_\delta \end{Bmatrix} + \left[\begin{array}{cc} M^{-1} & \\ \hline 0 & 0 \\ 0 & 0 \\ \hline 0 & 0 \\ \hline 0 & 0 \\ 0 & 0 \end{array}\right] \begin{Bmatrix} 0 \\ T_\delta \end{Bmatrix} + \left[\begin{array}{c} 0 \\ 0 \\ \hline 0 \\ 0 \\ \hline 0 \\ \omega_c^2 \\ 0 \end{array}\right] \alpha_{neural}, \tag{B.6}$$

where α_{neural} is the neural signal which is transformed into a steering torque output by the neuromuscular dynamics. This control signal has the form,

$$\alpha_{neural} = \begin{Bmatrix} K_{\phi d} & K_{\delta d} & K_{\phi p} & K_{\delta p} & K_{\delta i} \end{Bmatrix} \begin{Bmatrix} \dot{\phi} \\ \dot{\delta} \\ \phi \\ \delta \\ \int \delta \end{Bmatrix}, \tag{B.7}$$

then equation (B.7) and (B.6) can be combined and reduced to,

$$\begin{Bmatrix} \ddot{\phi} \\ \ddot{\delta} \\ \dot{\phi} \\ \dot{\delta} \\ \delta \\ \ddot{T}_\delta \\ \dot{T}_\delta \end{Bmatrix} = \left[\begin{array}{cc|cc|c|cc} -M^{-1}vC_1 & & -M^{-1}(gK_0 + v^2K_2) & & 0 & 0 & M^{-1}\begin{Bmatrix} 0 \\ 1 \end{Bmatrix} \\ \hline 1 & 0 & 0 & 0 & 0 & 0 & 0 \\ 0 & 1 & 0 & 0 & 0 & 0 & 0 \\ \hline 0 & 0 & 0 & 1 & 0 & 0 & 0 \\ \hline \omega_c K_{\phi d} & \omega_c K_{\delta d} & \omega_c K_{\phi p} & 0 & \omega_c K_{\delta i} & -2\zeta\omega_c & -\omega_c^2 \\ 0 & 0 & 0 & 0 & 0 & 1 & 0 \end{array}\right] \begin{Bmatrix} \dot{\phi} \\ \dot{\delta} \\ \phi \\ \delta \\ \int \delta \\ \dot{T}_\delta \\ T_\delta \end{Bmatrix}, \tag{B.8}$$

C

Damping Coefficient Extraction

An attempt has been made at identifying the eigenvalues of the motions, such that the characteristics of the motion could be quantified for larger perturbations. To identify the eigenvalues, an harmonic function is fitted to the numerical integration solution. This function has the following form,

$$f(t) = (Asin(\omega t) + Bcos(\omega t))e^{-\beta t} + E, \tag{C.1}$$

where the eigenvalues could be extracted using $Im(\lambda_{weave}) = \omega$ & $Re(\lambda_{weave}) = \beta$. The function is fitted onto the roll rate solution. The approach is taken from Kooijman *et al.*, whom used it for the experimental validation of the lateral dynamics of a bicycle on a treadmill [12].

For the solution that crash within t_{sim} seconds, the last 1/8th part of the signal has been cut to prevent bad fits.

Attempt 1: Unbounded Fminsearch & Roll Rate

The harmonic function is applied to the lean rate solutions for a velocity range of 0 to 10 ms^{-1} and the system is perturbed using 0.10 $rads^{-1}$ steer rate perturbations. The harmonic functions is fitted using the command FMINSEARCH with no bounds. The results are given in figure C.1. To observe how accurate the fit is, the eigenvalue diagram of the uncontrolled bicycle is plotted in the background. This could gave more insight than using the error of the fit.

In the lower velocity region, a vague trend can be seen but a significant amount of points lie far from the calculated eigenvalues. The fit gets more accurate upon reaching the stable region and has a slight struggle when the real eigenvalues cross. A large part of the points are off.

Attempt 2. Unbounded Fminsearch & Steer Rate

The algorithm struggles to fit correctly across the velocity range where the weave motion dominates. This motion is characterized by the pivoting motion of the front assembly across the handlebars. Therefore, the steer rate was considered for the fit as well. To prevent the steer rate disturbance from influencing the fit, the first part of the signal has been eliminated.

Attempt 3. Bounded Fmincon & Roll Rate

The roll rate proved to be a better fit and is used here as well as for all undocumented attempts in between here and the previous section. To acquire a proper fit with the eigenvalues, bounds had been set on the magnitude of the signal. This still did not give the desired result. From the previous fits, it could already be observed that the motion is dominated by the least negative eigenvalue. Therefore, the crossing points of the real eigenvalues had been used to switch the harmonic function to one that suits capsize motion. This had the following form,

$$f(t) = De^{-\gamma t}, \tag{C.2}$$

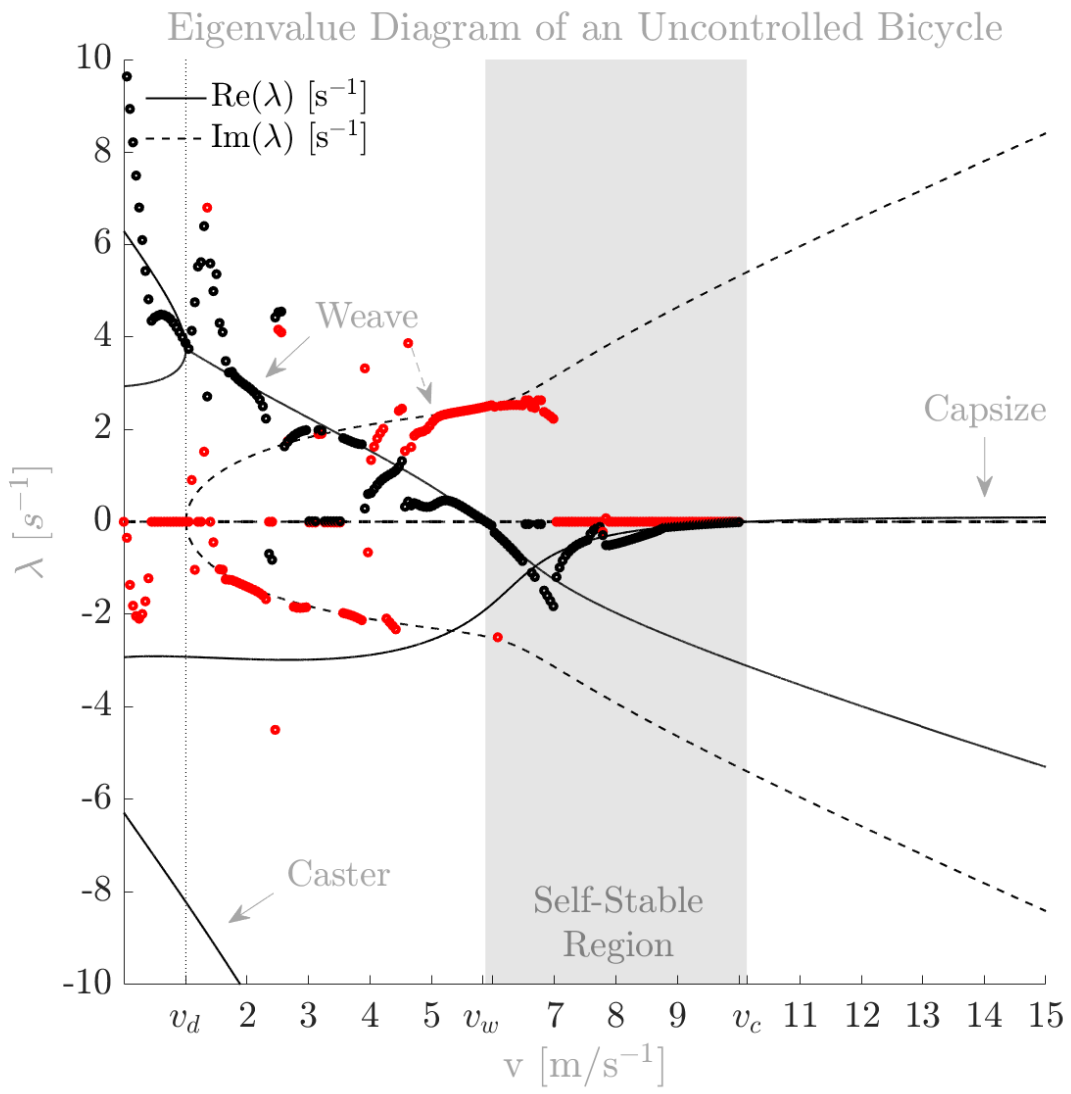

Figure C.1: Eigenvalue estimation from numerical integration solution of the nonlinear equations of motion[2] of the WCBM bicycle model. The correct eigenvalues derived from the linear equations of motion [20] are displayed in gray on the background. The red dots are the estimated frequencies and the black dots the damping coefficient of the motion. The extraction is done via the fitting of an harmonic function onto the lean rate solution. The algorithm is a fminsearch without bounds. All simulations have been performed using 0.1 rads^{-1} steer rate disturbance.

for which γ has been plotted by the yellow dots in C.3. On top of it, most outliers had been removed which had an error considered too high. Only then, a fairly decent fit with the eigenvalue diagram could be made.

Discussion Eigenvalue Extraction

The problem with this approach is that the velocity of the most negative real eigenvalue will likely change for larger perturbations. Also, the error for outlier eliminated has been picked by changing the value and observing the fit w.r.t the eigenvalue diagram. On top of that, a heuristically chosen part of the signal has been fitted to. It is not known is that is the same crucial part for larger disturbances.

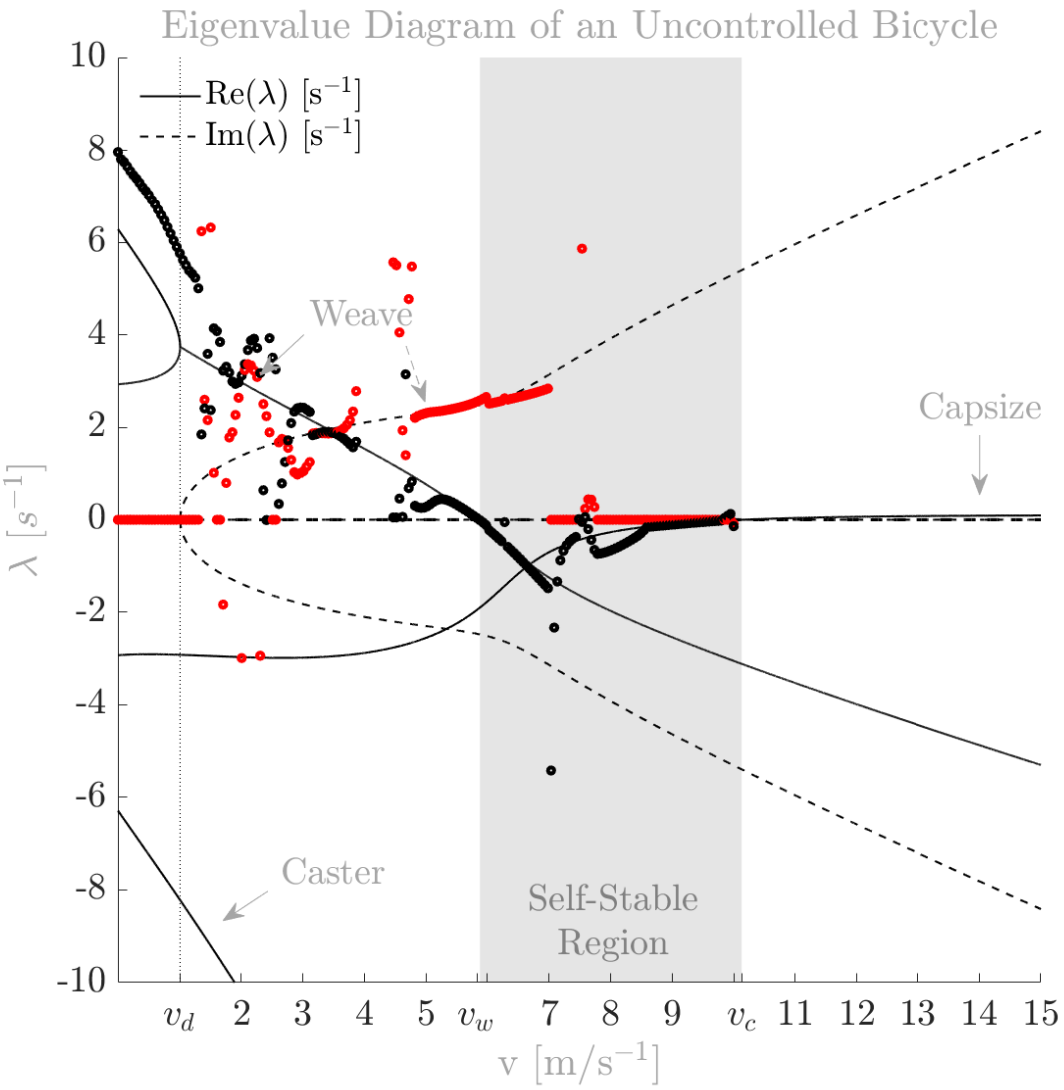

Figure C.2: Eigenvalue estimation from numerical integration solution of the nonlinear equations of motion[2] of the WCBM bicycle model. The correct eigenvalues derived from the linear equations of motion [20] are displayed in gray on the background. The red dots are the estimated frequencies and the black dots the damping coefficient of the motion. The extraction is done via the fitting of an harmonic function onto the steer rate solution. The algorithm is a fminsearch without bounds. All simulations have been performed using 0.1 rads^{-1} steer rate disturbance.

Conclusion

The results of the eigenvalue diagram are thought to be unreliable. Therefore, it has not been used in this thesis.

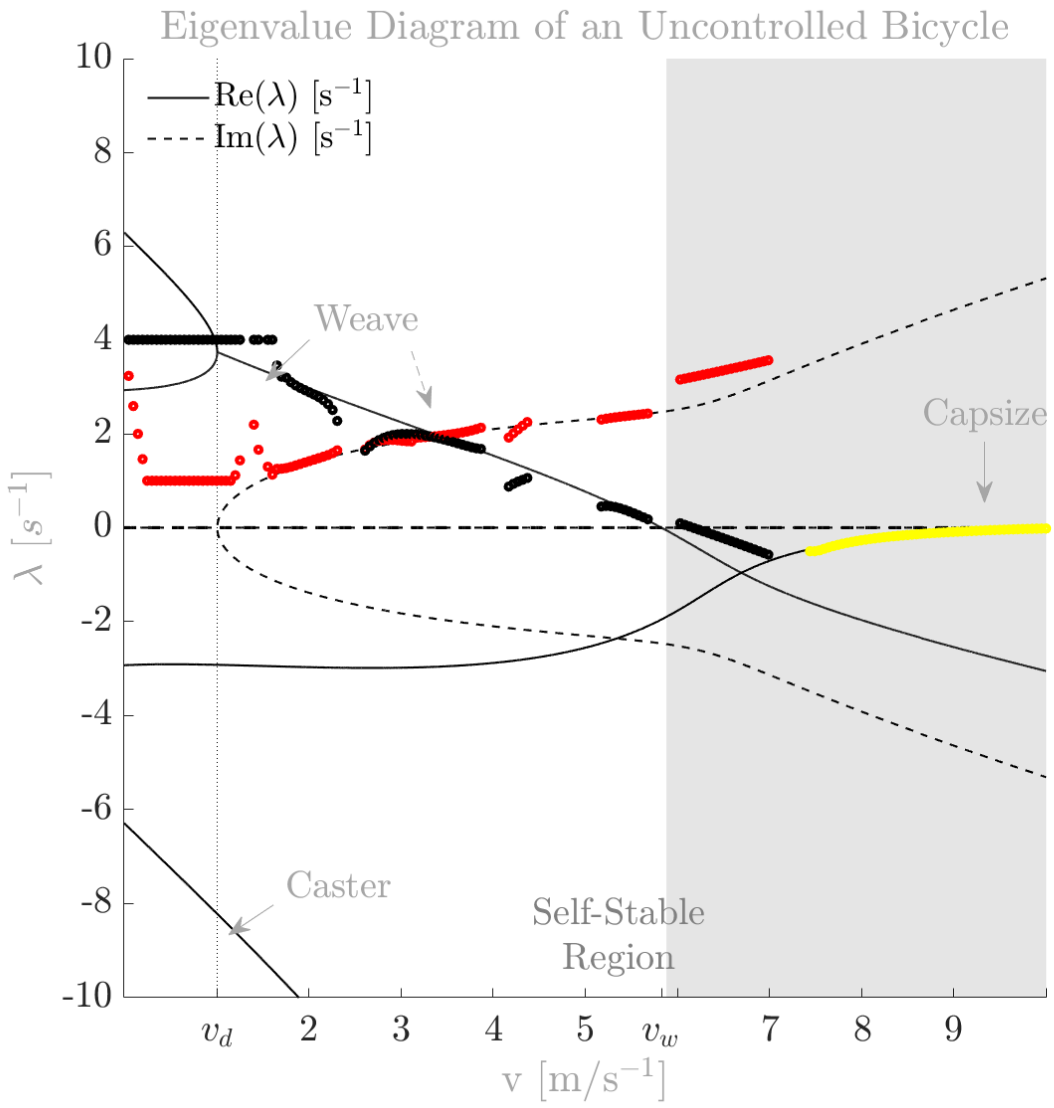

Figure C.3: Eigenvalue estimation from numerical integration solution of the nonlinear equations of motion[2] of the WCBM bicycle model. The correct eigenvalues derived from the linear equations of motion [20] are displayed in gray on the background. The red dots are the estimated frequencies of the motion, the black dots the damping coefficient of the weave motion and the yellow dots of the capsize motion. The extraction is done via the fitting of an harmonic function onto the roll rate solution. At 7 ms^{-1} the harmonic functions changes to adapt itself to the capsize motion. The algorithm is a fmincon with bounds put on the function based on the derived eigenvalues. All simulations have been performed using 0.1 $rads^{-1}$ steer rate disturbance.

D

Convergence Study

The errors accumulating in the process of integration the equations of motion are dependent on the solver and its settings used in the integration process. Those errors are truncation errors and round-off errors which emerge in the integration process and they can significantly influence the outcome, especially if the problem at hand is highly sensitive to small changes in its variables. Therefore, a convergence study is performed.

To do a convergence study, several integration methods have to be chosen. Since a large collection of methods exist, all for different purposes and accuracy's, a selection has to be made beforehand. The choices made are explained in section D.1. Once the solvers have been chosen, they will integrate the problem for several different initial conditions. Picking multiple initial conditions is necessary since some solution may be smooth whereas others may contain high frequency components which might be harder to integrate, causing the integrator to "step over" those components leading to a deviating solution. The simulation points are chosen in section D.2.

The error estimation method chosen for this problem and for the solvers is elaborated upon in section D.3 after which the results of the convergence study are shown in D.6. The results are discussed in section D.7.

D.1. Numerical Methods Selection

Several methods for ordinary differential equations exists, of which commonly used are the Runge-Kutta methods. The MATLAB ODE-functions are also based on these methods. The main difference between both are the integration steps used; MATLAB's function has been written such that it uses tolerances on the errors to determine optimized step sizes whereas a general Runge-Kutta scheme is based on a fixed time-step.

To find the solver and their settings which are most suitable for the bicycle equations of Basu-Mandal, convergence tests are required. Chosen for comparison are a Runge-Kutta 4 and Runge-Kutta-Fehlberg 45 scheme with fixed time steps, the ode45 function from MATLAB which they recommend to be your first choice for variable time steps and the ode15s which is more suited for stiff equations.

If the solution reaches a stiff area, the ode45 might get "stuck" since it will need a lot of integration steps due to its tolerances which results in large computation times. The ode15s uses a different process for the determination of the required time steps and uses more time steps on the stiff areas but quickly enlarges the time-steps after. Moreover, the ode15s can solve algebraic equations which are present in the equations resulting from the Newton-Euler approach. The ode15s solver might be more suitable for the evaluation of the bicycle equations, since especially near the border of the stability region, stiff regions in the solutions are expected.

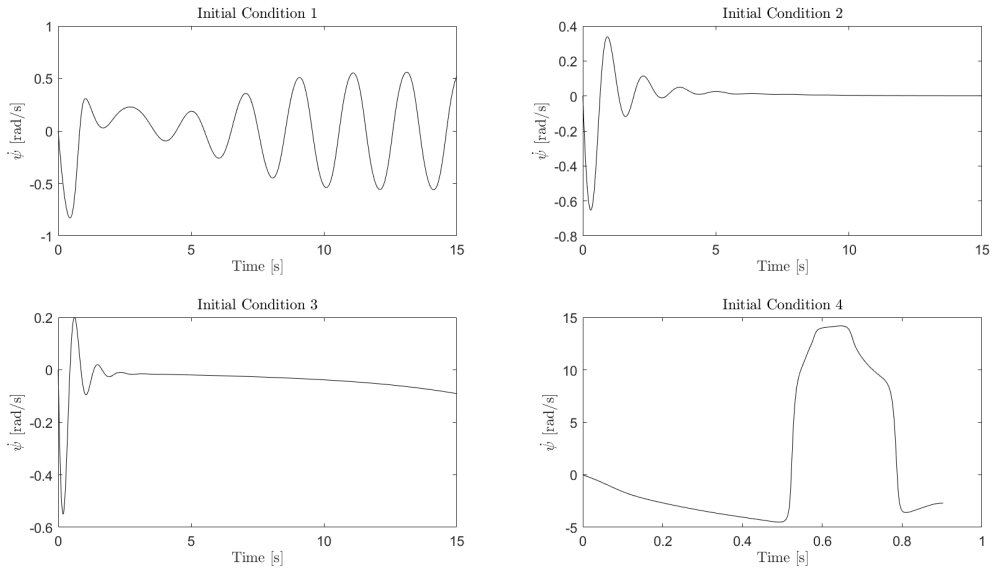

Figure D.1: The solutions of the simulation points used for the convergence study. The left-top plot shows the solution for the initial conditions from the weave region. The top-right plot shows the solution for the initial conditions from the stable region. The left-bottom plot shows the solution for the initial conditions from the capsize region and the right-bottom plot shows the solution for the initial conditions from the unstable, chaotic area.

The Runge-Kutta-Fehlberg 45 scheme is of a higher order than the Runge-Kutta 4 and, thus, evaluates the function at more points. It produces both a fourth and fifth order solution, only the fifth is chosen to be displayed in the graphs.

D.2. Evaluation Points

Prior to comparing the four solver amongst each other, it is necessary to find the optimal settings of each solver. This is done by comparing the solver for several tolerances or time steps amongst themselves. For one initial value problem and various tolerances the solver may converge to be nearly identical, whereas for other initial value problems this may not be the case.

To prevent picking an inappropriate tolerance, four initial conditions from four regions of the uncontrolled bicycle mentioned in Meijaard *et al.* have been chosen. The first initial condition evaluated, an initial velocity and disturbance of 4 m/s and 0.5 rad/s, respectively, lies in the weave area and is named "Initial Condition 1". The second, an initial velocity and disturbance of 5 m/s and 0.5 rad/s, respectively, lies in the stable region and is named "Initial Condition 2". The third, an initial velocity and disturbance of 7 m/s and 0.5 rad/s, respectively, lies in the capsize zone and the last, with an initial velocity and disturbance of 3 m/s and 3 rad/s, respectively, is suspected to lie in the unstable region due to the large magnitude of the disturbance and the low velocity. The last two conditions are named "Initial Condition 3" and "Initial Condition 4", respectively. Using the ode45 solvers for a tolerances of 10^{-9} the bicycle equations are integrated for 15 seconds to give insight in the solutions of the chosen simulation points. These solutions are displayed in figure D.1

D.3. Numerical Methods and Estimated Errors Explained

Since numerical methods make an estimation of the unknown, true solution, the error is not known as well. However, since most numerical methods make use of a truncated part of the Taylor expansion for their integration schemes, the order of the truncation error is known as well. The exact derivation is irrelevant for this research, but the sources of the errors and the integration schemes will be explained in this section for both the ode solvers and the Runge-Kutta schemes.

D.4. Numerical Scheme and Estimated error of the Runge-Kutta method

The Runge-Kutta schemes make use of a fixed time step between which the function is evaluated at various points dependent on the scheme used. The scheme of the Runge-Kutta 4 method is,

$$k_1 = dt\frac{dy}{dt}(t_n, y_n) \tag{D.1}$$
$$k_2 = dt\frac{dy}{dt}(t_n + \frac{1}{2}dt, y_n + \frac{1}{2}k_1) \tag{D.2}$$
$$k_3 = dt\frac{dy}{dt}(t_n + \frac{1}{2}dt, y_n + \frac{1}{2}k_2) \tag{D.3}$$
$$k_4 = dt\frac{dy}{dt}(t_n + dt, y_n + k_3) \tag{D.4}$$
$$y_{n+1}^{[4]} = y_n + \frac{1}{6}(k_1 + 2k_2 + 2k_3 + k_4) \tag{D.5}$$

and the scheme for the Runge-Kutta-Fehlberg method is,

$$k_1 = dt\frac{dy}{dt}(t_n, y_n) \tag{D.6}$$
$$k_2 = dt\frac{dy}{dt}(t_n + \frac{1}{4}dt, y_n + \frac{1}{4}k_1) \tag{D.7}$$
$$k_3 = dt\frac{dy}{dt}(t_n + \frac{3}{8}dt, y_n + \frac{3}{32}k_1 + \frac{9}{32}k_2) \tag{D.8}$$
$$k_4 = dt\frac{dy}{dt}(t_n + \frac{12}{13}dt, y_n + \frac{1932}{2197}k_1 - \frac{7200}{2197}k_2 + \frac{7296}{2197}k_3) \tag{D.9}$$
$$k_5 = dt\frac{dy}{dt}(t_n + dt, y_n + \frac{439}{216}k_1 - 8k_2 + \frac{3680}{513}k_3 - \frac{845}{4104}k_4) \tag{D.10}$$
$$k_6 = dt\frac{dy}{dt}(t_n + \frac{1}{2}dt, y_n - \frac{8}{27}k + 28k_2 - \frac{3544}{2565}k_3 + \frac{1859}{4104}k_4 - \frac{11}{40}k_5) \tag{D.11}$$
$$y_{n+1}^{[5]} = y_n + (\frac{16}{135}k_1 + \frac{6656}{12825}k_2 + \frac{28561}{56430}k_4 - \frac{9}{50}k_5 + \frac{2}{55}k_6) \tag{D.12}$$

of which y is the estimated value of the true value, $\overline{y}$. The difference between the true and estimated value is dominated by the truncation and round-off errors. The truncation term is largely influenced by the truncation of the Taylor expansion series the scheme is based upon, hence the name, and its estimate takes on the form

$$E_{\text{truncation}} = C_1 dt^p \tag{D.13}$$

where p is the order of the integration scheme used and C_1 is a vector with unknown coefficients. Mere intuition should tell you that this error will decay with decreasing time steps and/or higher order schemes. It is the other way around for the round-off errors, each time the function is evaluated and its solution used another round-off error is added to the overall solution. The estimate of this type of error can be written as

$$E_{\text{round-off}} = C_2 \frac{1}{dt} \tag{D.14}$$

Taking into account the truncation and round-off errors, it can be said that the estimated value of the true value is,

$$y = \overline{y} + C_1 dt^p + C_2 \frac{1}{dt} \tag{D.15}$$

This leaves us with three unknowns, the two error vectors containing the constants and the vector containing the truth. However, an important characteristic can be seen and used. There is only one step size for which the global error is the smallest and the estimate the closest to the true value since both error term are dependent of the time step in an opposite manner; the truncation error is non-linearly proportional whereas the round-off error is inversely proportional. Estimating the true value for a large step size and a slightly smaller step size, then looking at the difference will tell us about the decay of the truncation error since it is dominant in the large step size area. Repeating this process until the difference starts to grow again, will give us the optimal time step to use since if the difference starts to grow again it has to be the round-off errors accumulating.

D.5. Ode Tolerances

The tolerances set are bounds put on the estimated global error, whereas the global error is defined as:

$$\epsilon_{global} = \|y_n - \hat{y}_n\| \tag{D.16}$$

In this equation, the estimated states are indicated by $\hat{y}$. If the global error exceeds those bounds, a smaller time step is taken. For the tolerances of the ode solvers, only the absolute tolerance is taken into account since it is dominant for estimated state values close to zero. For clarity, the use of both tolerances will be explained.

D.5.1. Absolute and Relative Tolerances

The relative tolerance is multiplied by the estimated state values and if the estimated global error is larger than this value then the solver will repeat the integration at that time for a smaller time step. The absolute tolerance is the tolerance set on the estimated error itself and is thus the absolute, estimated difference between the true states and the estimated state of the solver (see equation (D.16)). Setting the tolerances will result in repeating an integration step for a smaller time step if,

$$\epsilon_{global} > \text{AbsTol} \tag{D.17}$$

$$\text{or} \tag{D.18}$$

$$\epsilon_{global} > \text{RelTol} \cdot \|\hat{y}_n\| \tag{D.19}$$

Since MATLAB's ode solver do not output their error and the solvers make use of Runge-Kutta schemes, the error can be estimate in a similar way as has been done for the Runge-Kutta schemes. Having a lower tolerance will result in smaller time steps, which will lead to an accumulation of round-off errors and a larger tolerance will lead to truncation errors.

D.6. Convergence Results

For both Runge-Kutta schemes, the results are shown in figure D.2. As has been explained above and can now be seen, the point where the decline stops and the growth of the global error starts. The lowest point differs but is approximately the same for the first three initial conditions and lies around 10^{-4} for the Runge-Kutta 4 scheme. A time step this size would result in a solution closest to the truth, yet is has the drawback which is a large computational time.

For the last set of initial conditions, no convergence of the estimated error can be found and its magnitude lies in the range $0.1<0<1.5$ which is significantly large compared to the maximum value found in the estimated solution corresponding to this set of conditions. Also, several red markers are visible indicating a solution which crashed. These crashes lead to large differences in the resulting states

and as a result the global error estimated are inaccurate and unreliable. However, it is known that the Runge-Kutta schemes and their fixed time steps are often led astray by the presence of stiffness in the solution which would explain the crashes for non-sequential time steps. The unreliability of the error estimated also renders the Runge-Kutta 4 scheme unreliable.

For the Runge-Kutta-Fehlberg no minimum is found, merely a timestep for which the gradient changes. This change might be due to the start of the accumulation of the round-off errors. The truncation errors still decline faster for smaller times steps than the round-off errors grow, preventing the sign change of the gradient.

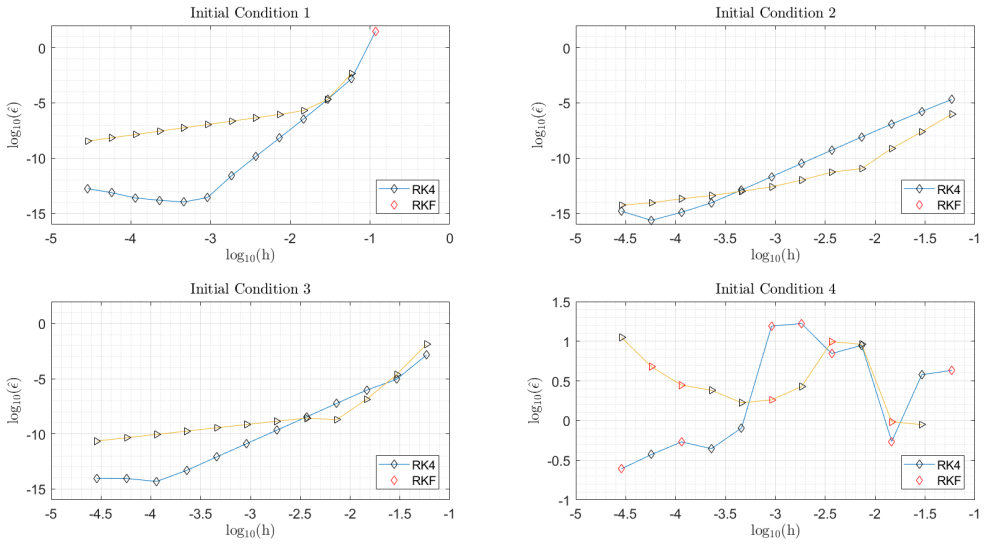

Figure D.2: The estimated errors for the Runge-Kutta 4 and the Runge-Kutta-Fehlberg method for various stepsizes. Initial condition 1 lies in the weave region, initial condition 2 in the stable region, initial condition 3 in the capsize region and initial condition 4 in an unstable chaos area. The red marker indicate a solution with a shorter simulation time due to the discontinuation of the integration process by the stopping criteria. The simulations have been performed for 15 seconds.

The graphs displaying the results of the ODE solvers, see figure D.3, have a similar overall shape compared to the results of the Runge-Kutta 4 scheme shown in figure D.2. Note that the main difference between the schemes and the solvers is the variable on the x-axis. The estimated error is plotted versus the tolerance, whereas for the RK schemes the time steps were used.

As can be seen for the first three initial conditions, the ode45 solver carries a smaller error estimate until an absolute tolerance of approximately 10^{-15} has been taken. At this point the error estimate stagnates which is due to the build-up of round-off errors since for such a tolerance the solvers will take very small time-steps. The result for the fourth condition is different, due to stiffness being present in the solution. The ode15s is build to conquer the stiffness present in the solution, whereas as expected, the ode45 has trouble minimizing its error. The difference is significant, ode45 has a minimum error estimate of about 10^{-5} which stagnates for a tolerance of 10^{-12} and the ode15s has an minimum error estimate of approximately 10^{-10} for a tolerance of 10^{-15}. Do note that the tolerances set in MATLAB for the ode solvers are merely bounds set on the local discretization errors and the errors estimated here are global; the error estimates in figure D.3 can exceed their corresponding tolerance.

D.7. Discussion

The Runge-Kutta schemes are not able to handle the high frequency components present in the solution of the fourth initial condition. The ode45 is able to reach a minimal estimated error of 10^{-6} for the chaotic conditions for a tolerance of approximately 10^{-14} which is a decent error, yet a very small tolerance. The ode15s, however, can have an estimated error as small as 10^{-10} at a tolerance slightly smaller than 10^{-12}, for the same initial conditions. The remaining question is which error is acceptable, since

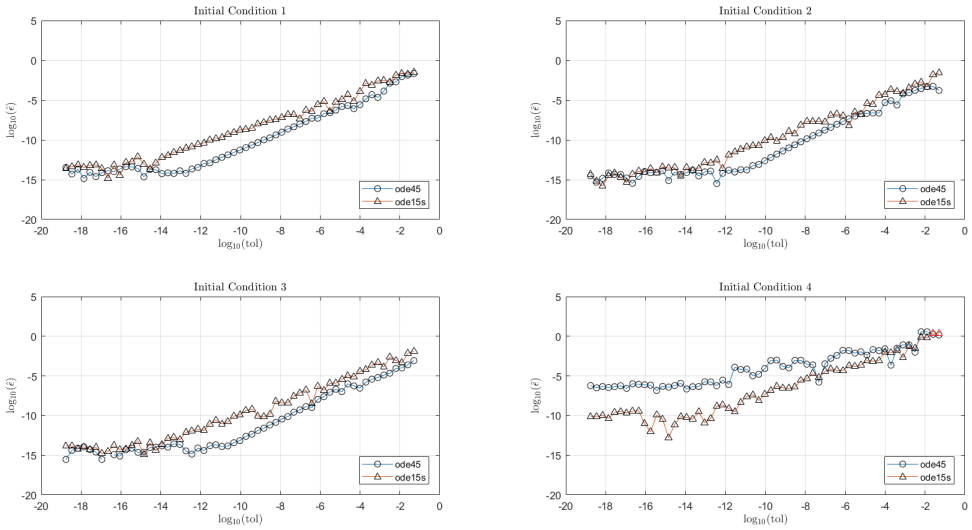

Figure D.3: The estimated errors for the ode45 and ode15s solvers for various tolerances. Initial condition 1 lies in the weave region, initial condition 2 in the stable region, initial condition 3 in the capsize region and initial condition 4 in an unstable chaos area. The red marker indicate a solution with a shorter simulation time due to the discontinuation of the integration process by the stopping criteria. The simulations have been performed for 15 seconds.

the numerical method choice is a trade-off between computational time and accuracy. It is unknown whether those four evaluated initial conditions are representative for all the conditions to be evaluated and which error magnitude has a large influence on the solutions, however, the errors read from the graphs are the errors after 15 seconds of integration. An error smaller than 10^{-5} will be assumed to be more than sufficient and is reached by ode15s for the last initial condition at a tolerance of 10^{-8}, whereas the ode45 needs a tolerance of 10^{-12} to reach that value. Considering the trade-off between time and accuracy, the ode15s will be chosen, combined with a tolerance of 10^{-8}, for the numerical evaluation of the bicycle dynamics.

E

Mechanical Parameters of the Bicycle

The bicycle used in the experiments have been measured according to [37]. However, the 25 mechanical parameters and the coefficient matrices of [31], tables 6 & 7, do not match. Contact with the author revealed that the measurements has been redone, but only the matrices were updated before publication. This resulted in only a slight discrepancy which barely effects the open-loop dynamics of the bicycle. However, preferably, all unnecessary mistakes are eliminated. Therefore, the old and new values are given here. The old mechanical parameters are given in gray, those led to the coefficient matrices given in gray. The correct values are given in black.

Coefficient Matrices

The combined bicycle and rider properties result in the following coefficient matrices of the canonical linearized equations of motion given in equation (2.2),

$$M = \begin{bmatrix} 133.32(131.51) & 2.44(2.68) \\ 2.44(2.68) & 0.22(0.25) \end{bmatrix}, \quad K_0 = \begin{bmatrix} -116.73(-116.19) & -2.48(-2.76) \\ -2.48(-2.76) & -0.77(-0.95) \end{bmatrix}$$

$$C_1 = \begin{bmatrix} 0 & 44.66(42.75) \\ -0.32 & 1.46(1.60) \end{bmatrix}, \quad K_2 = \begin{bmatrix} 0 & 104.86(102.02) \\ 0 & 2.30(2.50) \end{bmatrix}$$

where the matrix values resulting from the old mechanical parameters have been put in gray. The mathematical derivation of these matrices is given in Appendix A of [20].

Parameter	Symbol	Value
wheel base	w	1.076 m
trail	c	0.060 - (0.072)m
steer axis tilt (π/2-head angle)	λ	0.317 - (0.350)rad
gravity	g	9.81 ms^{-2}
forward speed	v	various ms^{-1}
***R**ear wheel R*		
radius	r_R	0.336 m
mass	m_R	4.9 kg
mass moments of inertia	(I_{Rxx}, I_{Ryy})	(0.070,0.129) kg m^2
*rear **B**ody and frame assembly B*		
position centre of mass	(x_B, z_B)	(0.349,-1.027) - (0.332,-1.022)m
mass	m_B	106.4 kg
mass moments of inertia	$\begin{bmatrix} I_{Bxx} & 0 & I_{Bxz} \\ 0 & I_{Byy} & 0 \\ I_{Bzx} & 0 & I_{Bzz} \end{bmatrix}$	$\begin{bmatrix} 13.690 & 0 & -0.259 \\ 0 & 16.472 & 0 \\ -0.259 & 0 & 4.112 \end{bmatrix}$ kg m^2 $\begin{bmatrix} 13.997 & 0 & -0.611 \\ 0 & 15.463 & 0 \\ -0.611 & 0 & 4.428 \end{bmatrix}$ *kg m^2*
*front **H**andlebar and fork assembly H*		
position centre of mass	(x_H, z_H)	(0.809,-0.977) - (0.818,-0.986)m
mass	m_H	5.4 kg
mass moments of inertia	$\begin{bmatrix} I_{Hxx} & 0 & I_{Hxz} \\ 0 & I_{Hyy} & 0 \\ I_{Hzx} & 0 & I_{Hzz} \end{bmatrix}$	$\begin{bmatrix} 0.344 & 0 & -0.092 \\ 0 & 0.340 & 0 \\ -0.092 & 0 & 0.103 \end{bmatrix}$ kg m^2 $\begin{bmatrix} 0.338 & 0 & -0.100 \\ 0 & 0.340 & 0 \\ -0.100 & 0 & 0.109 \end{bmatrix}$ *kg m^2*
Front wheel F		
radius	r_F	0.336 m
mass	m_F	1.55 kg
mass moments of inertia	(I_{Fxx}, I_{Fyy})	(0.052,0.098) kg m^2

Table E.1: All 25 parameters which characterize the bicycle with their corresponding denotations. Given in gray are the bicycle parameters as given in [31]. Given in black are the parameters corresponding to the bicycle's mass, stiffness and damping matrices as given in [31]. The discrepancy was caused due to measurement being redone on the bicycle's properties.

F

Control Strategy of the Young Cyclist

This section elaborates on the control identification of the young cyclist. In section F.1, the control is identified for the discrete experimental velocities. Then, in section F.2, the control is made continuous over velocity. At last, in section F.3, the control strategy of the young cyclist is analyzed.

F.1. Part i. Crucial Feedback Gains

In this section, the crucial feedback gains for the young cyclist are sought. Those feedback gains are found using the parameter reduction process explained in section 2.1.3. This results of this reduction process are given in section F.1.1. Having found the reduced sets, the next step is to estimate its parameters. This is done in section F.1.2.

F.1.1. Reduction Process

The reduction process is performed for one data set per velocity group, due to the time consuming nature of the optimization process. The results of the parameter reduction process are given in table F.3. Since De Lange mentioned the unreliability of data set 248, the process is also performed for run 249.

Half of the data sets are described accurately using five feedback parameters. Those parameters are,

$$\theta(s) = [K_{\phi p}, K_{\phi d}, K_{\delta i}, K_{\delta d}, K_{\delta dd}]^T. \tag{F.1}$$

The most reduced parameter set which is able to describe their corresponding data set accurately; with a VAF of 90% or higher; are the highlighted rows of the table. Data set 256 is described fairly accurate, with a VAF of 88.66%, by those five parameters.

The data sets of the lowest two velocities, run 248 and 249, yield a completely different reduction and results. De Lange rendered the FIR model of run 248 unreliable due to the high signal to noise ratio. His hypothesis behind the ratio was the increased control, which dominates the output. Therefore, it is likely that this also effects the reduction of run 249.

Even though the parameter space optimum is seemingly different for the lowest velocities, these data sets only require three and two parameters for describing the data. Then, it is very likely that the data can also be described using the five parameters of (F.1). Therefore, those five feedback parameters will be used to describe the linear control response of the young cyclist.

F.1.2. Estimating the Reduced Parameter Sets

The reduced parameter set which dictates the control response of the young cyclist has been selected. To see whether those parameters are definitely able to describe the control response for all velocities accurately, their parameters are estimated for all fifteen data sets. The results are given in table F.2.

All parameter sets can describe their corresponding data accurately, or, in case of run 256, fairly accurately. And, as predicted, those five parameter sets are also able to describe the data sets of the lowest velocity groups accurately.

F.2. Part i. Velocity-Dependent Feedback Parameter Function

As explained in section 2.3, the feedback parameters need to be continuous over forward velocity. Therefore, a linear regression is performed per feedback parameter. The resulting parameter functions are of the form,

$$f_{\theta_{LR}}(v) = \begin{bmatrix} K_{\phi p} \\ K_{\phi d} \\ K_{\delta i} \\ K_{\delta d} \\ K_{\delta dd} \end{bmatrix} = \begin{bmatrix} -0.79 \\ -1.5 \\ 161.4 \\ -1.3 \\ -0.01454 \end{bmatrix} v + \begin{bmatrix} 59 \\ 51 \\ -356.5 \\ -0.64 \\ -0.1915 \end{bmatrix}, \tag{F.2}$$

which have been visualized in figure 3.1. Along with the linear regression, two functions based on interpolation are plotted in that figure as well. As a reminder, one interpolation is based on the parameter sets with the highest VAF per velocity group $f_{\theta_{LI,mean}}(v)$ and the other on the average parameter value per velocity group $f_{\theta_{LI,mean}}(v)$.

To quantify the quality of the fit, the R^2 is calculated for each feedback parameter for the three functions. The result is given in table F.1

R^2	$f(s,\theta_{LR}(v))$	$f(s,\theta_{LI,mean}(v))$	$f(s,\theta_{LI,HV}(v))$
$K_{\phi p}$	0.005	0.496	0.050
$K_{\phi d}$	0.107	0.740	0.532
$K_{\delta i}$	0.855	0.958	0.909
$K_{\delta d}$	0.797	0.930	0.881
$K_{\delta dd}$	0.130	0.732	0.596

Table F.1: Coefficients of determination R^2 between three functions $f(s,\theta(v))$ which predict five feedback gains over velocity. The three functions are based on a linear regression $f(s,\theta_{LR}(v))$, linear interpolation between the mean parameters per velocity group f$(s,\theta_{LI,mean}(v))$ and linear interpolation between the parameter with the highest VAF per velocity group f$(s,\theta_{LI,HV}(v))$. All coefficients of determination below 0.2 have been marked gray.

Overall, all functions describe the trend of the mean and some of the variation of the parameters which indicates decent fits. The linear regression, however, has three coefficients <0.2. This indicates a high variance of those three parameters, which is not captured by the regression and is best captured by the interpolation between the mean values.

F.3. Part i. Control Response Analysis

The control of the rider is now continuous and the gray box model can be used for the identification of its BoA. But, what does the control response tell us about the young cyclist? Does the inclusion of nonzero time delay yield significant different feedback parameters compared to [31]?

Similar to the findings in the rider identification paper [31], the integral steer parameter $K_{\delta i}$ significantly increases over time. This makes sense since the integral steering seems to be related to the heading, hence, at larger velocities the heading will accumulate much faster and will quickly result in a heading error which is unwanted when cycling on a narrow treadmill. The proportional and derivative roll feedback, $K_{\phi p}$ and $K_{\phi d}$ resp., are always positive, which is as expected since they then correspond to the principle of steer-into-the-fall. The integral of the roll angle $K_{\phi i}$ is eliminated in every case and also has no further logical, physical interpretation.

The fifth crucial feedback parameter is the steering acceleration feedback parameter $K_{\delta dd}$. An acceleration feedback functions in a sense like a lead, and it is likely that this feedback is used to compensate

for the presence of the neural time delay τ_d of 30 ms. This would explain the addition of this crucial feedback parameter to the identified, reduced parameter set of [31].

Model τ_d=30 ms	$K_{\phi p}$	$K_{\phi d}$	$K_{\delta i}$	$K_{\delta d}$	$K_{\delta dd}$	**VAF**
248 K(s,θ(v=2.1 m/s))	44.08	51.7	45.18	-3.92	-0.29	93.82
249 K(s,θ(v=2.2 m/s))	71.05	56.1	68.65	-4.12	-0.26	96.97
250 K(s,θ(v=2.2 m/s))	43.21	46.94	45.24	-3.876	-0.19	93.90
184 K(s,θ(v=3.2 m/s))	34.51	37.78	98.74	-4.82	-0.18	93.76
185 K(s,θ(v=3.2 m/s))	57.10	42.39	135.5	-4.79	-0.20	97.81
186 K(s,θ(v=3.2 m/s))	51.64	44.86	121.1	-4.99	-0.23	96.93
251 K(s,θ(v=4.3 m/s))	121.8	59.65	475.90	-6.31	-0.35	97.59
252 K(s,θ(v=4.3 m/s))	65.52	47.87	321.43	-5.82	-0.28	96.47
253 K(s,θ(v=4.3 m/s))	61.73	44.88	279.90	-5.928	-0.25	96.41
190 K(s,θ(v=6.0 m/s))	46.54	36.78	512.69	-7.25	-0.23	98.43
191 K(s,θ(v=6.1 m/s))	37.27	32.88	445.1	-7.13	-0.18	94.55
192 K(s,θ(v=6.1 m/s))	33.61	27.98	377.60	-6.18	-0.14	91.98
255 K(s,θ(v=7.3 m/s))	44.79	42.38	812.7	-10.77	-0.30	91.64
256 K(s,θ(v=7.3 m/s))	57.45	50.12	956.08	-13.65	-0.42	88.66
257 K(s,θ(v=7.4 m/s))	64.66	48.63	1106.0	-10.54	-0.37	93.67

Table F.2: Estimation results of the reduced parameter set using various experimental data sets acquired at a range of forward velocities v, based on the gray box model consisting of controller K(s, θ), neuro-muscular dynamics G_{nm} and an effective neural time delay, $G_{\tau d}$, of 30 ms. The identified parameter vectors θ consist of a roll proportional gain $K_{\phi p}$ (Nm/rad), roll derivative gain $K_{\phi d}$ (Nm s/rad), steer integral gain $K_{\delta i}$ (Nm/(s rad)), steer derivative gain $K_{\delta d}$(Nm s/rad) and steer 2^{nd} derivative gain $K_{\delta dd}$ (Nm s^2/rad) and is given with its Variance Accounted For (VAF) (%).

Model τ_d=30 ms	$K_{\phi p}$	$K_{\phi i}$	$K_{\phi d}$	$K_{\phi dd}$	$K_{\delta p}$	$K_{\delta i}$	$K_{\delta d}$	$K_{\delta dd}$	***VAF***
run 248: **K**(s,θ(v=2.1))	-5.31	0.57	4.13	3.10	-1.23	0.37	0.82	0.05	94.53
	29.21	199.45	52.32	-2.11	-8.08		-5.75	-0.33	91.31
		2.02	3.29	2.94	-2.54		0.70	0.05	93.08
			2.59	3.03	-2.55		0.80	0.05	93.06
				3.62	-2.96		1.32	0.03	91.43
				4.04	-2.80		1.51		90.27
				5.49			2.18		65.86
run 249: **K**(s,θ(v=2.2))	63.02	-31.57	36.17	1.98	-0.79	53.96	-1.96	-0.16	99.03
	54.90	-28.08	34.44	2.17		49.23	-1.74	-0.15	99.03
	45.16		33.91	2.01		39.99	-1.85	-0.14	98.83
	19.89		16.65	3.49		17.38		-0.07	97.56
	7.25		11.99	3.04		6.71			94.75
			10.83	2.91		2.42			92.82
			10.18	3.03					92.10
				6.82					0
run 184: **K**(s,θ(v=3.2))	121.71	-81.55	49.65	-1.42	-25.90	205.33	-7.11	-0.46	98.27
	81.85	-63.72	37.67		-13.40	151.32	-4.55	-0.32	98.12
	61.82		33.41		-11.72	102.94	-4.45	-0.25	97.07
	34.51		37.78			98.74	-4.82	-0.18	93.76
	11.78		21.77			44.68	-3.05		77.36
run 252: **K**(s,θ(v=4.3))	171.27	-225.36	75.63	-2.14	-34.48	696.76	-10.34	-0.63	99.00
	108.02	-168.89	55.58		-5.37	500.28	-5.78	-0.41	98.66
	101.60	-181.49	58.20			521.55	-5.86	-0.40	98.50
	65.52		47.87			321.43	-5.82	-0.28	96.47
	18.49		22.56			80.09	-4.13		72.86
			20.39			27.75	-4.14		65.39
			20.264				-4.53		66.84
							-2.74		0
run 190: **K**(s,θ(v=6.0))	67.64	-55.22	45.87	-0.59	-15.34	722.08	-9.38	-0.35	98.91
	54.82	-49.47	40.89	-0.03		636.84	-7.47	-0.29	98.84
	54.71	-48.61	40.42			629.50	-7.34	-0.29	98.84
	46.54		36.78			512.69	-7.25	-0.23	98.43
	29.16		22.58			285.19	-4.72		89.90
run 256: **K**(s,θ(v=7.3))	188.30	-255.69	70.25	-1.40	-122.43	1913.58	-18.70	-0.87	95.58
	123.48	-206.75	59.12		-35.91	1543.74	-13.47	-0.64	95.19
	88,00	-225.54	62.54			1603.80	-13.63	-0.55	93.70
	57.45		50.12			956.08	-13.65	-0.42	88.66
			15.37			10.71	-6.99	0.06	64.86
			15.08				-6.98	0.06	64.45
			17.17				-8.13		64.10
			0.064						0

Table F.3: Parameter estimation and reduction results using various experimental data sets at a range of forward velocities v, based on the gray box model consisting of controller K(s,θ), neuro-muscular dynamics G_{nm} and an effective neural time delay, $G_{\tau d}$, of 30 ms. A full parameter vector θ consists of a roll proportional gain $K_{\phi p}$ (Nm/rad), roll integral gain $K_{\phi i}$ (Nm/(s rad)), roll derivative gain $K_{\phi d}$ (Nm s/rad), roll 2^{nd} derivative gain $K_{\phi dd}$ (Nm s^2/rad), steer proportional gain $K_{\delta p}$ (Nm/rad), steer integral gain $K_{\delta i}$ (Nm/(s rad)), steer derivative gain $K_{\delta d}$(Nm s/rad) and steer 2^{nd} derivative gain $K_{\delta dd}$ (Nm s^2/rad) and is given with its Variance Accounted For (VAF) (%).

G

Control Strategy of the Smart, Old Cyclist

This section elaborates on the control identification of the smart, old cyclist. In section G.1, the control is identified for the discrete experimental velocities. Then, in section G.2, the control is made continuous over velocity. At last, in section G.3, the control strategy of the young cyclist is analyzed.

G.1. Part ii. Crucial Feedback Gains

In this section, the crucial feedback gains for the smart, old cyclist are sought. Those feedback gains are found using the parameter reduction process explained in section 2.1.3. This results of this reduction process are given in section G.1.1. Having found the reduced sets, the next step is to estimate its parameters. This is done in section G.1.2.

G.1.1. Reduction Process

Again, the reduction process is performed for one data set per velocity group and, additionally, for data set 249 as well. The results are less uniform compared to the results of the young cyclist, but nearly all data sets could be described by five feedback parameters.

The parameter elimination is not constant over velocity and neither are the sets of remaining parameters after reducing the parameter set until the VAF drops below 90%. Also, the signs of $K_{\phi p}$, $K_{\delta d}$ and $K_{\phi i}$ are not constant over velocity. This might have two possible causes,

- Parameter redundancy, which leads to the existence of multiple optima per data set in parameter space
- Unique optima per data set, but different parameter spaces for the data sets

However, for the same data sets and 30 ms neural time delay, a somewhat uniform optimum was found; there were no sudden order or sign changes of the parameters over the different data sets. Therefore, the latter cause is less likely.

So let's assume that there is a uniform crucial reduced parameter space for which all data sets have the same optimum. With the same optimum, it is not meant that the same parameter values for all data sets are expected. It is meant that all optimized parameter value will have a form of coherence over velocity. This space is hard to find, which is why De Lange introduced the reduction technique. But if this technique does not yield desired result, another approach is required.

What would be the implications of using a parameter set larger than the most reduced? The loss will be the insight in the basic control strategy of the older cyclist, but it should not hinder the quest to

identify its BoA. Multiple optima will likely be found again. But perhaps, a consistency can be found.

Therefore, all feedback gains are retained except the integral roll feedback $K_{\phi i}$ since it is the only feedback parameter eliminated for all runs of the reduction process as well as that no physical meaning could be found behind this parameter. The selected reduced parameter set is then,

$$\theta(s) = [K_{\phi p}, K_{\phi d}, K_{\phi dd}, K_{\delta p}, K_{\delta i}, K_{\delta d}, K_{\delta dd}]^T, \tag{G.1}$$

The next step is to perform the parameter estimation for the selected reduced parameter set using all data sets. As a reminder, in the end the requirement is a parameter set which accurately describes the cyclist's control. It is unrealistic if the values and their signs significantly change across the data sets and this will also prevent fitting a proper velocity function on the parameter values. Therefore, the parameter estimation process proceeds until a decent set is found.

G.1.2. 7 Feedback Parameter Estimation

Having selected the reduced parameter set of the 7 parameters given in (3.5), can more consistency of the resulting parameter values be found if all fifteen data sets are used? The results are given in table G.4. As can be seen, the sign change per data set of $K_{\phi p}$, $K_{\delta i}$ and $K_{\delta d}$ still occurs.

Assuming data set 248 to contain a bad FIR model, only three data sets (185, 190 and 192) seem to have a positive $K_{\phi p}$. Therefore, it is more likely that the optimum with negative $K_{\phi p}$ lies closer to the truth. Then, can we also find a solution with negative $K_{\phi p}$ for those three sets? Bounding the optimization for those sets yields the results given in table G.1,

Id	velocity [ms^{-1}]	$K_{\phi p}$	$K_{\phi d}$	$K_{\phi dd}$	$K_{\delta p}$	$K_{\delta i}$	$K_{\delta d}$	$K_{\delta dd}$	VAF
185	3.2	0	0	16.75	3.94	16.57	34.57	-0.16	98.68
190	6.0	0	10.52	3.12	61.08	109.77	2.45	-0.15	98.66
192	6.1	0	11.21	1.87	45.15	114.99	0.23	0.04	95.42

Table G.1: The parameter sets and their corresponding Variance-Accounted-For found for three data sets for controller K with neural time delay $G_{\tau d}$=60 ms. The feedback parameter $K_{\phi p}$ has been forced to be negative. The optimization algorithm forces $K_{\phi p}$ to the set boundary by setting it to zero.

As can be seen, the optimization algorithm forces $K_{\phi p}$ to the boundary by setting it to zero. Thereby, it shows that the system is overparametrized; the absence of nonzero $K_{\phi p}$ is compensated for by the other parameters. This is not odd, since $K_{\phi d}$ and $K_{\phi dd}$ influence the future position of ϕ and thereby, indirectly $K_{\phi p}$ as well. But it does pose a problem in finding a consistent parameter set. Seeking correlations, the parameter estimation has been repeated for the 7 state feedback for all data sets once for a zero upper boundary and once for a zero upper boundary on $K_{\phi p}$. The result is given in table H.4, appendix H, due to its lenght.

Every velocity group has at least one set with negative $K_{\phi p}$, which can not be said for the sets with positive $K_{\phi p}$. Therefore, the parameter sets with negative $K_{\phi p}$ are used for the continualization.

G.1.3. 6 State Feedback

One interesting observation of table H.4 is that the algorithm managed to find a solution with $K_{\phi p}$ set to zero for all but data set 248 and 191. However, $K_{\phi p}$ is a feedback deemed crucial for the young cyclist and in [31]. Also, it is likely that the algorithm might also find a more reduced set upon the elimination of any other parameter. There is no substantiation behind the elimination of $K_{\phi p}$ and therefore, the 7 state feedback is used for the older cyclist. However, the option of the 6 state feedback with $K_{\phi p}$ being eliminated, has been explored in appendix H since it yielded more solutions for the parameter sets compared to the 7 state feedback sets with negative or positive $K_{\phi p}$.

G.2. Part ii. Velocity-Dependent Feedback Parameter Function

Again, to make the parameter sets continuous over forward velocity, a linear regression is applied onto the estimated parameter sets. The estimated parameter sets are the sets containing negative $K_{\phi p}$ of table G.4. This led to the linear functions given in (G.2). Apart from the linear regression, also the mean and highest vaf linear interpolation methods are applied again. The estimated parameters and their parameter functions are displayed in figure 3.3.

$$f_{\theta_{LR}}(v) = \begin{bmatrix} K_{\phi p} \\ K_{\phi d} \\ K_{\phi dd} \\ K_{\delta p} \\ K_{\delta i} \\ K_{\delta d} \\ K_{\delta dd} \end{bmatrix} = \begin{bmatrix} -1.73 \\ -0.65 \\ -0.02 \\ 25.89 \\ -0.30 \\ 1.11 \\ -0.03 \end{bmatrix} v + \begin{bmatrix} -6.24 \\ 8.61 \\ 4.41 \\ -64.13 \\ 2.39 \\ -1.62 \\ 0.03 \end{bmatrix} \tag{G.2}$$

To quantify the quality of the fit, the R^2 is calculated for each feedback parameter for the three functions. The result is given in table G.2

R^2	$f(s, \theta_{LR}(v))$	$f(s, \theta_{LI,mean}(v))$	$f(s, \theta_{LI,HV}(v))$
$K_{\phi p}$	0.433	0.688	0.342
$K_{\phi d}$	0.289	0.414	-0.248
$K_{\phi dd}$	0.002	0.674	0.348
$K_{\delta p}$	0.947	0.989	0.987
$K_{\delta i}$	0.097	0.716	0.500
$K_{\delta d}$	0.897	0.958	0.941
$K_{\delta dd}$	0.369	0.535	0.200

Table G.2: Coefficient of determination of the three functions $f(s, \theta_{LR}(v))$, $f(s, \theta_{LI,mean}(v))$ and $f(s, \theta_{LI,HV}(v))$ which are fitted through the feedback parameters of parameter set $\theta(v)$.

The coefficients of determination between the linear regression and the feedback parameters $K_{\phi dd}$ and $K_{\delta i}$ are really low, indicating that the linear regression does not grasp the variance of the parameters but merely the mean values. For the remaining parameters, it shows a decent fit.

The linear interpolation between the mean values predicts all parameters fairly well. The linear interpolation between the values with the highest VAF predicts does not capture the variance of $K_{\phi d}$ and also does not follow the trend of the mean. For the remaining parameters, it is a decent fit.

G.3. Part ii. Control Response Analysis

The control of the older cyclist is harder to interpret than the young cyclist due to the larger number of feedback states. The control analyse here is done with respect to the feedback parameters of the young cyclist.

Roll Feedback

The roll rate feedback changed sign, thereby it does not follow the principle of the fall anymore. The roll rate feedback became nearly an order smaller, but still does follows the principle. Based on those parameters, the cyclist would be less stable. However, this is compensated for by the presence of roll acceleration which does follow the principle. All roll feedback has negative proportionality with velocity, indicating a decline for the principle for increasing velocity. This does make sense, since stronger stabilization control is required for long velocities.

Steer Feedback

The steer acceleration feedback $K_{\delta dd}$ seems relatively unaffected by the addition of $K_{\delta p}$, whereas the dependency of $K_{\delta d}$ on the velocity changed sign and $K_{\delta i}$ nearly became negligible due to a order reduction of two. The steer feedback $K_{\delta p}$ seems to functions similar to what $K_{\delta i}$ did for the young cyclist; it induces a fall, causing a change in heading. The steer rate feedback $K_{\delta d}$ excites the steering angle, but is opposed by the acceleration feedback $K_{\delta dd}$.

Conclusively

Overall, it seems that there are feedback parameters which are opposing one another (e.g. $K_{\delta d}$ and $K_{\delta dd}$) or which nearly doing anything at al (e.g. $K_{\delta i}$) and, therefore, it is clear that there is redundancy. This redundancy clouds the interpretation of the cyclist's control. The VAF of the estimated parameter sets is high, so presumably, the control of the rider is still well-described.Therefore, the parameter functions are used for the identification of the BoA of the older cyclist.

Model τ_d=60 ms	$K_{\phi p}$	$K_{\phi i}$	$K_{\phi d}$	$K_{\phi dd}$	$K_{\delta p}$	$K_{\delta i}$	$K_{\delta d}$	$K_{\delta dd}$	***VAF***
Run 248: **K**(s,θ(v=2.1 m/s))	69.22	-5.94	28.43	1.97	-8.35	37.88	-2.07	-0.30	96.01
	67.98		28.77	1.91	-8.38	36.63	-2.14	-0.30	96.00
	93.06		36.28		-13.42	43.89	-3.90	-0.37	92.68
	-12.62		37.09			1.08	-3.62	-0.24	77.24
Run 249: **K**(s,θ(v=2.2 m/s))	-8.62	-0.64	8.27	5.16	3.07	0.73	1.04	-0.09	99.26
	-9.72	-0.018	7.99	5.18	3.16		1.07	-0.09	99.25
	-9.73		7.99	5.18	3.16		1.07	-0.09	99.25
			4.48	5.02			1.15	-0.10	97.68
				6.52			2.32	-0.15	93.93
				5.22			1.73		46.41
Run 184: **K**(s,θ(v=3.2 m/s))	48.00	-38.63	23.74	1.77	-4.48	89.52	-2.14	-0.28	97.67
	32.90	-29.25	19.78	2.21		68.99	-1.33	-0.23	97.62
	23.78		17.06	2.11		44.38	-1.30	-0.19	96.74
	19.13		9.98	2.68		26.11		-0.17	94.10
	7.55		4.44	2.01		1.95			81.66
Run 252: **K**(s,θ(v=4.3 m/s))	-18.19	0.87	5.34	4.67	41.68	-2.84	3.50	-0.06	98.61
	-17.45		5.63	4.64	41.40		3.45	-0.06	98.61
	-20.68		6.31	4.19	41.18		2.87		96.65
			5.77	3.04	22.13		1.25		88.93
	-12.20		10.03	2.59	25.05				87.11
Run 190: **K**(s,θ(v=6.0 m/s))	19.69	-19.65	21.00	2.35	43.05	292.79	-0.74	-0.27	98.89
	15.35	-16.63	18.80	2.54	47.59	255.7		-0.25	98.88
	12.34		17.11	2.48	46.36	208.10		-0.22	98.71
			16.65	2.55	58.67	177.09		-0.12	95.14
			13.20	2.09	48.95	130.12			92.72
			7.00	1.96	36.45				81.27
Run 256: **K**(s,θ(v=7.3 m/s))	-20.82	0.26	4.93	4.60	137.43	-0.04	6.39	-0.41	95.23
	-20.81	0.25	4.93	4.60	137.42		6.38	-0.41	95.23
	-19.91		4.87	4.58	135.81		6.36	-0.42	95.25
			5.12	3.86	96.58		4.36	-0.43	92.06
			8.33	2.47	67.14			-0.19	86.90

Table G.3: Parameter estimation and reduction results using various experimental data sets at a range of forward velocities v, based on the gray box model consisting of controller K(s, θ), neuro-muscular dynamics G_{nm} and an effective neural time delay, $G_{\tau d}$, or 60 ms. The identified parameter vectors θ consist of a roll proportional gain $K_{\phi p}$ (Nm/rad), roll derivative gain $K_{\phi d}$ (Nm s/rad), roll 2^{nd} derivative gain $K_{\phi dd}$ (Nms^2/rad), steer proportional gain $K_{\delta p}$ (Nm/rad), steer integral gain $K_{\delta i}$ (Nm/(s rad)), steer derivative gain $K_{\delta d}$(Nm s/rad) and steer 2^{nd} derivative gain $K_{\delta dd}$ (Nm s^2/rad) and is given with its Variance Accounted For (VAF) (%). The second parameter elimination of Dataset 252 (v = 4.3 m/s) led to two parameters having high autocovariance and an extra reduction has been performed upon eliminating either of them.

Model τ_d=60 ms	$K_{\phi p}$	$K_{\phi d}$	$K_{\phi dd}$	$K_{\delta p}$	$K_{\delta i}$	$K_{\delta d}$	$K_{\delta dd}$	**VAF**
Run 248: K(s,θ(v=2.1 m/s))	67.96	28.76	1.91	-8.38	36.62	-2.14	-0.30	96.00
Run 249: K(s,θ(v=2.2 m/s))	-9.75	2.98	5.18	3.16	-0.02	1.07	-0.09	99.25
Run 250: K(s,θ(v=2.2 m/s))	-8.9	13.94	4.30	3.67	4.61	0.20	-0.1	97.58
Run 184: K(s,θ(v=3.2 m/s))	-7.90	6.43	3.27	10.45	4.98	1.01	-0.06	98.04
Run 185: K(s,θ(v=3.2 m/s))	11.59	21.45	3.28	13.15	53.33	-0.50	-0.18	98.94
Run 186: K(s,θ(v=3.1 m/s))	-10.59	7.22	4.23	13.44	3.54	1.58	-0.10	98.98
Run 251: K(s,θ(v=4.3 m/s))	-16.73	7.90	6.10	55.10	0.18	4.92	-0.13	98.40
Run 252: K(s,θ(v=4.3 m/s))	-17.51	5.61	4.65	41.44	-0.16	3.45	-0.06	98.61
Run 253: K(s,θ(v=4.3 m/s))	-16.61	6.44	4.55	38.91	1.27	3.18	-0.11	98.11
Run 190: K(s,θ(v=6.0 m/s))	9.36	15.55	2.63	49.85	184.69	0.57	-0.20	98.71
Run 191: K(s,θ(v=6.0 m/s))	-10.54	2.90	3.10	63.23	0.06	3.88	-0.03	96.99
Run 192: K(s,θ(v=6.0 m/s))	1.62	11.71	1.79	42.63	122.92	-0.04	0.03	95.44
Run 255: K(s,θ(v=7.3 m/s))	-18.41	2.96	4.03	124.86	-0.47	6.36	-0.17	96.02
Run 256: K(s,θ(v=7.3 m/s))	-20.62	5.02	4.60	137.19	2.14	6.35	-0.42	95.24
Run 257: K(s,θ(v=7.3 m/s))	-19.41	3.76	4.34	142.30	-1.17	7.16	-0.14	96.33

Table G.4: Estimation results of the reduced parameter set using various experimental data sets acquired at a range of forward velocities v, based on the gray box model consisting of controller K(s, θ), neuro-muscular dynamics G_{nm} and an effective neural time delay, $G_{\tau d}$, of 60 ms. The identified parameter vectors θ consist of a roll proportional gain $K_{\phi p}$ (Nm/rad), roll derivative gain $K_{\phi d}$ (Nm s/rad), steer integral gain $K_{\delta i}$ (Nm/(s rad)), steer derivative gain $K_{\delta d}$(Nm s/rad) and steer 2^{nd} derivative gain $K_{\delta dd}$ (Nm s^2/rad) and is given with its Variance Accounted For (VAF) (%).

H

Six State Feedback of the Older Cyclist

For the older cyclist, it would be interesting to see if there would be solutions for describing the data using six feedback states instead of seven. The optima here have been split up using the sign of the $K_{\phi p}$ and the algorithm was forced to find a solution for positive sign and the next run for a negative sign. The data sets for which the algorithm could not abide by those bounds ánd return a nonzero $K_{\phi p}$ were eliminated. But perhaps a better approach would have been to eliminate $K_{\phi p}$ instead, which is a feedback parameter deemed relatively crucial since it was not eliminated for the other controllers.

In table H.4, the estimated parameter solutions for which the algorithm set $K_{\phi p}$ to zero, are marked gray. This data set seems a lot more coherent than the data used for the smart, old cyclist. The elimination of the proportional roll feedback makes sense if the roll velocity and acceleration feedback are of the same positive sign, since then they follow the principle of steer-into-the-fall.

Moreover, as said previously, an acceleration feedback functions like a lead and, therefore, precedes the proportional feedback rendering the latter more useless for control. However, one might also argue that the elimination of the proportional steer angle would have been a more intuitive choice. Since for the 30 ms neural time delay, the steer acceleration feedback gains was added to the set of parameters of the undelayed rider. This set did contain a proportional roll feedback gain, however, did not contain a proportional steer feedback gain. Then, upon increasing the neural time delay, it would seem more intuitive to proceed with the previous set and add the remaining acceleration gain.

The solution to this debate might be given by the following question; if various combinations of parameters are able to describe the experimental data equally well, then are their basins of attraction similar as well? If so, it should not matter which combination is chosen. Therefore, the procedure of estimated parameters for extracting the stability region is repeated for the set of six parameters of the gray marked rows of table H.4.

If the resulting stability regions are approximately the same of those given in figure 3.4, then the debate is settled. Repeating the previous procedures of making the estimated parameters continuous for the data of table H.4 yields the solution given in figure H.2. The linear regression equations are given in (H.1), and the stability regions of the parameter functions are compared with the stability regions of the seven parameter feedback controller in figure H.3.

Gain Comparison

The estimated parameters for the further reduced parameter set of 6 feedback gains versus the parameters of the controller using 7 feedback states is given in figure H.1. For each state feedback, the R^2 is given in table H.1. Visually, as well as from the coefficient, it seems that for all but the integral steer feedback the trend of the found parameter values over forward velocity is retained. The elimination of

the proportional roll feedback results in an increase of the integral feedback.

Discussion Six State Feedback

From figure H.3, a discrepancy of the stability regions between the used parameter sets made continuous by the linear regression. The controllers based on the linear interpolation of the mean values seem to agree quite well (RMSE=0.42). The interpolations between the parameter sets with the highest VAF's do result in a significant larger difference (RMSE=0.95). This indicates that the mean better represents the data sets regardless of the chosen dimension of the parameter sets. It also indicates that there is quite a variance between the responses of individual data sets. Therefore, it would be wise to acquire more data per data set such that the median data sets can be used for parameter estimation. To be more sure of the influence of the estimated parameter sets of single data sets on the maximum allowable perturbations, a sensitive study has been performed in appendix I.

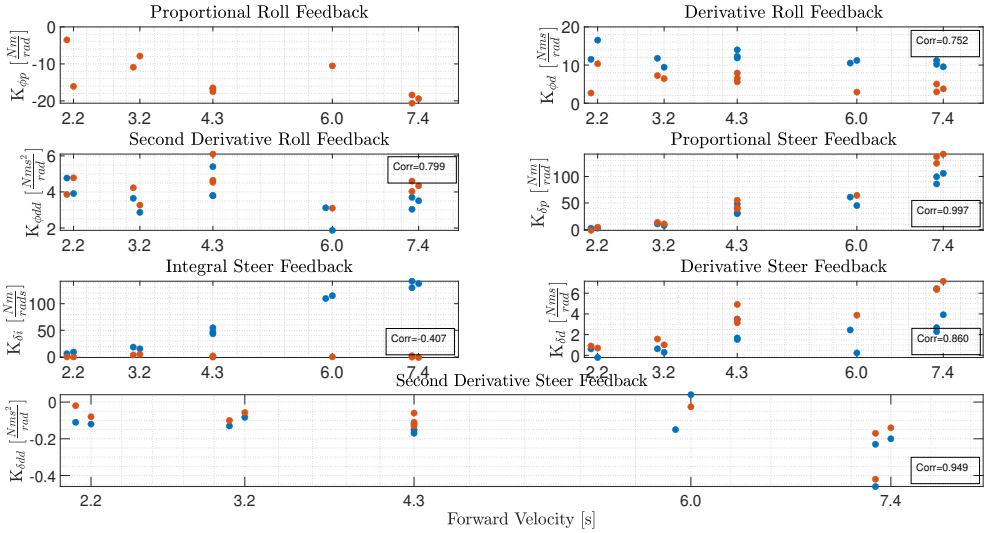

Figure H.1: Estimated parameters for the controller $K(s,\theta)$ with neuro-muscular dynamics G_{nm} and effective neural time delay G_{τ_d} of 60 ms based on two different sets of estimated parameters θ. In blue are the estimated parameters given for six state feedback and in orange for seven state feedback. All estimated parameter sets had VAF of above 90% with the experimental data.

R^2	$f(s,\theta_{LR}(v))$	$f(s,\theta_{LI,mean}(v))$	$f(s,\theta_{LI,HV}(v))$
$K_{\phi d}$	0.282	0.485	0.006
$K_{\phi dd}$	0.177	0.631	0.026
$K_{\delta p}$	0.920	0.965	0.914
$K_{\delta i}$	0.974	0.994	0.990
$K_{\delta d}$	0.457	0.676	0.141
$K_{\delta dd}$	0.223	0.568	0.239

Table H.1: Coefficient of determination of the three functions $f(s,\theta_{LR}(v))$, $f(s,\theta_{LI,mean}(v))$ and $f(s,\theta_{LI,HV}(v))$ which are fitted through the feedback parameters of parameter set $\theta(v)$.

$$K(s) = \begin{bmatrix} K_{\phi d} \\ K_{\phi dd} \\ K_{\delta p} \\ K_{\delta i} \\ K_{\delta d} \\ K_{\delta dd} \end{bmatrix} = \begin{bmatrix} -0.54 \\ -0.19 \\ 18.28 \\ 27.20 \\ 0.47 \\ -0.03 \end{bmatrix} v + \begin{bmatrix} 14.27 \\ 4.541 \\ -43.81 \\ -61.75 \\ -0.06181 \\ -0.02 \end{bmatrix} \tag{H.1}$$

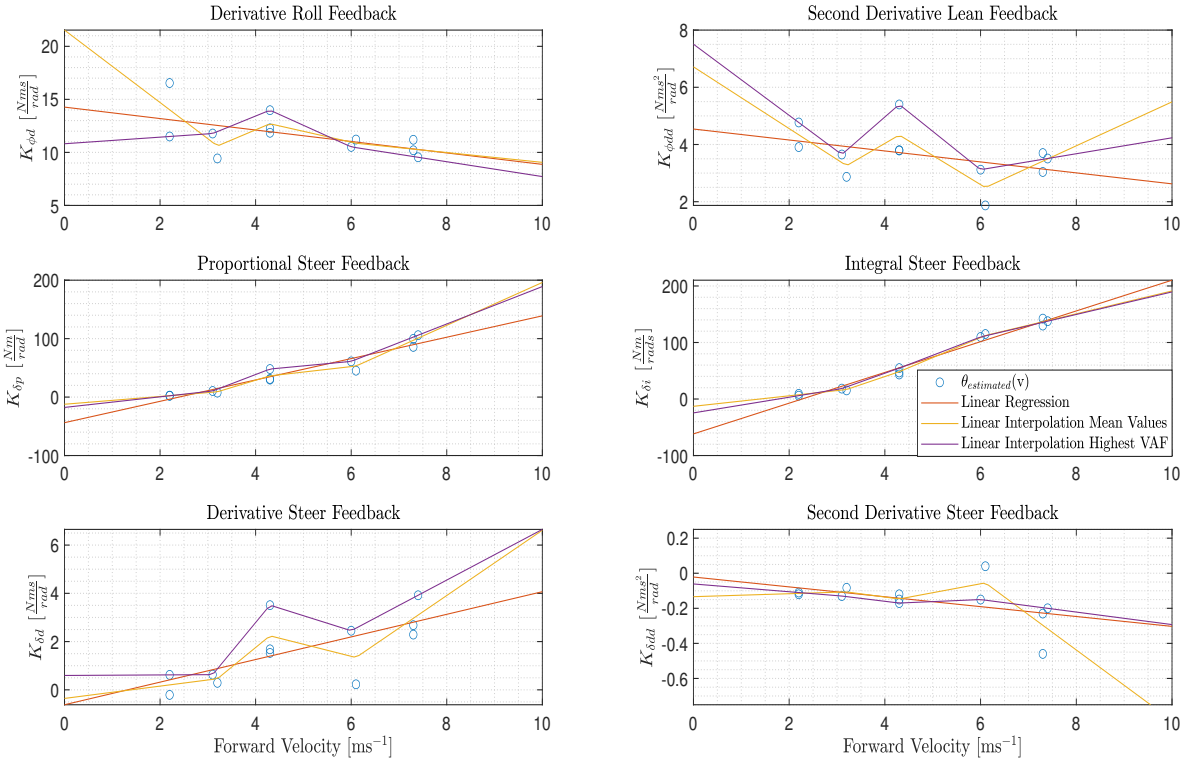

Figure H.2: The discrete, estimated six state parameters $\theta(v) = (K_{\phi d}, K_{\phi dd}, K_{\delta p}, K_{\delta i}, K_{\delta d}, K_{\delta dd})$ resulting from gray box identification. The gray box consists of controller K with neural time delay τ_d=60 ms. Also displayed are potential functions to make the discrete data continuous over forward velocity. The estimated parameters are the blue circles. The orange line is a linear regression, the yellow line a linear interpolation between the mean values of the estimated parameters per velocity group and the purple line a linear interpolation between the parameter sets with the highest VAF per velocity. A velocity group consists of three parameter sets for close velocities. The top-left figure contains the data concerning the derivative roll parameter, $K_{\phi p}$, the mid-left figure concerning the integral steer parameter, $K_{\phi p}$, the mid-right figure concerning the derivative steer and the bottom figured displays the second derivative steer parameter fits.

RMSE	$K(s, f_{\theta_{LR}}(v))$	$K(s, f_{\theta_{LI,mean}}(v))$	$K(s, f_{\theta_{LI,HV}}(v))$	**Surface Area [radms^{-2}]**	**Average Basin Height [rads^{-1}]**
$K(s, f_{\theta_{LR}}(v))$	-	1.01	0.73	17.55	3.15
$K(s, f_{\theta_{LI,mean}}(v))$	1.01	-	0.67	21.72	3.83
$K(s, f_{\theta_{LI,HV}}(v))$	0.73	0.67	-	18.26	3.26

RMSE		**n=7**			**n=6**		
		$K(s, f_{\theta_{LR}}(v))$	$K(s, f_{\theta_{LI,mean}}(v))$	$K(s, f_{\theta_{LI,HV}}(v))$	$K(s, f_{\theta_{LR}}(v))$	$K(s, f_{\theta_{LI,mean}}(v))$	$K(s, f_{\theta_{LI,HV}}(v))$
n=7	$K(s, f_{\theta_{LR}}(v))$	-	2.32	2.51	1.51	2.34	1.87
	$K(s, f_{\theta_{LI,mean}}(v))$	2.32	-	0.45	1.03	0.42	0.71
	$K(s, f_{\theta_{LI,HV}}(v))$	2.51	0.45	-	1.30	0.58	0.95
n=6	$K(s, f_{\theta_{LR}}(v))$	1.51	1.03	1.30	-	1.02	0.73
	$K(s, f_{\theta_{LI,mean}}(v))$	2.34	0.42	0.58	1.02	-	0.67
	$K(s, f_{\theta_{LI,HV}}(v))$	1.87	0.71	0.95	0.73	0.67	-

Table H.2: Root-mean square error (RMSE) between the basin of attraction outlines of a controller based on [31] with 60 ms effective, neural time delay τ_d, combined with the nonlinear Whipple (-Carvallo) benchmark bicycle from [2]. One controller is based on six-state feedback (n=6) and the other on seven-state feedback (n=7). The control of the rider is made continuous over forward velocity by linear interpolation between the mean $K(s, f_{\theta_{LI,mean}}(v))$, linear interpolation between the parameter sets with the highest variance-accounted-for $K(s, f_{\theta_{LI,HV}}(v))$ and by a linear regression $K(s, f_{\theta_{LR}}(v))$

The estimated parameter of controller $K_{s,\theta}$ with neuro-muscular dynamics G_{nm} and neural time delay τ_d=60 ms. Bounds were put for the optimization algorithm, such that it was forced to seek solutions in the direction of one of the two identified optima. For each dataset, the first search had a lower 0 bound

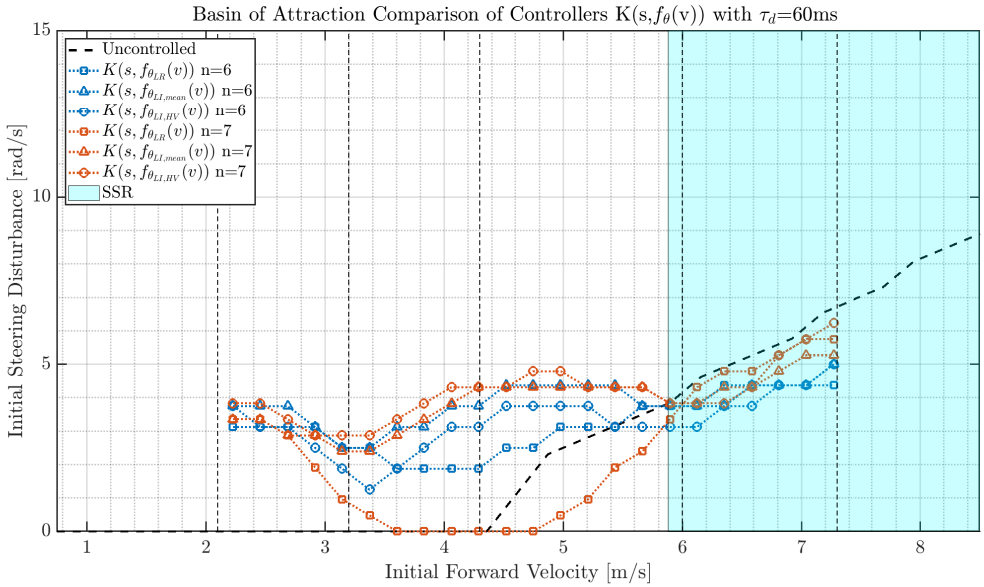

Figure H.3: Stability region outlines of bicycle-rider system consisting of the WCBM combined with a rider, based on the gray box model consisting of controller K, second-order neuro-muscular dynamics G_{nm} and an effective neural time delay, τd, of 60 milliseconds based on 6 (blue) versus 7 (red) feedback gains. The blue shaded region is the self-stable region of the uncontrolled bicycle and ranges from 5.88 to 10.13 ms^{-1}. The dashed, vertical lines are the velocities at which the experimental data was acquired and the parameter sets were estimated. These velocities are approximately 2.1, 3.2, 4.3, 6.0 and 7.3 ms^{-1}. The line with square markers represents the control model for which the parameter sets, θ, were made continuous over velocity using a linear regression. The parameters of the controller corresponding to the line with triangles, were linearly interpolated mean parameters. For the line with circle markers, the parameters were linearly interpolated between the parameter containing the highest VAF.

	Basin of Attraction [$radms^{-2}$]		
dim.	n=7	n=6	Change
$K(s, f_{\theta_{LI,mean}}(v))$	21.41	21.72	1.45%
$K(s, f_{\theta_{LI,HV}}(v))$	23.05	18.26	-20.78%

Table H.3: Changes in the basins of attraction of a bicycle-rider system with 60 ms neural time delay. The bicycle-rider system consists of the nonlinear equations of motion of Basu-Mandal [2], internal controller $K(s, f_\theta(v))$, neuro-muscular dynamics G_{nm} and neural time delay τ_d. The feedback parameter function is based on linear interpolation between either the mean estimated parameters, $f_{\theta_{LI,mean}}$ or between the estimated parameters with the highest variance accounted for $f_{\theta_{LI,HV}}$. The percentage difference is taken with respect to n=7.

on $K_{\phi p}$ and the second an upper 0 bound.

Id	**velocity** [ms^{-1}]	$K_{\phi p}$	$K_{\phi d}$	$K_{\phi dd}$	$K_{\delta p}$	$K_{\delta i}$	$K_{\delta d}$	$K_{\delta dd}$	**VAF**
248	2.1	68.00	28.76	1.91	-8.38	36.63	-2.14	-0.30	96.00
		-3.52	2.67	3.86	-1.68	-0.034	0.90	-0.02	93.63
249	2.2	0	11.50	4.77	2.25	5.94	0.62	-0.11	99.17
		-9.75	7.98	5.18	3.16	-0.02	1.07	-0.09	99.25
250	2.2	0	16.54	3.91	2.49	9.14	-0.21	-0.12	97.46
		-16.08	10.34	4.78	4.37	-0.12	0.70	-0.08	97.47
184	3.2	0	9.43	2.87	7.63	15.24	0.29	-0.083	97.79
		-7.88	6.44	3.27	10.44	5.00	1.01	-0.057	98.04
185	3.2	11.58	21.44	3.28	13.15	53.31	-0.49	-0.18	98.94
		0	0	16.75	3.94	16.57	34.57	-0.16	98.68
186	3.1	0	11.78	3.65	10.41	18.42	0.63	-0.13	98.73
		-10.90	7.23	4.23	13.43	3.57	1.58	-0.10	98.98
251	4.3	0	13.98	5.40	47.99	54.68	3.51	-0.17	98.29
		-16.72	7.90	6.10	55.09	0.18	4.92	-0.13	98.40
252	4.3	0	11.85	3.79	30.99	46.96	1.68	-0.12	97.98
		-17.50	5.61	4.65	41.43	-0.17	3.45	-0.06	98.61
253	4.3	0	12.27	3.80	29.88	43.37	1.53	-0.15	97.69
		-16.47	6.56	4.54	38.83	1.95	3.15	-0.11	98.11
190	6.0	9.46	15.90	2.62	49.74	185.46	0.55	-0.2	98.71
		0	10.52	3.12	61.08	109.77	2.45	-0.15	98.66
191	6.1	43.23	24.63	1.09	-1.00	338.84	-4.43	-0.38	96.89
		-10.54	2.90	3.10	64.23	0.055	3.88	-0.026	96.99
192	6.1	1.60	11.70	1.79	42.65	122.76	-0.04	0.04	95.44
		0	11.21	1.87	45.15	114.99	0.23	0.04	95.42
255	7.3	0	10.20	3.04	85.88	142.25	2.29	-0.23	94.69
		-18.41	2.96	4.03	124.86	-0.47	6.46	-0.17	96.02
256	7.3	0	11.19	3.70	99.57	129.94	2.68	-0.46	93.92
		-20.62	5.02	4.60	137.17	2.14	6.35	-0.42	95.24
257	7.4	0	9.54	3.51	105.89	137.67	3.92	-0.20	95.36
		-19.41	3.76	4.34	142.30	-1.14	7.16	-0.14	96.33

Table H.4: The parameter sets and their corresponding Variance-Accounted-For found for each dataset for controller K with neural time delay $G_{\tau d}$=60 ms. For the first row of every dataset $K_{\phi p}$ has been forced to be positive. The the second row of each dataset $K_{\phi p}$ has been forced to be negative. Only for datasets 248 and 191 two optima could be found.

I

BoA Sensitivity to Parameter Dimension

This chapter is dedicated to the minor research performed regarding the sensitivity of the stability of the bicycle-rider system with respect to the parameter estimation and reduction. The majority of the data sets are well described (VAF>90%) using the gray-box model with a parameter set containing in between 5 and 8 feedback states. Then, do the identified controllers also describe the same behaviour for larger perturbations? If this is not the case, then the observed differences in the results from section 3.1 and 3.2 are not merely the result of the time delay. This would render the results less reliable.

In tables I.1 and I.2, the parameter reductions are given for 6 data sets of the controllers with 30 and 60ms neural time delay, respectively. For each set with VAF>90%, simulations have been performed at the corresponding velocity untill the bicycle-rider system fell. The maximum allowable perturbations $\pm$ 0.1 rads^{-1} has been plotted in figure I.1 and are given in the most right column of the tables. This process has been done for both the young and older cyclist with adapted control strategy.

Results 30ms Delayed Cyclist

As one can observe, for run 248 there is quite a difference between the second parameter set and the other sets. For run 249, a significant decline is observed upon further elimination of parameters. Less significant, but opposite behaviour is seen for run 252. Therefore, there does not seem to be a clear correlation between the eliminated states and the perturbation rejection. The average basin height for all sets with corresponding VAF>90% is 7.11 rads^{-1}. The average for all lowest values per data set is 6.58 rads^{-1}.

To find the source behind the discrepancies, the experimental and simulated data of the rider model are compared. For several data sets, some simulations are compared to seek a correlation. The simulation results are given in figure I.2 to I.6. The actual data is longer, but the response immediate after the perturbation is crucial. Therefore, all the graphs contain part which are zoomed in. Visual comparison has been done, but no clear correlation could be found. If a correlation exists, it is likely to be be clouded due to the change of motion characteristics of the bicycle over forward velocity.

Results 60ms Delayed Cyclist

The results for the older cyclist concerning the maximum basin height, seem to have less variance compared to the young cyclist. The average maximum basin height would be 4.99 rads^{-1}. The average for the maximum values per data set would be 5.33 rads^{-1}. Then, in case the least stable parameters of the young cyclist would lie closest to the truth and vice versa for the old cyclist, the height of the basin of attraction would still decline by 19.00%.

Overall Observation

A similar VAF for two parameters sets does not necessarily mean that they describe the first part of the data set equally well. Whereas, the first part of the signal describes the most crucial behaviour for perturbation rejection. The three controllers $K(s, f_\theta(v))$ are, however, based on three data sets per velocity which do have results around the same optima. Therefore, those results are more likely to lie closer to the truth. The results here merely indicate the high sensitivity and that VAF might not be the best measure for validating a gray box model combined seeking the limitations of stability of such a model. Future recommendations are to only estimated on the crucial part of the data and to have sufficient data per velocity such that the median data set can be used.

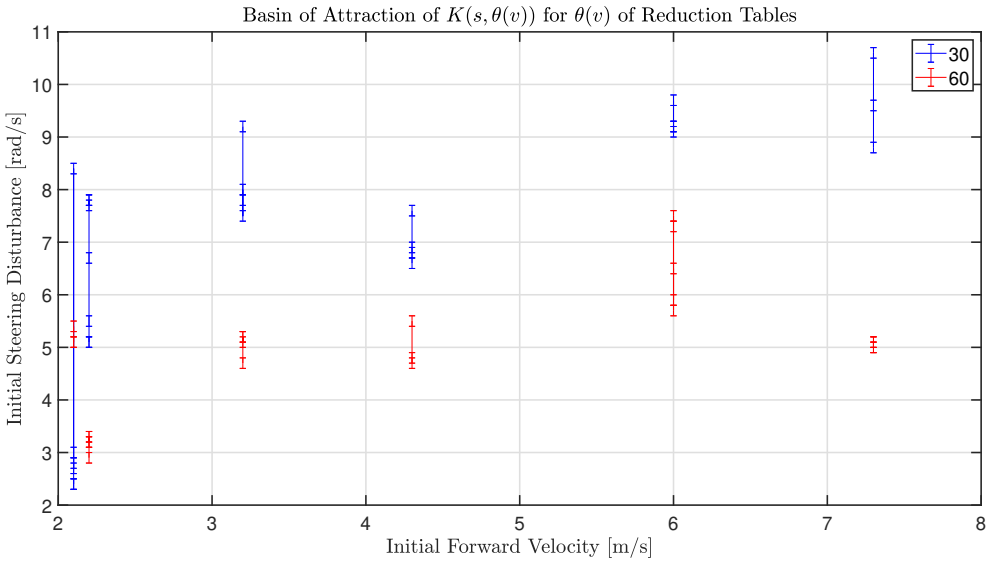

Figure I.1: Maximum allowable perturbations for a bicycle-rider system with Whipple(-Carvallo) benchmark bicycle from [20] and controller $K(s, \theta(v))$ with neuro-muscular dynamics G_{nm} and single, effective neural time delay G_{td} with τ_d is 30 ms (blue) and 60 ms (red). The feedback parameters $\theta(v)$ are based on tables F.3 and G.3.

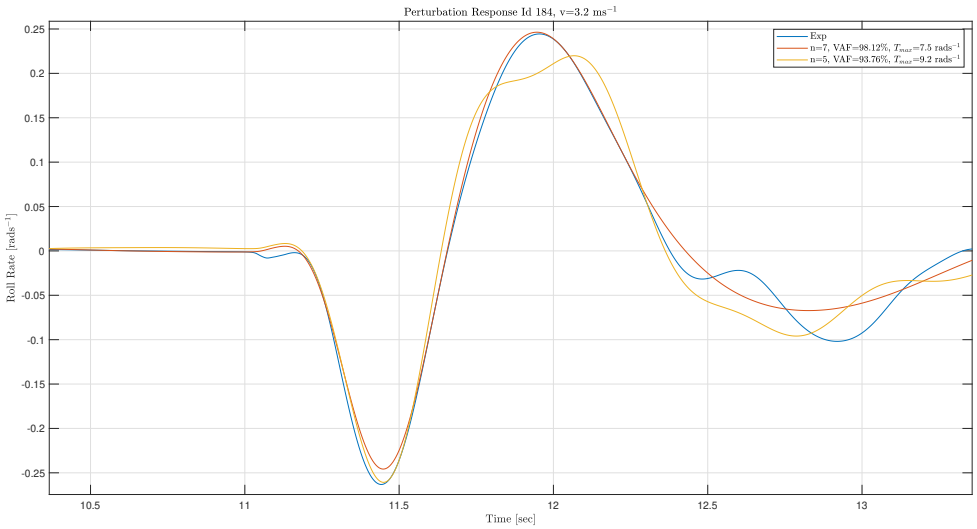

Figure I.2: Perturbation response of the gray-box model to the experimental disturbances for different state feedback parameters. This perturbation response belongs to experimental data Id. 184 which was taken at a forward velocity of 3.2 ms^{-1}.

Model τ_d=30 ms	$K_{\phi p}$	$K_{\phi i}$	$K_{\phi d}$	$K_{\phi dd}$	$K_{\delta p}$	$K_{\delta i}$	$K_{\delta d}$	$K_{\delta dd}$	***VAF***	$T_{\delta,max} \pm 0.1 \text{rads}^{-1}$
run 248: **K**(s,θ(v=2.1))	-5.31	0.57	4.13	3.10	-1.23	0.37	0.82	0.05	94.53	2.7
	29.21	199.45	52.32	-2.11	-8.08		-5.75	-0.33	91.31	8.4
		2.02	3.29	2.94	-2.54		0.70	0.05	93.08	3
			2.59	3.03	-2.55		0.80	0.05	93.06	2.8
				3.62	-2.96		1.32	0.03	91.43	2.4
				4.04	-2.80		1.51		90.27	2.4
				5.49			2.18		65.86	
run 249: **K**(s,θ(v=2.2))	63.02	-31.57	36.17	1.98	-0.79	53.96	-1.96	-0.16	99.03	7.8
	54.90	-28.08	34.44	2.17		49.23	-1.74	-0.15	99.03	7.7
	45.16		33.91	2.01		39.99	-1.85	-0.14	98.83	7.8
	19.89		16.65	3.49		17.38		-0.07	97.56	6.7
	7.25		11.99	3.04		6.71			94.75	5.5
			10.83	2.91		2.42			92.82	5.1
			10.18	3.03					92.10	5.1
				6.82					0	
run 184: **K**(s,θ(v=3.2))	121.71	-81.55	49.65	-1.42	-25.90	205.33	-7.11	-0.46	98.27	8
	81.85	-63.72	37.67		-13.40	151.32	-4.55	-0.32	98.12	7.5
	61.82		33.41		-11.72	102.94	-4.45	-0.25	97.07	7.8
	34.51		37.78			98.74	-4.82	-0.18	93.76	9.2
	11.78		21.77			44.68	-3.05		77.36	
run 252: **K**(s,θ(v=4.3))	171.27	-225.36	75.63	-2.14	-34.48	696.76	-10.34	-0.63	99.00	6.6
	108.02	-168.89	55.58		-5.37	500.28	-5.78	-0.41	98.66	6.8
	101.60	-181.49	58.20			521.55	-5.86	-0.40	98.50	6.9
	65.52		47.87			321.43	-5.82	-0.28	96.47	7.6
	18.49		22.56			80.09	-4.13		72.86	
			20.39			27.75	-4.14		65.39	
			20.264				-4.53		66.84	
							-2.74		0	
run 190: **K**(s,θ(v=6.0))	67.64	-55.22	45.87	-0.59	-15.34	722.08	-9.38	-0.35	98.91	9.2
	54.82	-49.47	40.89	-0.03		636.84	-7.47	-0.29	98.84	9.2
	54.71	-48.61	40.42			629.50	-7.34	-0.29	98.84	9.1
	46.54		36.78			512.69	-7.25	-0.23	98.43	9.7
	29.16		22.58			285.19	-4.72			89.90
run 256: **K**(s,θ(v=7.3))	188.30	-255.69	70.25	-1.40	-122.43	1913.58	-18.70	-0.87	95.58	8.8
	123.48	-206.75	59.12		-35.91	1543.74	-13.47	-0.64	95.19	9.5
	88.00	-225.54	62.54			1603.80	-13.63	-0.55	93.70	10.6
	57.45		50.12			956.08	-13.65	-0.42	88.66	12.2
			15.37			10.71	-6.99	0.06		64.86
			15.08				-6.98	0.06		64.45
			17.17					-8.13		64.10
			0.064						0	

Table I.1: Parameter estimation and reduction results using various experimental data sets at a range of forward velocities v, based on the gray box model consisting of controller K(s, θ), neuro-muscular dynamics G_{nm} and an effective neural time delay, $G_{\tau d}$, of 30 ms. A full parameter vector θ consists of a roll proportional gain $K_{\phi p}$ (Nm/rad), roll integral gain $K_{\phi i}$ (Nm/(s rad)), roll derivative gain $K_{\phi d}$ (Nm s/rad), roll 2^{nd} derivative gain $K_{\phi dd}$ (Nm s^2/rad), steer proportional gain $K_{\delta p}$ (Nm/rad), steer integral gain $K_{\delta i}$ (Nm/(s rad)), steer derivative gain $K_{\delta d}$(Nm s/rad) and steer 2^{nd} derivative gain $K_{\delta dd}$ (Nm s^2/rad) and is given with its Variance Accounted For (VAF) (%).

Model τ_d=60 ms	$K_{\phi p}$	$K_{\phi i}$	$K_{\phi d}$	$K_{\phi dd}$	$K_{\delta p}$	$K_{\delta i}$	$K_{\delta d}$	$K_{\delta dd}$	***VAF***	$T_{\delta,max}$ $\pm$0.1rads^{-1}
Run 248: **K**(s,θ(v=2.1 m/s))	69.22	-5.94	28.43	1.97	-8.35	37.88	-2.07	-0.30	96.01	5.1
	67.98		28.77	1.91	-8.38	36.63	-2.14	-0.30	96.00	5.1
	93.06		36.28		-13.42	43.89	-3.90	-0.37	92.68	5.4
	-12.62		37.09			1.08	-3.62	-0.24	77.24	
Run 249: **K**(s,θ(v=2.2 m/s))	-8.62	-0.64	8.27	5.16	3.07	0.73	1.04	-0.09	99.26	3.3
	-9.72	-0.018	7.99	5.18	3.16		1.07	-0.09	99.25	3.2
	-9.73		7.99	5.18	3.16		1.07	-0.09	99.25	3.2
			4.48	5.02			1.15	-0.10	97.68	3.3
				6.52			2.32	-0.15	93.93	2.9
				5.22			1.73		46.41	
Run 184: **K**(s,θ(v=3.2 m/s))	48.00	-38.63	23.74	1.77	-4.48	89.52	-2.14	-0.28	97.67	5.2
	32.90	-29.25	19.78	2.21		68.99	-1.33	-0.23	97.62	5.1
	23.78		17.06	2.11		44.38	-1.30	-0.19	96.74	5.2
	19.13		9.98	2.68		26.11		-0.17	94.10	4.7
	7.55		4.44	2.01		1.95			81.66	
Run 252: **K**(s,θ(v=4.3 m/s))	-18.19	0.87	5.34	4.67	41.68	-2.84	3.50	-0.06	98.61	5.5
	-17.45		5.63	4.64	41.40		3.45	-0.06	98.61	4.8
	-20.68		6.31	4.19	41.18		2.87		96.65	4.7
			5.77	3.04	22.13		1.25		88.93	
	-12.20		10.03	2.59	25.05				87.11	
Run 190: **K**(s,θ(v=6.0 m/s))	19.69	-19.65	21.00	2.35	43.05	292.79	-0.74	-0.27	98.89	5.7
	15.35	-16.63	18.80	2.54	47.59	255.7		-0.25	98.88	6.5
	12.34		17.11	2.48	46.36	208.10		-0.22	98.71	5.9
			16.65	2.55	58.67	177.09		-0.12	95.14	7.3
			13.20	2.09	48.95	130.12			92.72	7.5
			7.00	1.96	36.45				81.27	
Run 256: **K**(s,θ(v=7.3 m/s))	-20.82	0.26	4.93	4.60	137.43	-0.04	6.39	-0.41	95.23	5.1
	-20.81	0.25	4.93	4.60	137.42		6.38	-0.41	95.23	5.1
	-19.91		4.87	4.58	135.81		6.36	-0.42	95.25	5
			5.12	3.86	96.58		4.36	-0.43	92.06	5
			8.33	2.47	67.14			-0.19	86.90	

Table I.2: Parameter estimation and reduction results using various experimental data sets at a range of forward velocities v, based on the gray box model consisting of controller K(s,θ), neuro-muscular dynamics G_{nm} and an effective neural time delay, $G_{\tau d}$, or 60 ms. The identified parameter vectors θ consist of a roll proportional gain $K_{\phi p}$ (Nm/rad), roll derivative gain $K_{\phi d}$ (Nm s/rad), roll 2^{nd} derivative gain $K_{\phi dd}$ (Nms^2/rad), steer proportional gain $K_{\delta p}$ (Nm/rad), steer integral gain $K_{\delta i}$ (Nm/(s rad)), steer derivative gain $K_{\delta d}$(Nm s/rad) and steer 2^{nd} derivative gain $K_{\delta dd}$ (Nm s^2/rad) and is given with its Variance Accounted For (VAF) (%). The second parameter elimination of Dataset 252 (v = 4.3 m/s) led to two parameters having high autocovariance and an extra reduction has been performed upon eliminating either of them.

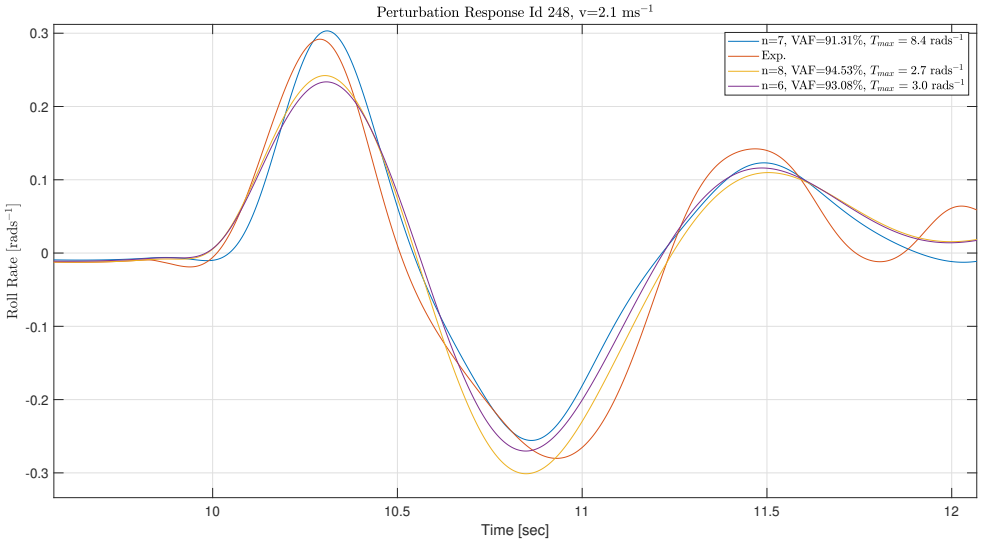

Figure I.3: Perturbation response of the gray-box model to the experimental disturbances for different state feedback parameters. This perturbation response belongs to experimental data Id. 248 which was taken at a forward velocity of 2.1 ms^{-1}.

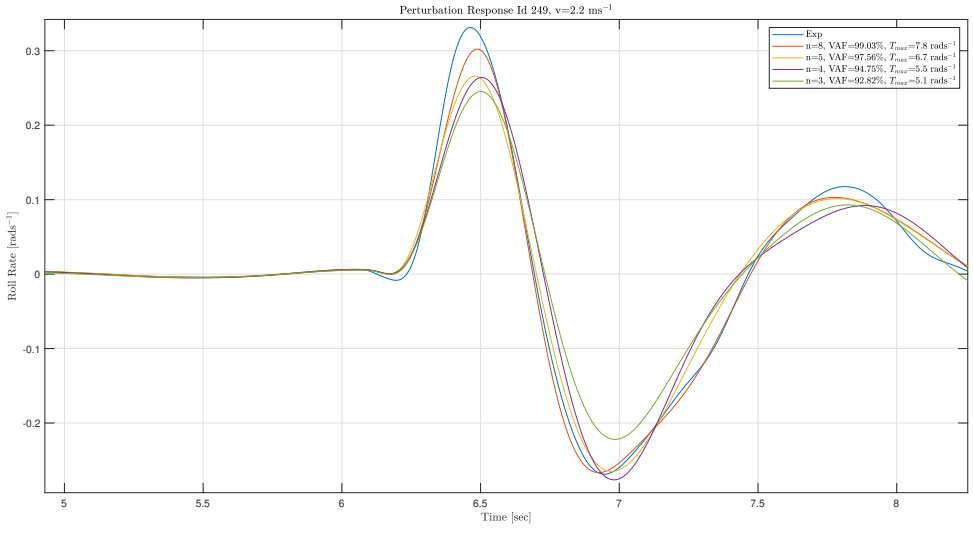

Figure I.4: Perturbation response of the gray-box model to the experimental disturbances for different state feedback parameters. This perturbation response belongs to experimental data Id. 248 which was taken at a forward velocity of 2.1 ms^{-1}.

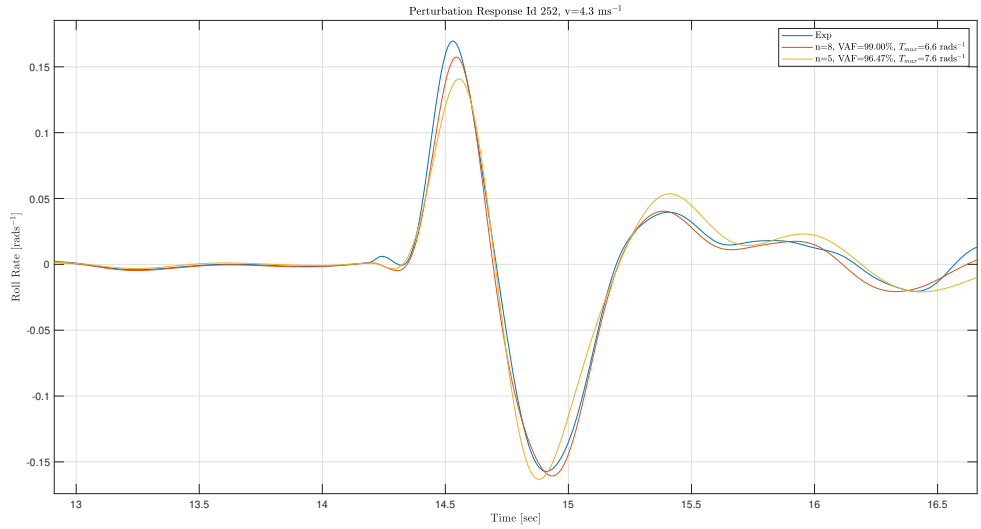

Figure I.5: Perturbation response of the gray-box model to the experimental disturbances for different state feedback parameters. This perturbation response belongs to experimental data Id. 252 which was taken at a forward velocity of 4.3 ms^{-1}.

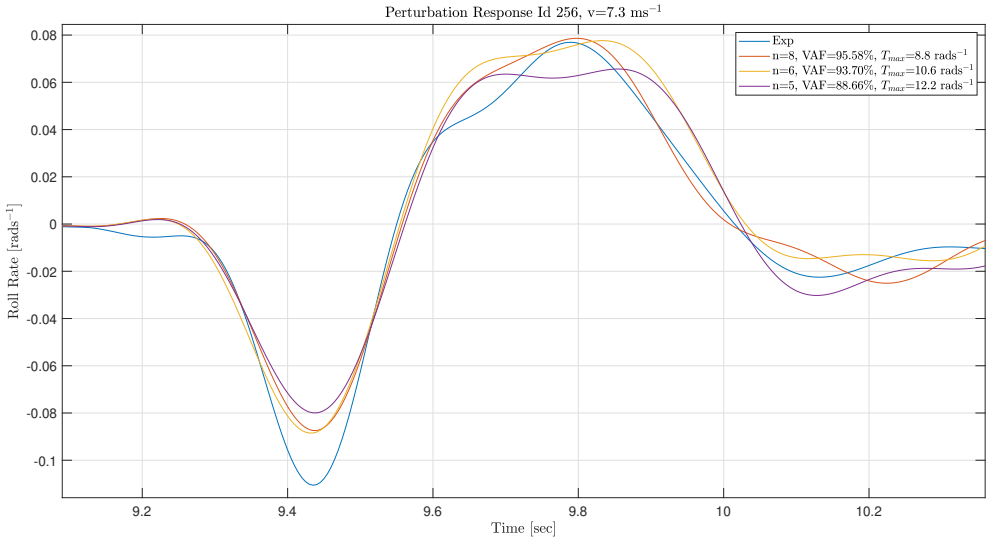

Figure I.6: Perturbation response of the gray-box model to the experimental disturbances for different state feedback parameters. This perturbation response belongs to experimental data Id. 256 which was taken at a forward velocity of 7.3 ms^{-1}.

J

Results for the Undelayed Rider

The parameter reduction process for the undelayed rider has already been performed by De Lange. This process is repeated after the mechanical bicycle parameter corrections and using the different modelling approach. This modelling approach is used to circumvent the numerical issues arising for nonzero neural time delays by the classical modelling approach, further details on this subject have been given in section 2.3. For the resulting parameter estimation, approximately the same values as published in table of [31] should be found, since De Lange also made use of a random search method to find the initial parameter vector θ_0 and the adapted modelling method yielded the same results according to the Nyquist values given in section 2.3. The reduced set is defined as the parameter set with the smallest number of feedback states while retaining a VAF above 80%.

J.0.1. Parameter Reduction using Autocovariances

After the genetic algorithm has entered the neighborhood of an optimum, the LSQNONLIN solver searches further to the optimum. Using information acquired during this search, the covariance matrix can be constructed. On the off-diagonal of this matrix one finds the covariances between parameters and on the diagonal are the autocovariances of the parameters. The parameter having the highest autocovariance is eliminated from the search and the process is repeated again. In [31], the parameter sets are reduced to the following four feedback gains,

$$\hat{\theta} = (K_{\phi p}, K_{\phi d}, K_{\delta i}, K_{\delta d}), \tag{J.1}$$

hence it is expected that upon repeating the reduction, the same reduced set will be found. Repeating the parameter reduction of the undelayed rider model gave some unexpected results. The results of the repeated reduction are given in table J.1.

Very similar results for data sets 248 and 249 are found, compared to De Lange his results; a proper reduction could be executed for 249, but not for 248. The values of the reduced parameter set for run 249 are close,

$$\hat{\theta}_{ri}^{249}(v = 2.2) = \begin{pmatrix} 28.97 & 32.85 & 29.02 & -2.50 \end{pmatrix}, \tag{J.2}$$

$$\hat{\theta}^{249}(v = 2.2) = \begin{pmatrix} 27.04 & 32.34 & 27.01 & -2.53 \end{pmatrix}, \tag{J.3}$$

where θ_{ri} refers to the found parameter set of [31]. De Lange attributes the failed reduction of data set 248 to the high signal-to-noise ratio and the inherent instability of the uncontrolled bicycle at the low velocity. For data set 256 at 7.3 ms^{-1}, a different reduction from [31] was found. The reduced parameter sets for both run 256 and 257 turn out to be,

$$\hat{\theta} = (K_{\phi p}, K_{\phi dd}, K_{\delta p}, K_{\delta d}), \tag{J.4}$$

which seems to be an alternative solution to describing the data while retaining a high VAF (>85%).

Model	$K_{\phi p}$	$K_{\phi i}$	$K_{\phi d}$	$K_{\phi dd}$	$K_{\delta p}$	$K_{\delta i}$	$K_{\delta d}$	$K_{\delta dd}$	***VAF***
Run 248: **K**(s,θ(v=2.1))	1553.99	77.16	696.32	-49.49	-132.76	870.67	-77.35	-6.86	94.88
	-2.85		6.35	2.27	-1.42	3.07	0.67	0.09	94.6
			7.59	2.18	-1.65	4.7	0.53	0.08	94.59
			12.03	1.7	-1.09	6.9		0.06	93.47
			14.82	1.95		9.82		0.04	92.63
Run 249: **K**(s,θ(v=2.2))	294.09	-109.79	95.3	-5.59	-23.08	192.03	-9.56	-0.52	99.22
	268.7		98.11	-6.36	-23.49	165.98	-10.32	-0.52	99.01
	62.35		48.33	-0.18		58.64	-3.39	-0.12	98.72
	59.96		46.41			56.22	-3.19	-0.11	98.71
	27.04		32.34			27.01	-2.53		93.22
Run 184: **K**(s,θ(v=3.2))	6.17	-10.06	12.27	1.38	4.51	32.84	-0.09	0.08	97.67
	4.85	-9.18	11.78	1.43	4.86	30.67		0.08	97.67
		-2.22	10.94	1.38	5.68	22.47		0.11	97.39
			10.74	1.37	5.42	20.99		0.11	97.34
			14.03	2	8.32	28.75			93.12
Run 252: **K**(s,θ(v=4.3))	263	-247.06	109.49	-7.71	-93.15	966.78	-20.13	-0.8	99.36
	83.78	-146.43	52.12	-0.64		452.83	-5.39	-0.21	98.18
	80.1	-127.57	44.01			389.71	-3.96	-0.19	97.77
	53.75		35.95			243.68	-3.85	-0.10	96.47
	41.31		28.23			174.11	-3.31		94.51
Run 190: **K**(s,θ(v=6.0))	-3.44	1.61	4.15	1.8	42.11	5.66	2.45	0.18	79.03
	-11.9	0.080	1.04	2.37	55.37		5.17	0.18	95.56
	-11.81		1.02	2.37	55.26		5.18	0.18	95.57
	-7.98			2.43	49.46		5.72	0.09	92.58
	-7.97			2.81	53.94		6.27		91.89
Run 256: **K**(s,θ(v=7.3))	-16.62	0.14	2.92	2.34	92.58	0.32	5.06	0.20	90.42
	-16.64	0.18	2.91	2.35	92.61		5.07	0.20	90.41
	-15.37		2.77	2.34	90.8		5.11	0.18	90.37
	-16.6		2.3	2.97	102.44		6.53		89.01
	-13.5			2.71	87		7.43		85.14
				2.18	59.18		6.13		79.3
				0.80			3.16		32.73
				1.06					16.27

Table J.1: Parameter estimation and reduction results using various experimental data sets at a range of forward velocities v. based on the gray box model consisting of controller K(s, θ), neuro-muscular dynamics G_{nm} and an effective neural time delay $G_{\tau d}$ with τ_d=0 ms. The identified parameter vectors θ consist of a roll proportional gain $K_{\phi p}$ (Nm/rad). roll derivative gain $K_{\phi d}$ (Nm s/rad). roll 2^{nd} derivative gain $K_{\phi dd}$ (Nm s^2/rad). steer proportional gain $K_{\delta p}$ (Nm/rad). steer integral gain $K_{\delta i}$ (Nm/(s rad)). steer derivative gain $K_{\delta d}$(Nm s/rad) and steer 2^{nd} derivative gain $K_{\delta dd}$ (Nm s^2/rad) and is given with its Variance Accounted For (VAF) (%).

J.1. Parameter Estimation - Four Feedback Gains

For both reduced sets consisting of four feedback states, the parameter estimation process is repeated for not just 6, but all 15 data sets. The estimated parameters for the same reduced parameter set of (J.1) are given in table J.2. The estimated parameters belonging to the alternative solution are given in J.3. For nearly all estimated parameter sets of table J.2, the model is able to describe the experimental data accurately (VAF>90%). The proportional and derivative roll parameters stay relatively constant over velocity and always have a positive sign. The integral parameter grows significantly over velocity and the steer rate feedback is always of negative sign and also relatively constant over forward speed.

For the alternative reduced parameter sets, the same optimization settings were used for the algorithm. Yet, the VAF is overall significantly lower for the alternative parameter set (see figure J.1).

Therefore, the alternative reduced parameter set is excluded and only the original set will be used for numerical integration.

Model τ_d=0 ms	$K_{\phi p}$	$K_{\phi d}$	$K_{\delta i}$	$K_{\delta d}$	**VAF**
248 K(s,θ(v=2.1))	4.316	27.02	13.53	-1.95	94.72
249 K(s,θ(v=2.2))	27.04	32.34	27.01	-2.53	96.48
250 K(s,θ(v=2.2))	22.69	32.03	24.79	-2.60	96.42
184 K(s,θ(v=3.2))	22.67	26.13	65.27	-3.06	96.88
185 K(s,θ(v=3.2))	42.90	30.35	92.02	-3.28	95.83
186 K(s,θ(v=3.1))	30.71	28.35	69.81	-3.00	92.25
251 K(s,θ(v=4.3))	72.38	32.41	202.53	-4.01	84.16
252 K(s,θ(v=4.3))	41.31	28.23	174.11	-3.31	93.22
253 K(s,θ(v=4.3))	45.32	29.02	165.60	-3.73	94.64
190 K(s,θ(v=6.0))	34.77	23.71	338.21	-3.68	88.83
191 K(s,θ(v=6.1))	30.13	23.21	326.29	-3.99	94.51
192 K(s,θ(v=6.1))	28.80	20.78	297.66	-3.44	94.88
255 K(s,θ(v=7.3))	37.74	27.09	536.91	-5.62	92.49
256 K(s,θ(v=7.3))	48.91	30.21	579.15	-7.36	89.76
257 K(s,θ(v=7.4))	46.32	27.43	619.52	-4.93	92.77

Table J.2: Estimated reduced parameter sets θ of controller $K(s,\theta)$ with neuro-muscular dynamics G_{nm} and effective neural time delay τ_d=0 ms, and the corresponding VAF (Variance Accounted For).

Model τ_d=0 ms	$K_{\phi p}$	$K_{\phi dd}$	$K_{\delta p}$	$K_{\delta d}$	**VAF**
248 K(s,θ(v=2.1))	-6.08	4.36	-1.52	2.12	85.34
249 K(s,θ(v=2.2))	-2.70	4.49	-1.06	2.15	90.32
250 K(s,θ(v=2.2))	-6.00	4.13	-1.17	2.05	86.62
184 K(s,θ(v=3.2))	-4.17	2.77	4.44	2.59	91.89
185 K(s,θ(v=3.2))	-1.98	3.26	6.04	3.00	87.61
186 K(s,θ(v=3.1))	-4.07	3.31	5.22	2.86	87.62
252 K(s,θ(v=4.3))	1.96	4.52	30.32	5.69	85.86
253 K(s,θ(v=4.3))	-6.15	3.75	25.28	4.83	90.58
254 K(s,θ(v=4.3))	-2.70	3.33	19.88	4.32	87.48
190 K(s,θ(v=6.0))	-7.97	2.81	53.94	6.27	81.33
191 K(s,θ(v=6.1))	-6.96	2.44	47.85	5.57	80.46
192 K(s,θ(v=6.1))	-11.17	2.62	55.72	6.26	81.10
255 K(s,θ(v=7.3))	-14.12	2.96	94.61	7.79	87.03
256 K(s,θ(v=7.3))	-13.50	2.71	87.00	7.43	85.14
257 K(s,θ(v=7.4))	-15.24	3.32	109.87	8.96	86.48

Table J.3: Estimated alternative reduced parameter sets θ of controller K(s,θ) with neuromuscular dynamics G_{nm} and effective neural time delay τ_d=0 ms, and the corresponding VAF (Variance Accounted For).

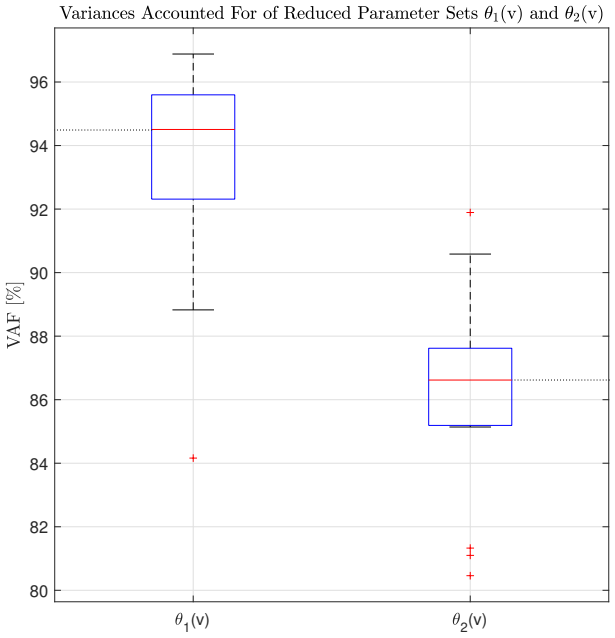

Figure J.1: Boxplots of the variance-accounted-for (VAF) found for the reduced parameter sets given in table J.2 and J.3 on the left and right, respectively.

J.2. Parameter Continualization

The stability of an uncontrolled bicycle is dependent on forward speed. Therefore, it is to be expected that the control strategy of the rider would also change with forward velocity. However, it is now known how a rider adapts its control to the bicycle's stability. Therefore, it will be assumed that the control of the rider changes linearly over forward velocity. A linear regression is applied to the reduced estimated parameter sets, and it denoted by θ_{LR}. This led to the linear functions given in equation J.5.

$$K(s,v) = \begin{bmatrix} K_{\phi p} \\ K_{\phi d} \\ K_{\delta i} \\ K_{\delta d} \end{bmatrix} = \begin{bmatrix} 3.42 \\ -0.8 \\ 103.38 \\ -0.58 \end{bmatrix} v + \begin{bmatrix} 19.99 \\ 31.59 \\ -240.72 \\ -1.09 \end{bmatrix} \tag{J.5}$$

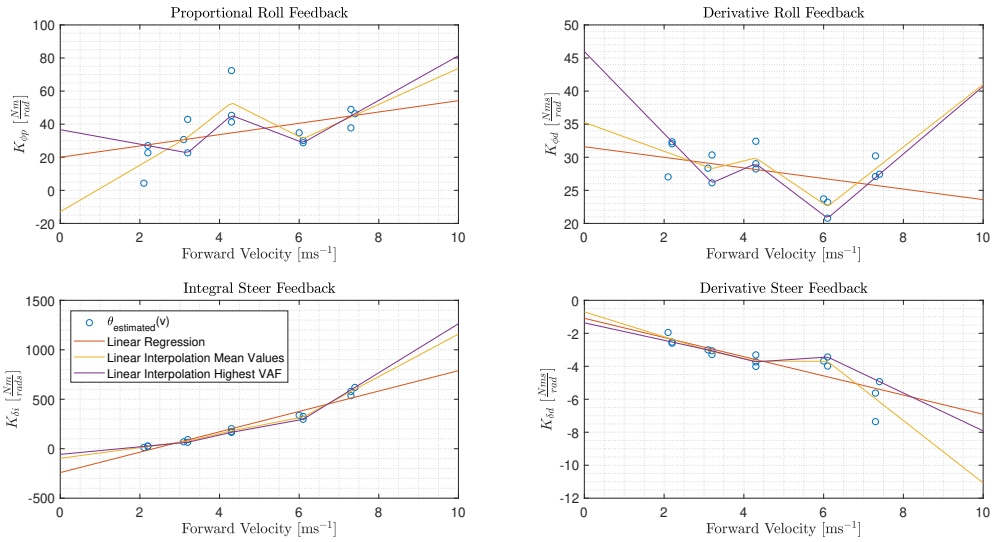

Figure J.2: The discrete, estimated four state parameters $\theta(v) = (K_{\phi p}, K_{\phi d}, K_{\delta i}, K_{\delta d})$ and their continualizations, resulting from gray box identification of controller $K(s,\theta)$ with neuro-muscular dynamics G_{nm} and neural time delay τ_d=0 ms. The discrete estimated parameters are the blue circles. The orange line is their linear regression, the yellow line a linear interpolation between the mean values of the estimated parameters per velocity group and the purple line a linear interpolation between the parameter sets with the highest VAF per velocity. A velocity group consists of three parameter sets for close velocities. The top-left figure contains the parameter functions of the proportional roll parameter, $K_{\phi p}$. The top-right figure of the derivative roll parameter, $K_{\phi p}$, the bottom-left of the integral steer parameter, $K_{\phi p}$, and the bottom-right figure of the derivative steer parameter $K_{\delta d}$.

Another option to make the parameter sets continuous over velocity, would be to use linear interpolation between the parameters. Since the parameter sets are not unique per velocity, a choice has to be made as to which sets will be used. Two options are considered for the linear interpolation; taking the parameter set with the highest VAF for each velocity group, denoted by $\theta_{LI,mean}$, or taking the average parameter sets per velocity group, denoted by $\theta_{LI,VAF}$. Velocity group refers to the velocities lying close together, such as 2.1, 2.2 and 2.2 m/s. All three velocity-dependent, continuous parameter functions are plotted versus forward velocity in figure J.2. If the systems sensitivity to the estimated parameters would be high, the controller K(s, θ_{LR}) will yield a significant different numerical integration result from the other two controllers. If the system is sensitive to specific combinations of parameters, controller K$(s, \theta_{LI,mean})$ would then also yield a different stability result. Then, if the system would be highly sensitive, at least controller K$(s, \theta_{LI,VAF})$ would return results closest to the true at the experimental velocities.

J.3. Control Strategy Analysis

It can be seen that $K_{\phi p}$ is positive for all forward velocities, this corresponds with a steering into the fall and indicates the systems compliance to perturbations. Then, $K_{\phi d}$ is always positive as well, thereby exciting the systems motion and also aiding the steer-into-the-fall principle. Then, $K_{\delta i}$ results in steering away from the straight ahead. A clear interpretation could not be found for this gain, it might be related to counter steering. The negative $K_{\delta d}$ has a damping influence of the system and partially eliminates oscillatory motion at the handlebars. For the proportional roll angle and rate feedback, there seems to be a change in control strategy between 4.3 and 6.1 ms^{-1}. The transition of the dynamic modes of the uncontrolled bicycle also occurs during that range, the bicycle's dynamics become stable and the weave motion is less present. It is also known that the weave motion is easily stabilized using roll rate feedback and that the capsize motion can be stabilized using roll angle feedback, which seems to be the

two feedback parameters changing the most for the mode change of the bicycle. For future research, it would be interesting to have a higher velocity resolution of rider data available between the above mentioned velocities such that the potential control strategy change can be more clearly portrayed.

J.4. Eigenvalue Analysis

The stability of the bicycle-rider system is evaluated based on the eigenvalues of the closed-loop system. The eigenvalues of controller K(s,θ), for the three gain parameter functions given in figure J.2, are displayed as a function of forward velocity in figure J.3. Two states are added due to the neuro-muscular dynamics and one more for the integral state, therefore the total number of states is 7 which results in 7 eigenvalues. The real parts of all eigenvalues are stabilized for the experimental velocities for both $K_{\theta_{LI,VAF}}$ and $K_{\theta_{LI,mean}}$. Controller $K_{\theta_{LR}}$ is unstable for 2.2 ms^{-1}. For the remainder, all controllers are stable within the range dictated by the experimental velocities. Controller $K_{\theta_{LR}}$ is only marginally stable at 4.3 ms^{-1} due to $\lambda_{2,3}$, for which is deviates significantly from the other controllers. In figure J.2, the linear regression does not capture the kink observed for $K_{\phi p}$ and $K_{\phi d}$ at 4.3 ms^{-1}. The linear regression deviates at both 4.3 ms^{-1} and 6.0 ms^{-1}, but the eigenvalues do not deviate as much for 6.0 ms^{-1}. This might be due to the linear regression having a larger, positive value of $K_{\phi d}$ which is likely partially cancelled by the more negative value of $K_{\delta d}$. Due to the discrepancy between the linear interpolation functions and the linear regression, it is expected that this difference will be observed for 4.3 ms^{-1} for their basins of attraction.

		Gain Parameters			
Name	**Symbol**	$K(s,\theta_{LR})$	$K(s,\theta_{LI,mean})$	$K(s,\theta_{LI,VAF})$	**Unit**
Weave Velocity	v_w	2.34	1.77	1.50	[ms^{-1}]
Capsize Velocity	v_c	10.71	10.55	8.95	[ms^{-1}]

Table J.4: blabla

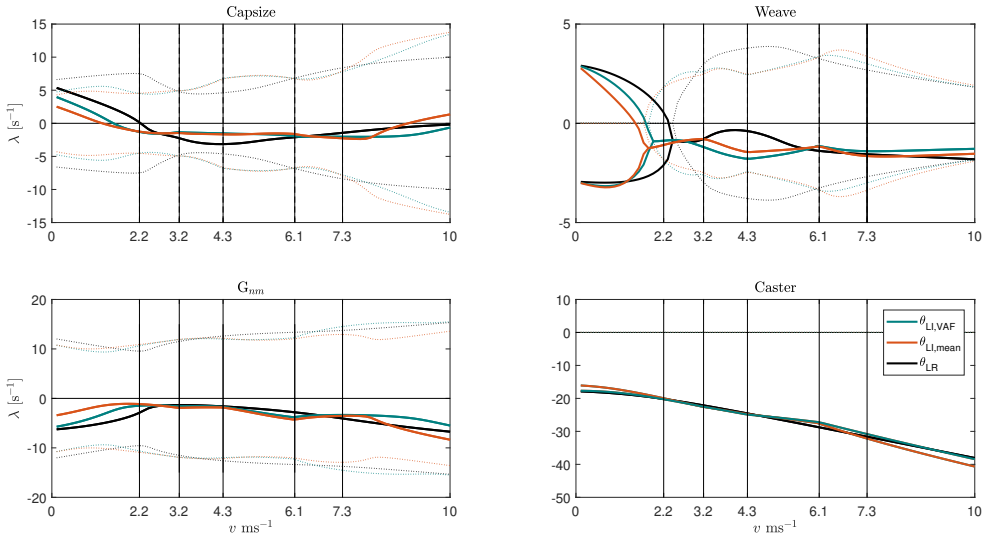

Figure J.3: of controller K(s,θ) with neuro-muscular dynamics G_{nm}, where the gain parameters θ have been made continuous over velocity using linear regression, denoted by θ_{LR}, linear interpolation between the mean values per velocity group, denoted by $\theta_{LI,mean}$ and linear interpolation between the VAF estimated for the highest VAF per velocity group, denoted by $\theta_{LI,VAF}$. VAF = Variance Accounted For. An example of a velocity group is 2.1,2.2 and ms^{-1}, which corresponds to the groups chosen for the experimental data.

Implementation Validation

Since the rider here has 0ms neural time delay, the rider implementation can be validated by comparing the velocity range for which stable solution are found for low perturbations, with the velocity range indicated by the eigenvalues. The basins of attraction given in figure J.4 will not exactly correspond to the stable velocities given by the eigenvalues due to the maximal simulation time. However, by simulating with 0.5 rads^{-1} and velocities around the utmost stable velocities and looking at the states over time, the stability transition should be visible. The critical stability velocities are given in table J.4.

J.5. Comparison of the Basins of Attraction

The outlines of the identified stability regions of the three controllers K(s, θ_{LR}), K$(s, \theta_{LI,mean})$ and K$(s, \theta_{LI,VAF})$ are compared in figure J.4.

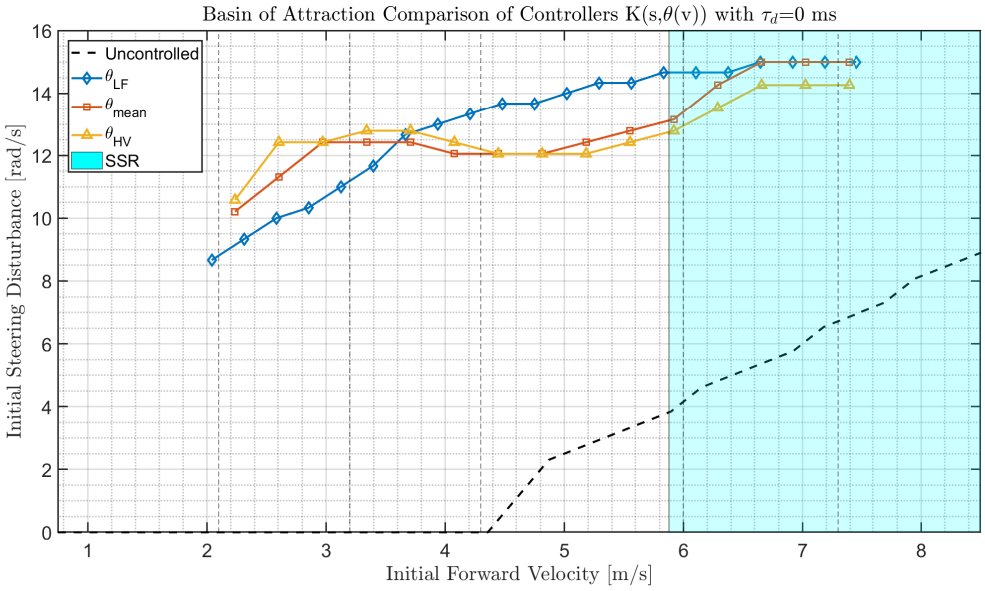

Figure J.4: Basin of attraction outlines of bicycle-rider system consisting of the WCBM combined with a rider, based on the gray box model consisting of controller K, second-order neuro-muscular dynamics G_{nm} and no neural time delay, τd= 0 ms. The blue shaded region is the self-stable region of the uncontrolled bicycle and ranges from 5.88 to 10.13 ms^{-1}. The dashed, vertical lines are the velocities at which the experimental data was acquired and the parameter sets were estimated. These velocities are approximately 2.1, 3.2, 4.3, 6.0 and 7.3 ms^{-1}. The orange line represents the control model for which the parameter sets, θ, were made continuous over velocity using a linear data fitting. The parameters of the controller corresponding to the yellow line, were linearly interpolated mean parameters. For the purple line, the parameters were linearly interpolated between the parameter containing the highest VAF.

The controller with no neural time delay, τ_d=0 ms, is capable of handling steer rate perturbation of up to approximately 15 rad/s. All three undelayed rider models seem to have somewhat a similar basin of attraction in terms of the range of maximum allowable perturbations. Controller K(s, θ_{LR}), however, does not follow the same trend as K$(s, \theta_{LI,mean})$ and K$(s, \theta_{LI,VAF})$. For the analysis of general influence on the basin of attraction, K(s, θ_{LR}) would provide a decent approximation. For more exact analysis, such as on the change of control over time, a higher order regression is likely to provide a more truthful image. The discrepancy of the outlines around the weave velocity, v=5.88ms^{-1}, again shows that a linear regression on the control parameters does not suffice.

J.6. Adding Time Delay Directly

Now that the basin of attraction of the rider with zero time delay from [31] has been identified, the influence of pure time delay can be studied by adding the time delay to the rider without altering the feedback parameters. Due to time limitations, only controller $K(s, f_{\theta_{LI,HV}})$ has been used and a low grid has been used. The result is given in figure J.5.

The detrimental effect of time delay on cycling stability is very obvious. For only 60 ms time delay, the basin of attraction of stability completely disappeared and for 30 ms time delay the basin became discontinuous over forward velocity.

Whether the elderly cyclist is properly represented by the older cyclist is not known, since the effective neural time delay of the elderly is unknown. For the young cyclists, the choice of 30ms neural time delay had been based on literature (see section **??**). Therefore, the result of the young cyclist is not realistic.

Since [31] estimated the feedback parameters based on a gray-box model with zero time delay, the actual time delay was compensated for by those estimated parameters. Adding the time delay on top of those gains, leads to the double incorporation of time delay. From the results here, one can deduce that time delay significantly influence stability and that a solution has to be found upon such that its influence can be studied properly.

It would make sense for a human to be unconsciously aware of the approximate time delay we suffer from. Therefore, without altering the gray box structure of [31], the feedback parameters require re-estimation and if no high VAF can be found with the 4 parameters of [31], the feedback parameter reduction also needs to be repeated.

By doing this, it is assumed that the older cyclist is more aware of the time delay it has since it is adapting its control to data from a young cyclist based on 60ms time delay. Therefore, the results of the older cyclist are likely to be somewhat overestimated.

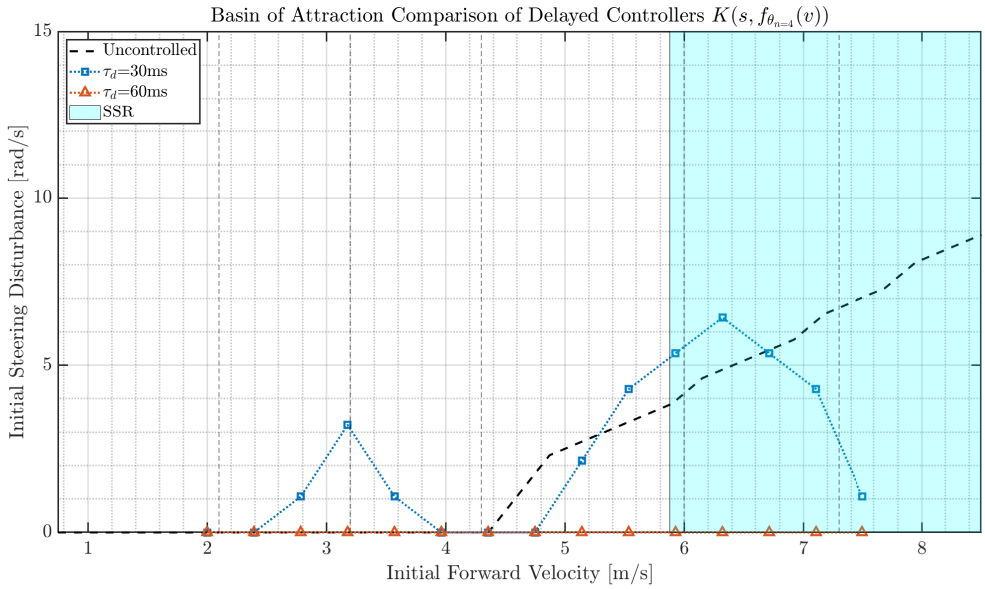

Figure J.5: Basin of attraction outlines of bicycle-rider system consisting of the WCBM combined with a rider, based on the gray box model consisting of controller K, second-order neuro-muscular dynamics G_{nm} and neural time delay τ_d. The blue shaded region is the self-stable region of the uncontrolled bicycle and ranges from 5.88 to 10.13 ms^{-1}. The dashed, vertical lines are the velocities at which the experimental data was acquired and the parameter sets were estimated. These velocities are approximately 2.1, 3.2, 4.3, 6.0 and 7.3 ms^{-1}. The orange line represents the control model for which the parameter sets, θ, were made continuous over velocity using a linear data fitting. The parameters of the controller corresponding to the yellow line, were linearly interpolated mean parameters. For the purple line, the parameters were linearly interpolated between the parameter containing the highest VAF.

K

Sensitivity Analysis

For the smart, old cyclist, using a linear regression on the estimated parameters resulted in an unexpected instability at 4.3 ms^{-1} (see figure 3.4). Therefore, a sensitivity analysis will be performed hoping that it gives more insight into the problem at hand.

Outline

First off, the problem is further explained in section K.1.

K.1. Problem Introduction

The parameter estimation of the smart, old cyclist (see appendix G.2) already revealed the possibility of existence of multiple control strategies. There is not just one unique solution by which the experimental data can be described using the 7-state feedback in the gray box model. This could be observed from the signs and order of the feedback values for different data sets at the same velocities and the disorderly trend of those values over velocity.

Then, if one were to interpolate values of two sets of parameters, one set of velocity x and of y, and those parameter sets would not lie within the proximity of the same optima, it would be no surprise that at an arbitrary velocity in between x and y instability would occur due to the wrong combination of parameters.

A similar effect could be expected if a linear regression would be applied and would pass in between two sets, again of different optima, but at one and the same velocity. However, run 251 to 253 all seem to have values close to one another (see table G.4), hence likely close to the same optimum, and the data fits do not seem to deviate much from them (see figure 3.3). Therefore, a sensitivity analysis is performed at the initial forward velocity of 4.3 ms^{-1}.

K.1.1. Parameter Solutions Comparison

To identify the cause of the sudden instability, the steering torque responses are plotted using the three discrete estimated parameter sets, θ_{251}, θ_{252} and θ_{253}, their mean values $\overline{\theta}(v = 4.3)$ and the linear regression values $f_{\theta_{LR}}(v = 4.3)$. The result is given on the right and the corresponding parameter sets for this velocity on the left of figure K.1. For the three parameter sets and their mean, a stable solution is found (see figure K.1).

Looking at the parameter sets, except for the $K_{\phi p}$, the values of θ_{LR} lie within the range stretched by the discrete estimated parameter sets. This leads to the expectation that $K_{\phi p}$ might be the cause of the unstable result of θ_{LR}. The next step is to identify main feedback gain at the cause of this stability discretion.

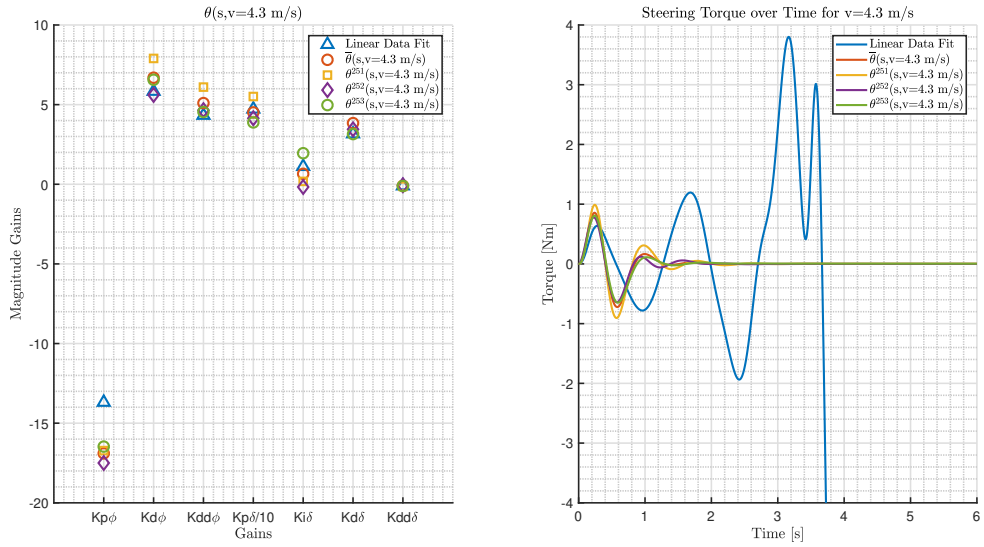

Figure K.1: The values of the estimated parameter sets $\theta(V)$ for data set 251, 252, 253 and their mean as well as the values from the data fit (left) and their corresponding steering torques over time for controller $K(\theta(s, v = 4.3m/s))$ for an initial forward velocity and disturbance of 4.3 m/s and 0.5 rad/s, respectively (right). All correspond to a forward velocity of 4.3 m/s. The proportional steer parameter is scaled down by 10.

K.1.2. Sensitivity Analysis of the Instability

To seek the most crucial parameter at the cause of the instability, a sensitivity study will be performed. Apart from $K_{\phi p}$, the remaining gains of $\theta_{LR}(v = 4.3)$ do not seem to deviate significantly from the estimated parameter sets nor their mean, yet do result in instability whereas the rest is stable. It is known that the mean parameters yield a stable result. Therefore, the percentage difference between $\theta_{LR}(v = 4.3)$ and $\overline{\theta}(v = 4.3)$ are given in table K.1 with respect to $\theta_{LR}(v = 4.3)$.

It can be seen that the largest percentage difference is found for $K_{\delta i}$. However, $K_{\delta i}$ had large values for the other controllers (e.g. see table 3.1). Therefore, it is unlikely that $K_{\delta i}$ is the cause of the instability. To see which gain is, multiple simulations will be performed using $\theta_{LR}(v = 4.3)$. For every simulation, one gain value will be substituted by the gain of the mean.

If no stable results are found for all individual parameter substitutions, this would indicate interaction, and hence dependency, between the parameters. Meaning that, if the unstable system can not be stabilized by the substitution of one of the individual parameters, it might be stabilized by the substitution of a group of parameters. That would leave us with a profusion of substitutions to try.

The results of this simple sensitivity analysis are given in figure K.2, where the resulting states over time are given. The single parameters which are substituted for the mean parameter value are given in the legend. The black dashed line represents the parameter set of the linear data fitting. The percentage differences between the mean parameters values and the linear regression parameter values with respect to the latter, are given in table K.1.

	$K_{\phi p}$	$K_{\phi d}$	$K_{\phi dd}$	$K_{\delta p}$	$K_{\delta i}$	$K_{\delta d}$	$K_{\delta dd}$
Mean Value $\overline{\theta}(v = 4.3)$	-16.90	6.69	5.10	45.12	0.65	3.84	-0.10
Linear Regression $\theta_{LR}(v = 4.3)$	-13.69	5.83	4.33	47.19	1.11	3.16	-0.11
Percentage Change [%]	18.99	-12.86	-15.10	4.59	70.77	-17.71	0.10

Table K.1: Mean and linear regression parameter values θ at 4.3 ms^{-1} forward velocity, of a rider control model $K(s, \theta)$ with neuro-muscular dynamics G_{nm} and 60 ms neural time delay τ_d, and their percentage difference with respect to the mean values $\overline{\theta}(v = 4.3)$. The values are based on three experimental data sets.

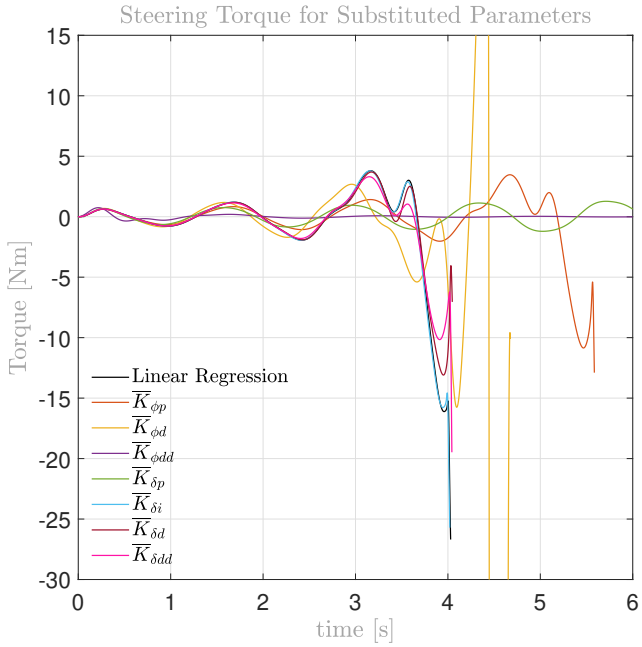

Figure K.2: Steering torque $T_\delta(t)$ of controller $K(s, \theta(v = 4.3))$ for various parameter solutions. The black, dashed line contains of an unstable controller with a parameter set based on a linear regression of the estimated parameter sets for v=4.3 m/s of the control group with negative $K_{\phi p}$. The simulation has been repeated for substituted mean parameter values, given in the legend. Substituting the mean roll acceleration parameter yields a stable solution, for all other substitutions the result remains unstable or becomes marginally stable. Table K.1 gives the corresponding parameters of the linear regression and the mean parameter values

From figure K.2, it can be seen that substituting the $\overline{K}_{\phi dd}$ stabilizes the solution completely. Substitution of $\overline{K}_{\delta p}$ also seems to improve stability. However, the result seems marginally stable. For all other parameter substitutions, stability is still lost.

The difference in roll acceleration feedback gains seemed minor from figure K.2 but has a significant percentage difference of 18.89%. An acceleration feedback functions as a lead and since the rider has a large neural time delay it is not surprising that a change in this feedback parameter will yield a large difference in the disturbance response. However, the influence of $\overline{K}_{\delta p}$ is interesting, since it induces quite the difference in the perturbation response while its percentage difference of -4.59% is fairly small.

Lowering $K_{\delta p}$ indicates less steering stiffness, hence, a lesser ability to steer into the fall. However, it also indicates that the displacement of the handlebars due to the perturbation will be higher, but apparently the trade-off suffices for marginal stability. It would be interesting to see if lowering the stiffness even further would induce instability again.

To conclude, the occurring instability at 4.3 ms^{-1} of the controller with $\theta_{LR}(v = 4.3)$ is the result of deviations in $K_{\delta p}$

To be able to properly compare the influence of the parameter changes, it would be interesting to, individually, change the mean parameter values by a fixed percentage and then study their influence on the perturbation response for all measured velocities. A fixed percentage makes it easier to compare amongst the parameters and using the main parameter values instead of the parameter of the linear regression will result in a clearer influence of the parameters since the mean parameter solutions are stable for all forward velocity.

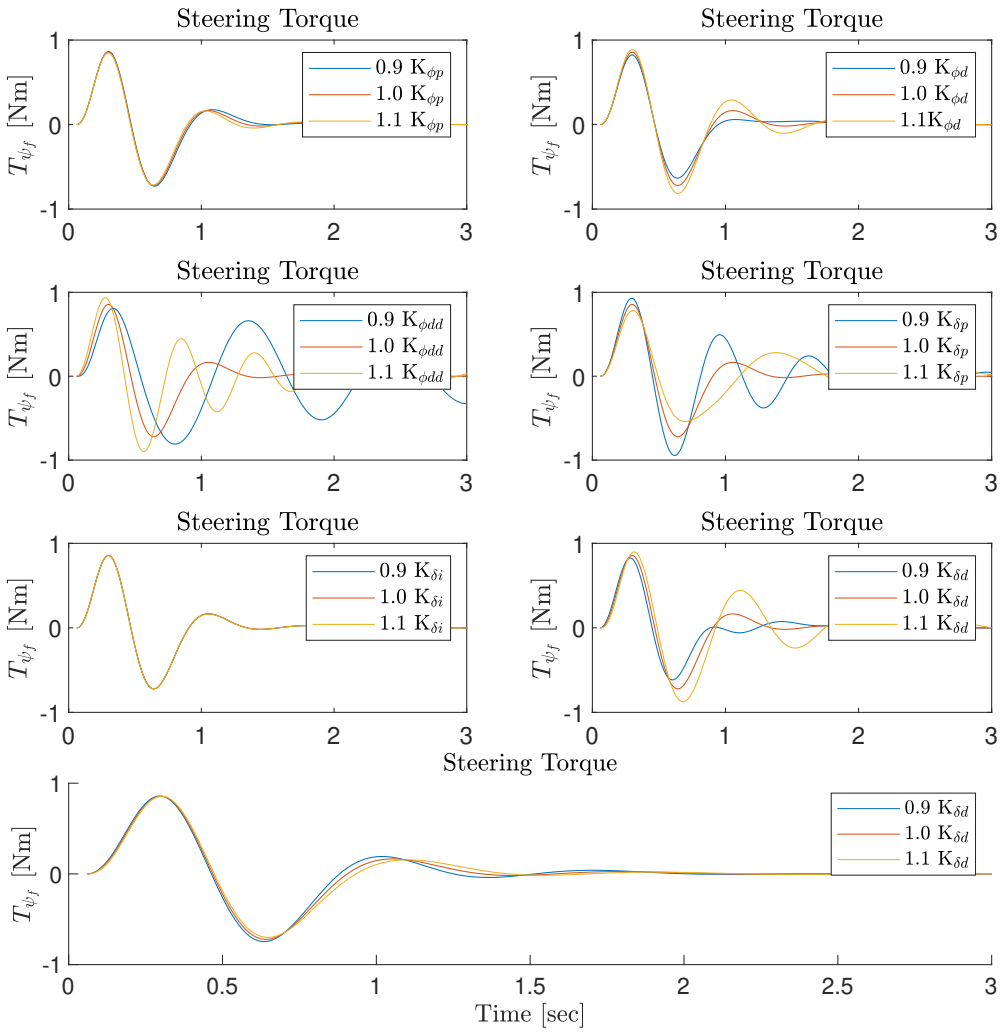

Figure K.3: A sensitivity analysis of the parameters of controller $K(s, \theta)$ with neuro-muscular dynamics G_{nm} and effective neural time delay τ_d of 60 ms for which the feedback parameters are averaged per velocity group. The torque response corresponds to a initial steer perturbation of 0.5 rads^{-1} and forward velocity of 4.3 ms^{-1}. The responses are visualized upon a 10% increase or decrease of the feedback parameter given in the legends. An example of a velocity group is the group of 2.1, 2.2 and 2.2 ms^{-1}. $\theta(v = 4.3)$=

$$-13.69, 5.83, 4.33, 47.19, 1.11, 3.16, -0.11$$

K.1.3. Sensitivity Analysis For All Experimental Velocities

For all experimental velocities, the mean estimated parameter values have been shifted one by one by 10%. The result at a forward velocity of 4.3 ms^{-1} is displayed in figure K.3, the results derived at the remaining experimental velocities have been suspended to Appendix **??** due to their length. The feedback parameters are multiplied by either 0.9, 1.0 or 1.1. To study the influence of these changes in parameter values, the sign of the original parameter value is of major importance. The mean parameter values and their signs at a forward velocity of 4.3 ms^{-1} are given in table K.1. The influence of the previously mentioned feedback parameters, $K_{\phi dd}$ and $K_{\delta p}$, is clearly visible. The roll acceleration feedback, $K_{\phi dd}$, is of positive sign. Increasing this feedback value corresponds to steering even more along with the roll acceleration. E.g., if a fall to the right starts to occur, the rider steers to the right as well; it steers-into-the-fall. Thereby, this feedback aids in preventing the fall. Since an acceleration feedback functions like a lead, it is a very important feedback parameter for the rider with a significant neural time

delay. Decreasing this values quickly destabilizes the system for all velocities and lowers the damping of the response. Increasing the value often leads to a slightly higher overshoot for the first period and a dampened, high frequency response. Interesting is the visible, opposite effect of the steering stiffness $K_{\delta p}$, between the linear regression analysis and the analysis of figure K.3. Since the sign of $K_{\delta p}$ is negative, a more appropriate term would be 'steering compliance'. Here, increasing the steering compliance by 10% leads to a more stable solution for the first period amplitudes whereas decreasing it induces a less critical damping which corresponds with stiffer behaviour, hence making the system less stable. For the linear regression analysis, it was found that swapping the linear regression parameter value of 47.19 by 45.12 led to an increased stability. This clearly indicates to an interdependence between the parameters since the increased value of the proportional steer parameter of the mean exceeds the value of the unstable, linear regression. The influence of the steer rate feedback $K_{\delta d}$ becomes more obvious for this analysis than from figure K.2. Here, it becomes clear that increasing the steer parameter excites the system. This makes sense, since the sign of the parameter is positive, whereas a negative sign would indicate steer dampening. This is visible for the lower value of $K_{\delta d}$ which clearly dampens the system. The system is significantly less sensitive to the remainder of the parameters.

K.1.4. Remaining Sensitivity Results

In this appendix the remaining results of the sensitivity analysis are given. The experimental velocities are approximately 2.1, 3.2, 4.3, 6.0 and 7.3 ms^{-1}. The figures have been order from the lowest velocity, v=2.1 ms^{-1}, in figure K.4 at the top to the highest velocity, v=7.3 ms^{-1}, in figure K.8 and the bottom.

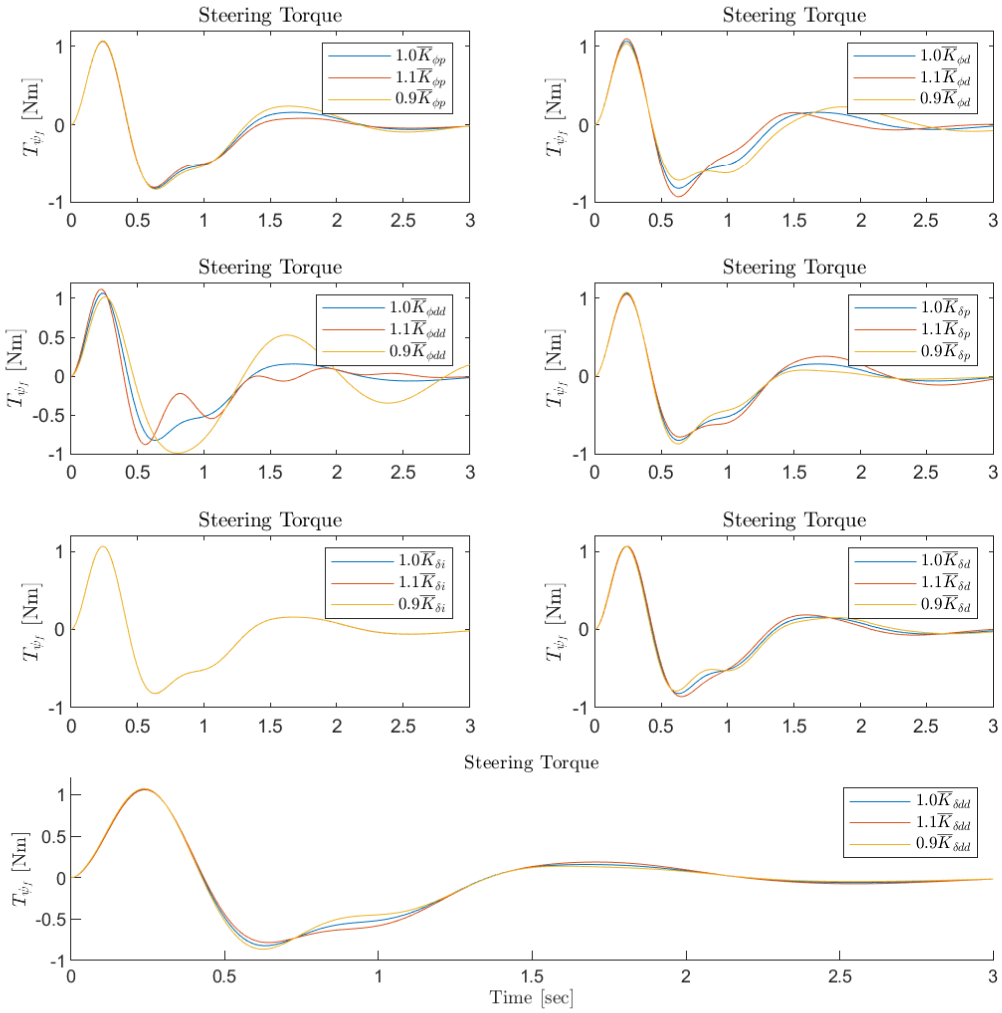

Figure K.4: A sensitivity analysis of the parameters of controller $K(s,\theta)$ with neuro-muscular dynamics G_{nm} and effective neural time delay τ_d of 60 ms for which the feedback parameters are averaged per velocity group. The torque response corresponds to a initial steer perturbation of 0.5 rads^{-1} and forward velocity of 2.2 ms^{-1}. The responses are visualized upon a 10% increase or decrease of the feedback parameter given in the legends. An example of a velocity group is the group of 2.1, 2.2 and 2.2 ms^{-1}.

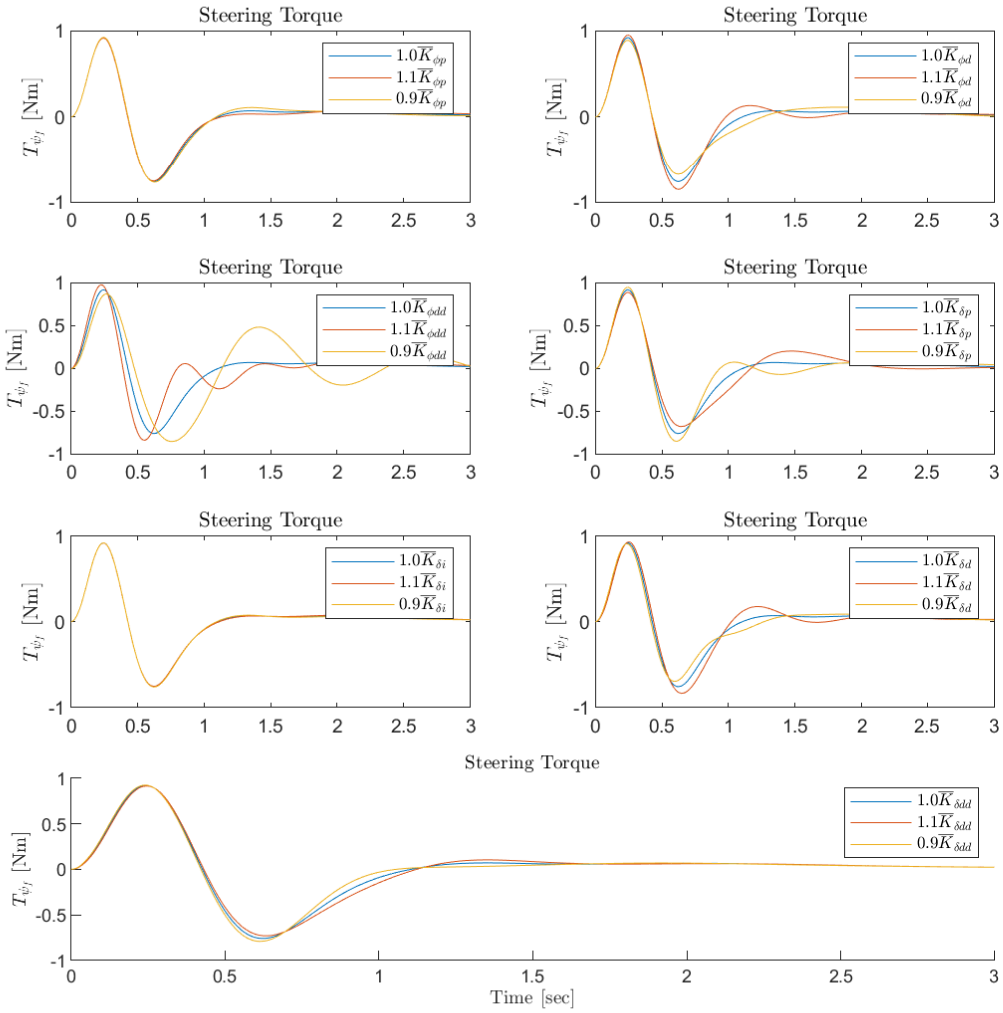

Figure K.5: A sensitivity analysis of the parameters of controller $K(s,\theta)$ with neuro-muscular dynamics G_{nm} and effective neural time delay τ_d of 60 ms for which the feedback parameters are averaged per velocity group. The torque response corresponds to a initial steer perturbation of 0.5 rads^{-1} and forward velocity of 3.2 ms^{-1}. The responses are visualized upon a 10% increase or decrease of the feedback parameter given in the legends. An example of a velocity group is the group of 2.1, 2.2 and 2.2 ms^{-1}.

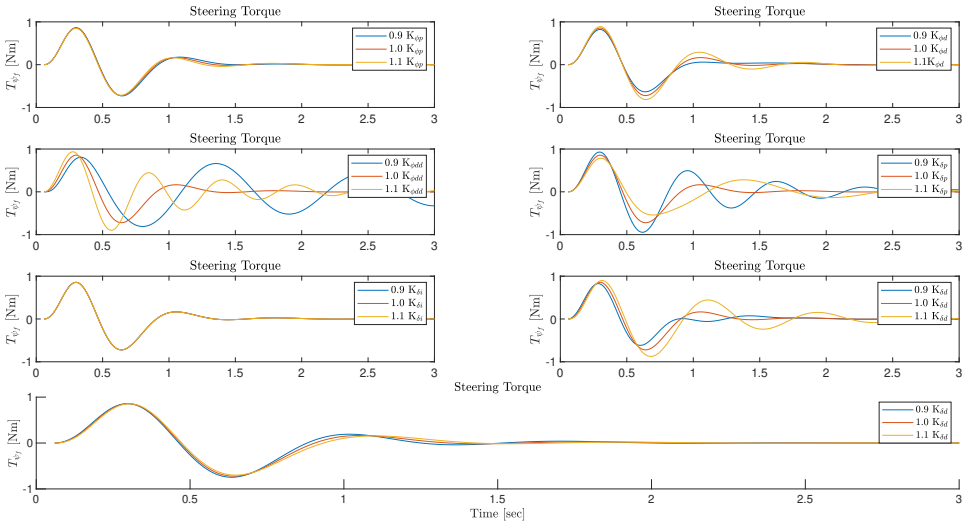

Figure K.6: A sensitivity analysis of the parameters of controller $K(s, \theta)$ with neuro-muscular dynamics G_{nm} and effective neural time delay τ_d of 60 ms for which the feedback parameters are averaged per velocity group. The torque response corresponds to a initial steer perturbation of 0.5 rads^{-1} and forward velocity of 4.3 ms^{-1}. The responses are visualized upon a 10% increase or decrease of the feedback parameter given in the legends. An example of a velocity group is the group of 2.1, 2.2 and 2.2 ms^{-1}.

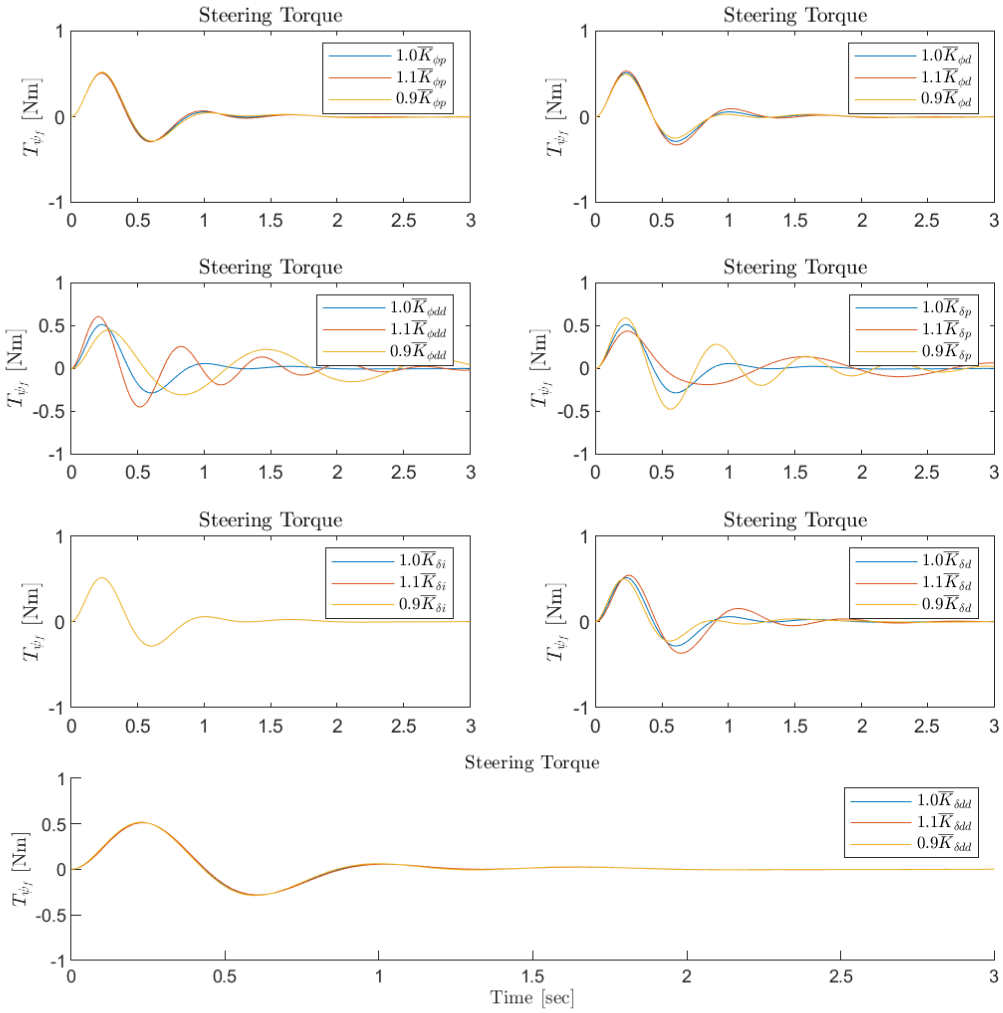

Figure K.7: A sensitivity analysis of the parameters of controller $K(s,\theta)$ with neuro-muscular dynamics G_{nm} and effective neural time delay τ_d of 60 ms for which the feedback parameters are averaged per velocity group. The torque response corresponds to a initial steer perturbation of 0.5 rads^{-1} and forward velocity of 6.0 ms^{-1}. The responses are visualized upon a 10% increase or decrease of the feedback parameter given in the legends. An example of a velocity group is the group of 2.1, 2.2 and 2.2 ms^{-1}.

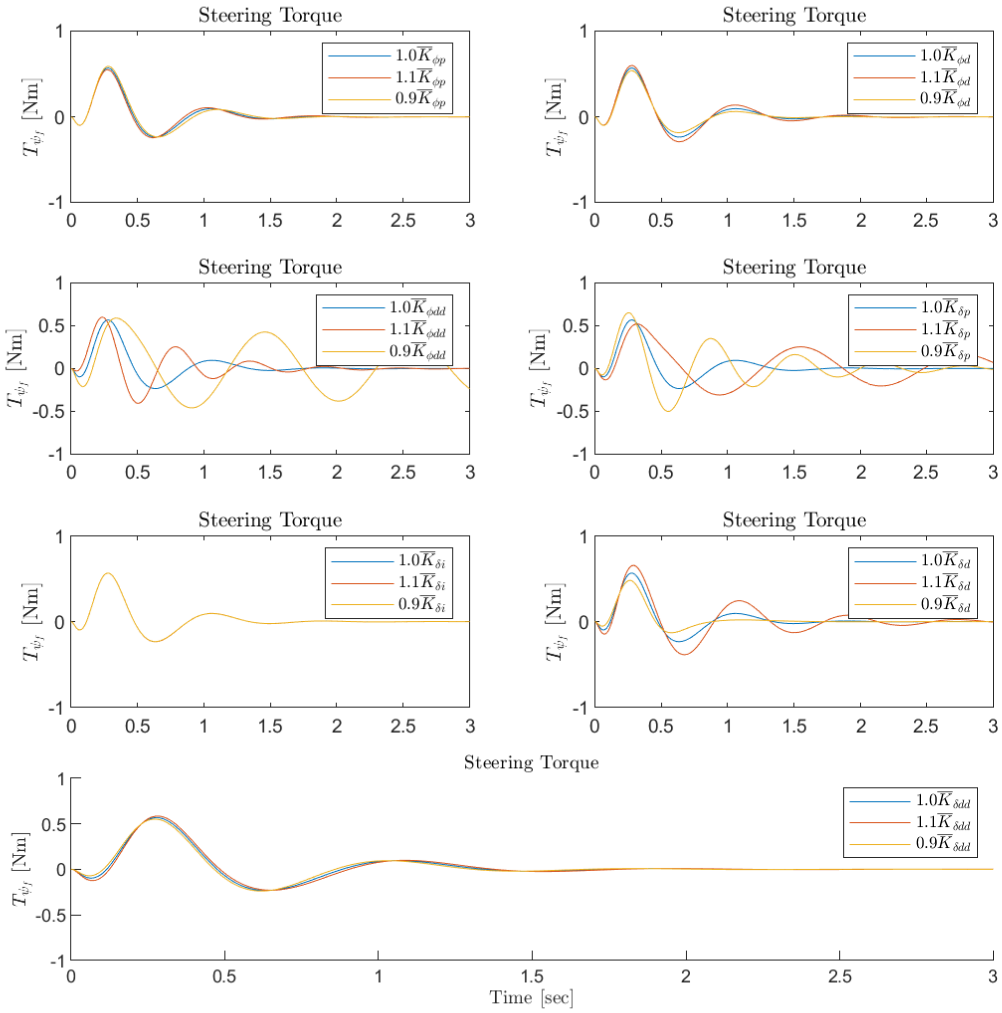

Figure K.8: A sensitivity analysis of the parameters of controller $K(s,\theta)$ with neuro-muscular dynamics G_{nm} and effective neural time delay τ_d of 60 ms for which the feedback parameters are averaged per velocity group. The torque response corresponds to a initial steer perturbation of 0.5 rads^{-1} and forward velocity of 7.3 ms^{-1}. The responses are visualized upon a 10% increase or decrease of the feedback parameter given in the legends. An example of a velocity group is the group of 2.1, 2.2 and 2.2 ms^{-1}.

Bibliography

[1] Dovilé Adminaité-Fodor and Graziella Jost. "How safe is walking and cycling in Europe?" In: (2020).

[2] Pradipta Basu-Mandal, Anindya Chatterjee, and Jim M Papadopoulos. "Hands-free circular motions of a benchmark bicycle". In: *Proceedings of the Royal Society A: Mathematical, Physical and Engineering Sciences* 463.2084 (2007), pp. 1983–2003.

[3] Vittore Cossalter, Alberto Doria, and Roberto Lot. "Steady turning of two-wheeled vehicles". In: *Vehicle system dynamics* 31.3 (1999), pp. 157–181.

[4] Erwin De Vlugt, Alfred C Schouten, and Frans CT Van Der Helm. "Quantification of intrinsic and reflexive properties during multijoint arm posture". In: *Journal of neuroscience methods* 155.2 (2006), pp. 328–349.

[5] Georgios Dialynas et al. "The effect of haptic feedback in the balance task of bicycling". In: ().

[6] Alberto Doria, Sergio Roa, and Luis Muñoz. "Stability analysis of bicycles by means of analytical models with increasing complexity". In: *Mechanical Sciences* 10.1 (2019), pp. 229–241.

[7] Anthony John Redfern Doyle. "The skill of bicycle riding." PhD thesis. University of Sheffield, 1987.

[8] G Franke, W Suhr, and F Rieß. "An advanced model of bicycle dynamics". In: *European Journal of Physics* 11.2 (1990), p. 116.

[9] Neil H Getz and Jerrold E Marsden. "Control for an autonomous bicycle". In: *Proceedings of 1995 IEEE international conference on robotics and automation*. Vol. 2. IEEE. 1995, pp. 1397–1402.

[10] Fumio Hamano. "Derivative of rotation matrix direct matrix derivation of well known formula". In: *arXiv preprint arXiv:1311.6010* (2013).

[11] H.and Koopman van der Kooij, B., and F van der Helm. *Human Movement Control Reader*. 2008.

[12] JDG Kooijman and AL Schwab. "Experimental validation of the lateral dynamics of a bicycle on a treadmill". In: *ASME 2009 International Design Engineering Technical Conferences and Computers and Information in Engineering Conference*. American Society of Mechanical Engineers Digital Collection. 2009, pp. 2029–2034.

[13] JDG Kooijman, AL Schwab, and Jacob Philippus Meijaard. "Experimental validation of a model of an uncontrolled bicycle". In: *Multibody System Dynamics* 19.1-2 (2008), pp. 115–132.

[14] Y Lajoie and SP Gallagher. "Predicting falls within the elderly community: comparison of postural sway, reaction time, the Berg balance scale and the Activities-specific Balance Confidence (ABC) scale for comparing fallers and non-fallers". In: *Archives of gerontology and geriatrics* 38.1 (2004), pp. 11–26.

[15] J. Langley et al. "Missing cyclists". In: *Injury Prevention* 9.4 (2003). cited By 52, pp. 376–379. DOI: 10.1136/ip.9.4.376. URL: https://www.scopus.com/inward/record.uri?eid=2-s2.0-1542542774&doi=10.1136%2fip.9.4.376&partnerID=40&md5=d90cecd4ecfaf28e1ca052cdd0681fbc.

[16] Anders Lennartsson. "Efficient multibody dynamics". PhD thesis. KTH Royal Institute of Technology, 1999.

[17] Duane T McRuer, Dunstan Graham, and Ezra S Krendel. "Manual control of single-loop systems: Part II". In: *Journal of the Franklin Institute* 283.2 (1967), pp. 145–168.

[18] Duane T McRuer, Raymond E Magdaleno, and George P Moore. "A neuromuscular actuation system model". In: *IEEE Transactions on Man-Machine Systems* 9.3 (1968), pp. 61–71.

[19] D.E. Meehan and A.L. Ruina. "Linear and nonlinear controllers of an autonomous bicycle have almost identical basins of attraction in a non-linear simulation". In: *Symposium on the Dynamics and Control of Single Track Vehicles* (2019).

[20] Jaap P Meijaard et al. "Linearized dynamics equations for the balance and steer of a bicycle: a benchmark and review". In: *Proceedings of the Royal society A: mathematical, physical and engineering sciences* 463.2084 (2007), pp. 1955–1982.

[21] Jason Keith Moore. *Human control of a bicycle*. University of California, Davis Davis, CA, 2012.

[22] J Patrick and KD Duncan. "THE ESSENTIAL HUMAN CONTRIBUTION TO BICYCLE RIDING". In: *Training, human decision making, and control* (1988), p. 351.

[23] ML Psiaki. "Bicycle stability: a mathematical and numerical analysis". In: *Undergraduate thesis* (1979).

[24] *Rider identification in bicycle: A preliminary analysis. Master's thesis*. 2011.

[25] Paul Schepers and K Klein Wolt. "Single-bicycle crash types and characteristics". In: *Cycling Research International* 2.1 (2012), pp. 119–135.

[26] Alfred C Schouten et al. "Quantifying proprioceptive reflexes during position control of the human arm". In: *IEEE Transactions on Biomedical Engineering* 55.1 (2007), pp. 311–321.

[27] AL Schwab. *ME41055 Multibody Dynamics B*. 2018.

[28] AL Schwab, George Dialynas, and Riender Happee. "Some Effects of Crosswind on the Lateral Dynamics of a Bicycle". In: *Multidisciplinary Digital Publishing Institute Proceedings*. Vol. 2. 6. 2018, p. 218.

[29] AL Schwab, JDG Kooijman, and Jacob Philippus Meijaard. "Some recent developments in bicycle dynamics and control". In: *4th European Conference on Structural Control, ECSC 2008*. Russian Academy of Sciences. 2008.

[30] AL Schwab, JP Meijaard, and JDG Kooijman. "Lateral dynamics of a bicycle with a passive rider model: stability and controllability". In: *Vehicle system dynamics* 50.8 (2012), pp. 1209–1224.

[31] AL Schwab et al. "Rider control identification in bicycling using lateral force perturbation tests". In: *Proceedings of the Institution of Mechanical Engineers, Part K: Journal of Multi-body Dynamics* 227.4 (2013), pp. 390–406.

[32] Arend L Schwab and JP Meijaard. "A review on bicycle dynamics and rider control". In: *Vehicle System Dynamics* 51.7 (2013), pp. 1059–1090.

[33] Everett X Wang et al. "Symbolic derivation of nonlinear benchmark bicycle dynamics with holonomic and nonholonomic constraints". In: *16th International IEEE Conference on Intelligent Transportation Systems (ITSC 2013)*. IEEE. 2013, pp. 316–323.

[34] David H Weir. "Motorcycle Handling Dynamics and Rider Control and the Effect of Design Configuration on Response and Performance, UCLA". PhD thesis. Ph. D. Thesis, 1972.

[35] Francis JW Whipple. "The stability of the motion of a bicycle". In: *Quarterly Journal of Pure and Applied Mathematics* 30.120 (1899), pp. 312–348.

[36] Jiaming Xiong, Nannan Wang, and Caishan Liu. "Stability analysis for the Whipple bicycle dynamics". In: *Multibody System Dynamics* (Oct. 2019). ISSN: 1573-272X. DOI: 10.1007/s11044-019-09707-y. URL: https://doi.org/10.1007/s11044-019-09707-y.

[37] Maurice R Yeadon and M Morlock. "The appropriate use of regression equations for the estimation of segmental inertia parameters". In: *Journal of biomechanics* 22.6-7 (1989), pp. 683–689.

[38] Jingang Yi et al. "Trajectory tracking and balance stabilization control of autonomous motorcycles". In: *Proceedings 2006 IEEE International Conference on Robotics and Automation, 2006. ICRA 2006.* IEEE. 2006, pp. 2583–2589.